LAPPEENRANTA UNIVERSITY OF TECHNOLOGY
LUT School of Energy Systems
LUT Mechanical Engineering

Pia Kaila

COMPUTATIONAL STUDIES OF DEFORMATION IN STAINLESS STEEL RINGS DUE TO TORCH HEATING

Examiners: Professor Timo Björk
Professor Robert Gooding
Supervisors: Aku Asikainen
Joonas Sorvari

ABSTRACT

Lappeenranta University of Technology
LUT School of Energy Systems
LUT Mechanical Engineering

Pia Kaila

Computational studies of deformation in stainless steel rings due to torch heating

Master's Thesis
2015
84 pages, 66 figures, 10 tables and 15 appendices.

Examiners: Professor Timo Björk, Professor Robert Gooding

Supervisors: Aku Asikainen, Joonas Sorvari

Keywords: Stainless steel, ring, torch heating, shrinkage, residual stress

A support ring of AISI 304L stainless steel that holds vertical, parallel wires arranged in a circle forming a cylinder is studied. The wires are attached to the ring with heat-induced shrinkage. When the ring is heated with a torch the heat affected zone tries to expand while the adjacent cool structure obstructs the expansion causing upsetting. During cooling, the ring shrinks smaller than its original size clamping the wires. The most important requirement for the ring is that it should be as round as possible and the deformations should occur as overall shrinkage in the ring diameter.

A three-dimensional nonlinear transient sequential thermo-structural Abaqus model is used together with a Fortran code that enters the heat flux to each affected element. The local and overall deformations in one ring inflicted by the heating are studied with a small amount of inspection on residual stresses.

A variety of different cases are chosen to be studied with the model constructed to provide directional knowledge; torch flux with the means of speed, location of the wires, heating location and structural factors. The decrease of heating speed increases heat flux that rises the temperature increasing shrinkage. In a single progressive heating uneven distribution of shrinkage appears to the start/end region that can be partially fixed with using speeded heating's to strengthen the heating of that region. Location of the wires affect greatly to the caused shrinkage unlike heating location. The ring structure affects also greatly to the shrinkage; smaller diameter, bigger ring height, thinner thickness and greater number of wires increase shrinkage.

TIIVISTELMÄ

Lappeenrannan teknillinen yliopisto
LUT School of Energy Systems
LUT Konetekniikka

Pia Kaila

Laskennallisten muodonmuutosten tutkimus ruostumattomissa teräs renkaissa aiheutuen poltin kuumennuksesta

Diplomityö
2015
84 sivua, 66 kuvaa, 10 taulukkoa ja 15 liitettä.

Tarkastajat: Professori Timo Björk, Professori Robert Gooding

Ohjaajat: Aku Asikainen, Joonas Sorvari

Hakusanat: Ruostumaton teräs, rengas, poltin kuumennus, kutistuma, jäännösjännitys

AISI 304L ruostumaton teräs rengas, joka tukee yhdensuuntaisia pystysuoria lankoja asetettuna kehän muotoon muodostaen sylinterin, tutkitaan. Langat kiinnitetään renkaaseen kuumennuksella aiheutetulla kutistumalla. Kun rengasta kuumennetaan polttimella, kuumennettu alue pyrkii laajenemaan viereisten viileämpien rakenteiden vastustaessa laajenemista aiheuttaen tyssääntymistä. Jäähtyessään rengas kutistuu alkuperäistä kokoaan pienemmäksi kiinnittäen langat. Renkaan tärkein vaatimus on säilyttää pyöreys ja muodonmuutosten tulisi tapahtua renkaan halkaisijan kokonaisvaltaisena kutistumana.

Kolmiulotteista, epälineaarista, tilapäistä sekä peräkkäisillä lämpö-rakenteellisilla vaiheilla olevaa Abaqus mallia käytetään yhdessä Fortran koodin kanssa, joka asettaa lämpövuon jokaiseen vaikutuksen alaiseen elementtiin. Kuumennuksesta aiheutuvia paikallisia ja kokonaisvaltaisia muodonmuutoksia tutkitaan yhdessä renkaassa hieman tarkastellen myös jäännösjännityksiä.

Erilaisten tapausten lajitelma valitaan tutkittavaksi rakennetulla mallissa tarjoamaan suuntaa-antavaa tietoa; polttimen vuo nopeuden avulla, lankojen sijainti, kuumennuksen sijainti ja rakenteelliset tekijät. Kuumennusnopeuden vähentäminen lisää lämpövuota nostaen lämpötilaa ja kasvattaen kutistumaa. Yhdessä etenevässä kuumennuksessa esiintyy epätasaisesti jakautuvaa kutistumaa aloitus/lopetus alueella joka voidaan osittain korjata käyttämällä nopeutettu kuumennuksia vahvistamaan kyseisen alueen kuumentamista. Lankojen sijainti vaikuttaa suuresti aiheutuvaan kutistumaan toisin kuin kuumennus sijainti. Renkaan rakenne vaikuttaa myös suuresti kutistumaan; pienempi halkaisija, suurempi renkaan korkeus, ohuempi paksuus ja suurempi määrä lankoja kasvattavat kutistumaa.

PREFACE AND ACKNOWLEDGEMENTS

I want to thank the workers at Aikawa Fiber Technologies Oy Varkaus for welcoming me amongst them and providing me knowledge and assist through this whole process. Especially big thanks to Aku Asikainen. Reza Mousivand, thank you for providing the model and a basic instruction guide on using it. However without the assist from Joonas Sorvari, I would have been lost with the model and the programs. Thank you for the long days working with the model and giving the strength to answer my endless amount of emails. Special thanks to IT Center for Science who gave me the access to Abaqus software and to their supercomputer. Timo Björk and Robert Gooding guided me through all this which is why I'm thankful for them. My family and friends had amazing patience and strength to listen to my problems and calm my nerves. There were lots of hardships but also many rewarding moments. As happy as I am for the thesis to be ready and me being finally able to graduate this is an end of an era.

Joroinen, May, 2015

Pia Kaila

CONTENTS

APPENDICES

FIGURES

TABLES

SYMBOLS AND ABBREVIATIONS

α	Expansion coefficient [mm/mK]
λ	Oxidation ratio
ξ	Presentation of the moving coordinate system
σ_r	Radial residual stress
c	Characteristic radius of heat flux distribution [mm]
C	Distribution width coefficient [m^{-2}]
k	Thermal conductivity [W/mK]
P	Contour height [mm]
q	Heat flux density [W/m^2]
Q	Energy input rate [W]
r	Radial distance [m]
S	Slot width [mm]
W	Wire width [mm]
x	X-coordinate for the element under calculation
x_m	Presentation of the moving coordinate system
x_0	X-coordinate for the center of the torch
y	Y-coordinate for the element under calculation
y_0	Y-coordinate for the center of the torch
CSC	IT Center for Science
FE	Finite element
FEM	Finite element method
HAZ	Heat affected zone
TMP	Thermomechanical pulping

1 INTRODUCTION

According to Sixta (2006, p. 8): “At present, more than 90 % of the pulp (virgin pulp fiber) produced worldwide is wood pulp.” Today’s emphasis on environmental factors is directed towards issues on product life cycles, natural resources, recycling and renewable energy (Metla, 2012). The second largest material after wood used to produce pulp is recovered paper. The usage of recovered fiber has grown substantially and continues to expand. Recovered fiber usage has increased from 22.5 % in 1978 to 33.5 % in 1992 and to 44 % in 2000 from the global usage of fiber. (Sixta, 2006, p. 14.)

There are two distinct processes used to produce pulp from wood: mechanical pulping and chemical pulping. Each was developed to produce pulp from wood efficiently. In chemical pulping, however, the yield of wood fibers relative to the incoming wood used is only about 45–55 %, whereas in mechanical pulping the yield is about 80–95 %. (Sixta, 2006, p. 1071.)

Kraft pulping is the predominant mode of chemical pulping process today accounting for 89% of all the chemical pulps and over 62 % of the total production of virgin fiber pulp (Sixta, 2006, p. 8). In kraft pulping, wood chips are mixed with high temperature cooking liquor in a digester. The digester breaks the chemical bonds in the lignin that bind the fibers together. After cooking, the fiber (in other words the pulp) is screened to separate the undesirable matter from the pulp and then washed. The pulp is typically bleached to whiten the fibers before the pulp is made into paper. After bleaching the pulp is formed into a sheet, dried and rolled. A simple schematic of a chemical-based pulp and paper mill with the main phases is illustrated in Figure 1. (Pulp and Paper Applications, 2008, p. 1.)

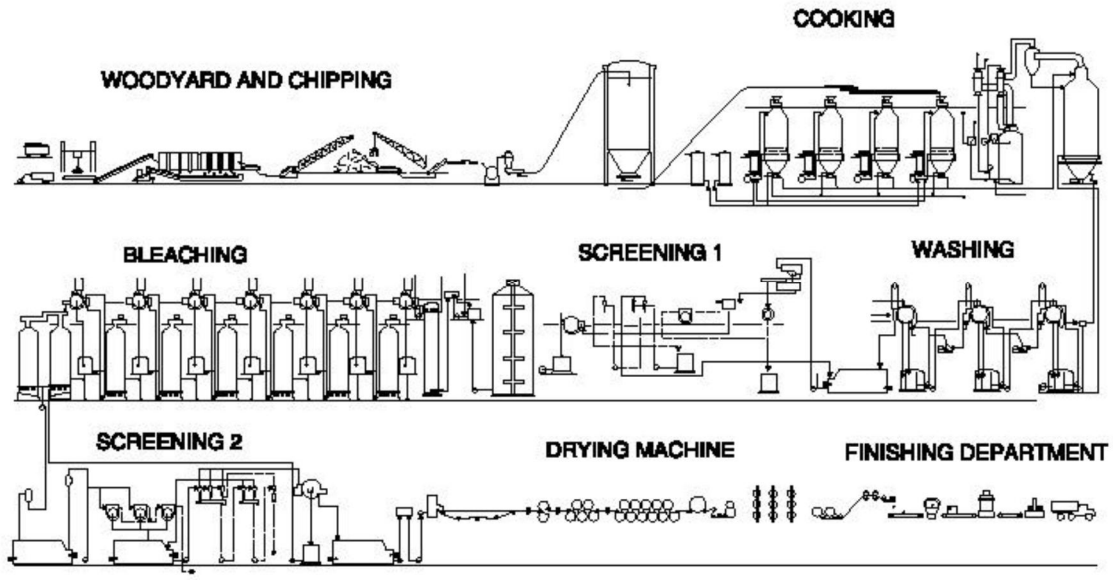

Figure 1. Simple schematic of a chemical pulp and paper mill (Pulp and Paper Applications, 2008, p. 1).

According to the Institute for Industrial Productivity (2015): "As the oldest form of pulping, mechanical pulping uses mechanical energy to weaken and separate fibers from wood via a grinding action." Mechanical pulping recovers more of the wood fibers than chemical pulping processes, but it does not dissolve lignin. The resulting pulp fibers are typically shorter that the kraft pulp fibers. Shorter fibers reduce the strength of the resulting paper, and the presence of lignin causes the paper to yellow. (The Institute for Industrial Productivity, 2015.) The resulting mechanical pulp is thus according to the Institute for Industrial Productivity (2015): "- - used for lower grade papers such as newsprint, magazines, and catalogues." Mechanical pulping processes are generally categorized as either groundwood pulping process or refiner pulping process (Sixta, 2006, p. 12). The Institute for Industrial Productivity (2015) states that "- - TMP is the most common mechanical process in use today." Thermomechanical pulping (TMP) is a type of refiner pulping process. Wood chips are softened with steaming and then ground between two grooved discs. After grinding, the pulp passes through similar processes as for chemical pulping, that are screening, cleaning, thickening, bleaching (in some cases) and finally the papermaking process (Figure 2). (The Institute for Industrial Productivity, 2015.)

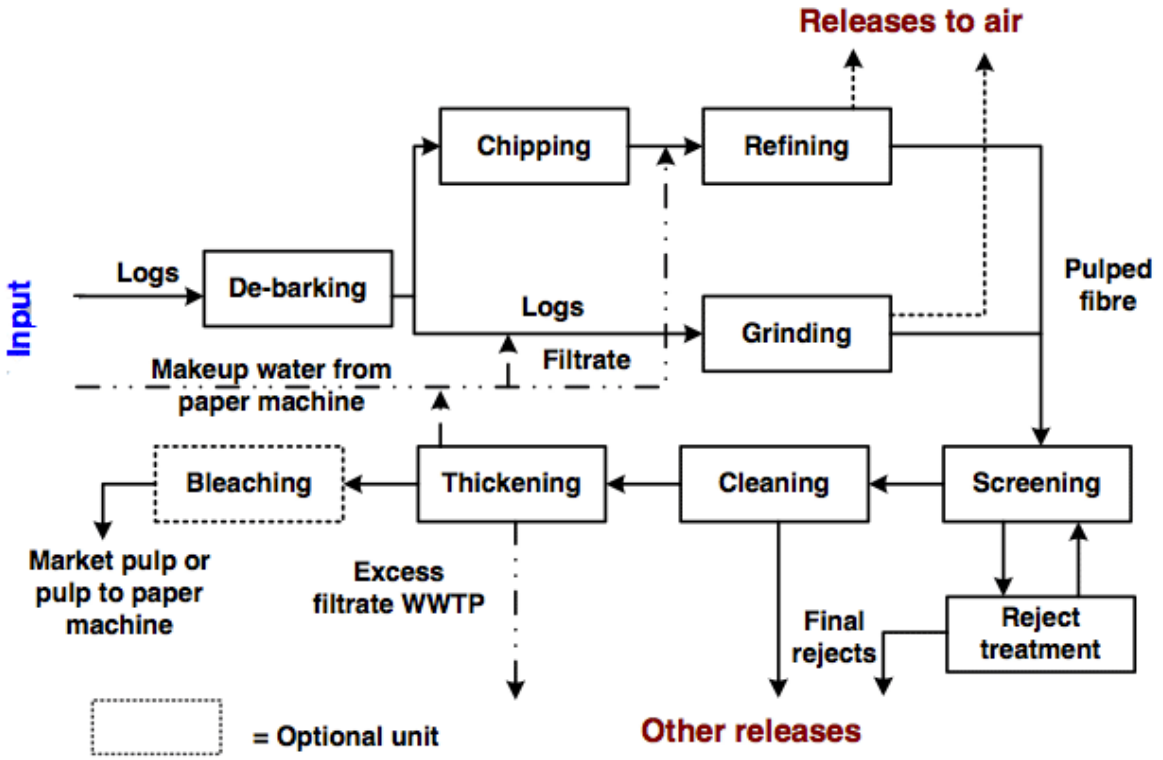

Figure 2. Main steps in mechanical pulping (The Institute for Industrial Productivity, 2015).

Both the chemical and mechanical pulping processes include the screening process. Screening is needed to remove oversize contaminants from the desired pulp fibers. The pulp can contain undesired wood components, such as fiber bundles and bark fragments, and non-wood contaminants. Non-wood contaminants are, for example, stones, sand, metal and plastic debris. (Sixta, 2006, p. 561.) According to Sixta (2006, p. 561) "- - certain non-wood contaminants are carried along with the wood chips or enter the pulp mill processes by other routes." The object of screening is to remove these impurities to protect the equipment, save bleaching chemicals and obtain a clean final product. The mechanism used in screening is separation by size through narrow screen apertures, where large contaminants are retained while the fibers pass through. (Sixta, 2006, p. 561–562.)

1.1 Background of the study

The details of the various means used to manufacturing screen cylinders by various manufacturers might not be found in public sources, because of the industry's competitive nature. Therefore this thesis is based on research articles and theses that consider the more fundamental aspects of cylinder manufacture.

A bachelor's thesis was done in Lappeenranta University of Technology to gather information and provide a literature review about controlling distortions and residual stresses when exposed to heat. Kaila (2014, p. 3) concentrated on finding information about how distortions and residual stresses are originated, manifested, measured and controlled. The different controlling methods she studied were prevention, reduction and removal. She also gathered information about studying distortions and residual stresses with modeling in general and through already made research studies. (Kaila, 2014, p. 3.)

The pulp screen cylinders have been studied in a master's thesis at the University of British Columbia. Towfighi (2011, p. 4) determined the material characteristics for stainless steel AISI 304L at elevated temperatures, which could not be found from the literature. He identified the possible mechanism that could change the support rings, on a microstructural level and by plastic deformations and residual stresses, when subjected to heat. With knowledge from these matters he constructed a LS-DYNA model to predict the state of the rings after heating, which he validated with experimental data gathered from laboratory tests. (Towfighi, 2011, p. 4.)

Another study at the University of British Columbia extended the work of Towfighi (2011) by analyzing different methods of heating. The results of this work are not yet published, but the model Towfighi used has been further developed. (Mousivand, 2015.)

1.2 Research problems and objectives

The research problem to be solved is to find factors and clarify the effects they have to the manufacturing process of screen cylinders by heating the support rings with a torch. From the effects the factors have to the manufacturing process the shrinkage of the ring is concentrated and a general conception of the distribution of residual stresses is obtained.

Thus far studies have only addressed outflow type cylinders. In this thesis the inflow type cylinders are studied. The difference between outflow and inflow cylinders are the location of the wires; in inflow cylinders the wires are located on the outer rim of the ring and in outflow cylinders on the inner rim of the ring. This study not only considers an improved model for analyzing the heat-induced shrinkage, but considers the influence of cylinder diameter, ring thickness and other common variables.

1.3 Structure of the thesis

The first chapter covers background information from pulp and paper industry via chemical and mechanical pulping to the process of screening. The research problems and objectives are gone through also to explain more the relevancy of this thesis.

In the second chapter pressure screens are inspected more closely getting a better picture about the screen cylinders idea, structure and manufacturing process through publically available information. In this chapter a closer look is done to screen cylinder structure where wedge-wires and continuous slots have been used.

Third chapter views the manufacturing procedure of a screen cylinder through the already done researches on the happening occasions when exposing a part to heat. The main affecting factors heating sequence, heat flux and the ring structure are discussed. The main idea of this thesis is to assess the computationally gathered data concerning the effects of different factors on deformation. Therefore different measurement, reduction and removal methods of deformations are discussed in the fourth chapter.

Fifth chapter tells more about modeling in general and the development of the model used in this thesis to conduct the computational studies. Towfighi (2011) created a model that was further improved. This model is now in use in this thesis modified to fit the studied cases. The studied cases and the needed model variations the studied cases need are explained in more detail in the sixth chapter along with the gain results.

Discussion and conclusions of the attained results is done in the seventh chapter. The discussion and conclusions consists of main findings, recommendations, evaluation of results and future research. After discussion and conclusions a summary of the thesis is made in chapter nine.

2 PULP SCREEN

The pulp screen commonly used to treat pulp before the paper making process usually comprises a vertical cylinder screen and a rotor. The rotor and cylinder are concentrically arranged inside the screen substantially close. In an outflow screen, the outer surface of the rotor and the inner surface of the screen define a screening zone for the pulp. There is an inlet for supplying the pulp to be screened, which is commonly on the upper end of the screening zone and outlets from an accept chamber surrounding the outer surface of the screen and a reject chamber connected to the lower end of the screening zone. The cylinder screen and the rotor are situated within an outer housing. (Pat. US 4634521 A, 1987, p. 4.) Figure 3 illustrates the main idea of a pressure screen described above.

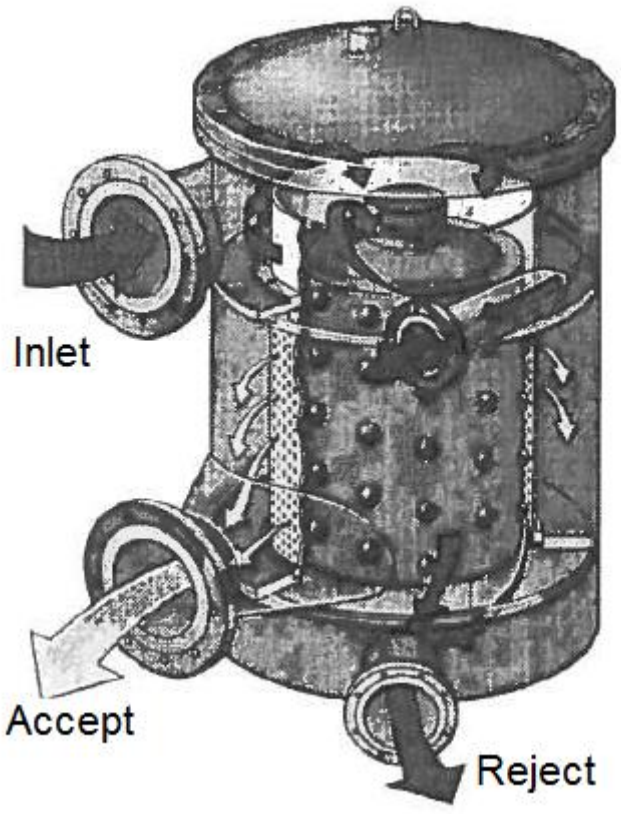

Figure 3. Pressure screen (Seppälä et al., 1999, p. 50).

The separation of solids according to Sixta (2006, p. 563): "- - with a pressure screen can be categorized by the type of physical separation mechanism." There are barrier separation

method and probability separation method (Sixta, 2006, p. 563). In barrier separation, the rejects are as Sixta (2006, p. 563) states: "- - physically larger than the aperture size in any orientation." In probability separation, accepts are selected based on the orientation of the particles while approaching the aperture. The pulp screen constitutes of two basic mechanical elements as mentioned above that control the separation, the screen and the rotor. Commonly the screen is a cylindrical shell fixed to the screen's outer housing. (Sixta, 2006, p. 563.) The apertures are as Sixta (2006, p. 563) describes: "- - either holes or slots and the screen surface may be smooth or contoured." Accepts pass through the apertures on the screen cylinder while rejects proceed on the inside of the screen to the reject outlet as you can see in the Figure 3. The rotor is situated inside the screen cylinder in an outflow-type screen. The rotor provides tangential velocity, turbulence and backflush pulses. Through these means it promotes the passage of pulp fibers through the cylinder apertures and keeps them clear of any blockages. (Sixta, 2006, p. 564.)

2.1 Screen Cylinder

The screen cylinder according to Sixta (2006, p. 572): "- - is fundamentally characterized by aperture size, aperture shape and aperture spacing, as well as the character of its surface." The aperture size has become the most dominating design factor for screen cylinders. Differing screen performance is caused by the apertures contour depth. The fiber length affects the aperture spacing. Longer fibers need wider distance between adjacent apertures than shorter fibers. (Sixta, 2006, p. 573.) Holed screens are favored stated by Sixta (2006, p. 573): "- - for their high capacity and reliable operation and easy control under varying conditions." For their robustness, the holed screens are ideal when screening larger contaminants. Typical hole diameters can be in the range of 1 to 10 mm. (Sixta, 2006, p. 573.)

When the use of slotted cylinders increased in early 1970's, the contaminant removal efficiency was superior, but the low capacity of these cylinders limited their use. Their capacity was greatly improved by the contoured slotted cylinders in 1980's. (Weckroth et al., 2002, p. 4; Sixta, 2006, p. 1117.) Developments in the screen construction in 1970's and the optimization of the screen contour in 1980's led slot width in slotted cylinders to decrease from 0.50 to 0.15 mm. The open area of slotted screen cylinders has since increased as a result of developments in cylinder technology, such as the wedge-wire

cylinder. (Weckroth et al., 2002, p. 4.) Wedge-wire screen cylinders are formed with wires arranged side by side forming continuous slots over the length of the screen cylinder (Sixta, 2006, p. 573). Cylinders with different open areas are compared in Figure 4. However the optimal open area depends on the required capacity and the needed slot width. (Weckroth et al., 2002, p. 4.)

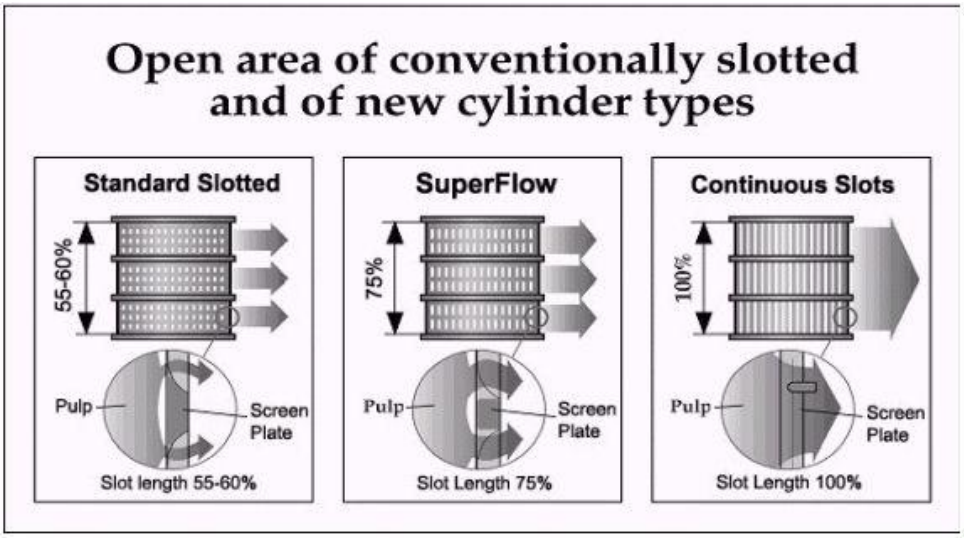

Figure 4. Cylinders with different open areas (Weckroth et al., 2002, p. 5).

The combination of contoured screen cylinders and wedge-wire designs according to Sixta (2006, p. 573): "- - have made today's narrow screen slots practical and widely accepted." Wedge-wire cylinders have provided improvements in contaminant removal, and enhanced physical pulp properties. The design of the wedge-wire cylinder consists of vertical, parallel wires arranged in a circle forming a cylinder and metal rings that hold the wires in place. The size of the slot, in other words the slot width *S*, between adjacent wires is precisely set typically to some value between 0.10 mm and 0.25 mm, though smaller and larger slots are used in certain applications. The wire cross-section resembles a wedge, but the exact shape differs between suppliers. The angle of the wedge and the resulting shape of the contour affect screen performance. An example of a wedge-wire shape is illustrated in Figure 5 where the wire width W, the slot width S and the contour height P are also shown. (Cannell, 1999, p. 1.)

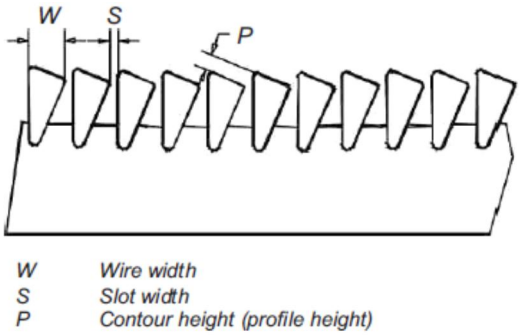

Figure 5. Example of a wedge-wire profile (Sixta, 2006, p. 1117).

2.2 Rotor

Different kind of shapes and local arrangements, bumps or foils, differentiate the rotors. Figure 6 illustrates examples of the pulp screen rotor designs with bumps and foils. (Sixta, 2006, p. 573.) The design factors of rotors have as Sixta (2006, p. 573) describes: "- - individual advantages regarding screen capacity, screening efficiency or power consumption." Rotor generates a pressure pulse which form as Sixta (2006, p. 573) states: "- - depends on the design of the pulsation element." The design of the pulsation element is varied with its shape, length and angle. There are many factors that affect the intensity of the pulse. (Sixta, 2006, p. 573.) These factors include according to Sixta (2006, p. 573): "- - the rotor shape, as well as the rotor tip velocity, the clearance between the pulsation element and the screen basket, as well as the pulp consistency and pulp furnish parameters." Figure 7 illustrates the example pressure pulse forms for a foil-type rotor and a step rotor.

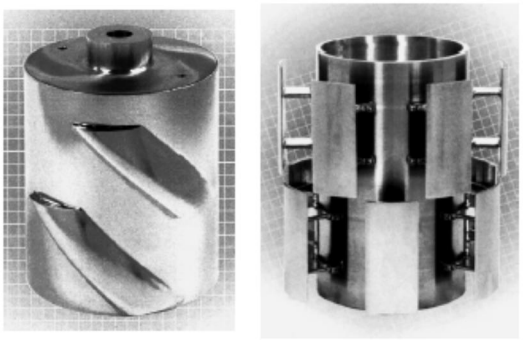

Figure 6. Pressure screen rotor designs, bumps (left) and foils (right) (Sixta, 2006, p. 1118).

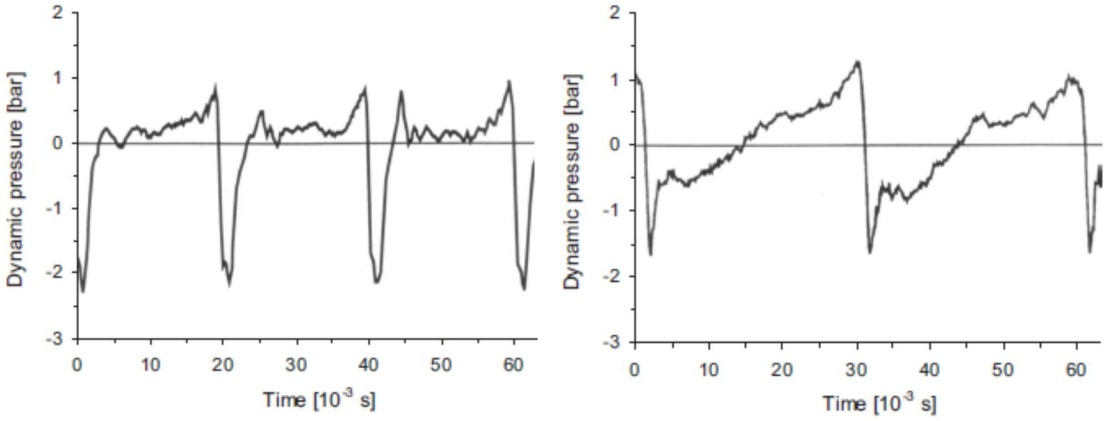

Figure 7. Example of pressure pulse forms for a foil rotor (left) and a step rotor (right) (Sixta, 2006, p. 574).

Sixta (2006, p. 574) describes the pressure pulse as such: "At a random point on the screen surface, there is in general a positive pressure pulse upstream of the rotor element, and a negative pressure pulse right after the smallest clearance between the rotor tip and the screen basket has passed by. The negative pressure is responsible for the backflush through the screen apertures." The clearance between the rotor (the pulsation element) and the screen cylinder differs among rotor designs, but is commonly set at a value between 3 and 10 mm. Reducing the clearance increases the pressure pulse intensity. (Sixta, 2006, p. 575.) Image of a rotor foil passing a screen cylinder is illustrated in Figure 8.

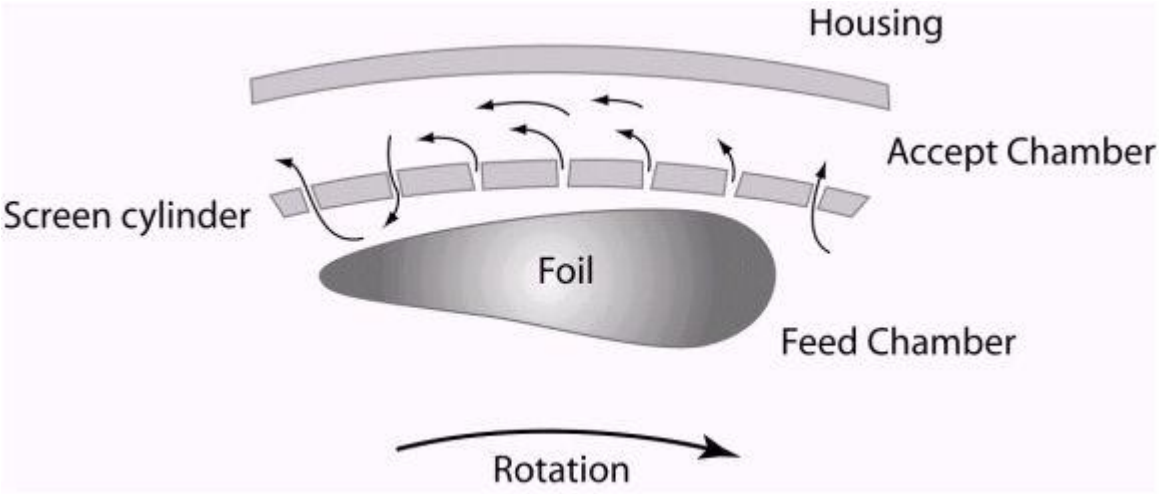

Figure 8. Image of a rotor foil passing a screen cylinder (Weckroth et al., 2002, p. 6).

3 HEATING PROCEDURE

Various means are used to create wedge-wire cylinders, and in particular the means to join the wires to the support structure. These means include riveting, welding, clamping, gluing and heat-induced shrinkage. This study focuses mainly on the method of heat-induces shrinkage. This manufacturing procedure has some elements that are comparable to heat straightening. The manifestation of distortions and residual stresses is comparable also to the distortions and residual stresses originating from the welding heat. In this chapter the methods and challenges of heat straightening are familiarized along with an inspection on the affecting factors on the deformations are discussed.

3.1 Heat-straightening

In heat straightening the heated component is locally heated to the material specific temperature where plastic deformations occur. The restricted expansion causes remaining deformations. During cooling the work piece is deformed leading to the desired change in length or shape. Heat straightening consist of three distinctive phases; heating, upsetting and shrinking (Figure 9). (Flame Straightening, 2013, p. 9.) In heat straightening the heating is done in different patterns with repetitive heating and cooling cycles (Federal Highway Administration, 2013, p. 6). According to Federal Highway Administration (2013, p. 6): “Heat straightening is a repair procedure in which controlled heat is applied - - to the plastically deformed regions of damaged steel - -.”

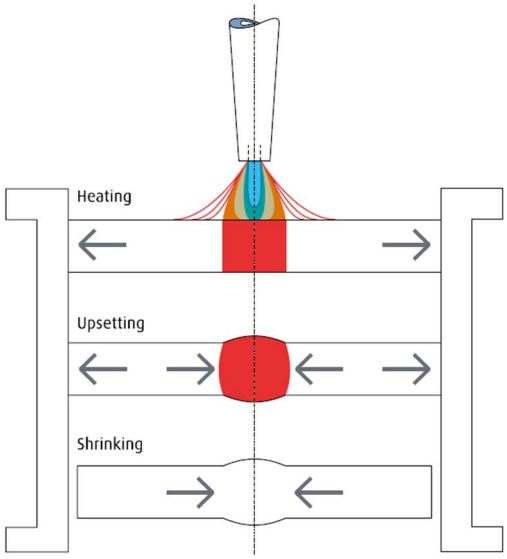

Figure 9. Three main phases in heat straightening (Flame Straightening, 2013, p. 9).

3.1.1 Heat straightening phases

Figure 10 illustrates the theory of heat induced deformations in a bar in ideal situation. The effects of heat straightening are easiest explained with a bar fixed from both ends to a clamp much stronger than the bar itself. The bar is heated partially (Figure 10). (Federal Highway Administration, 2013, p. 7.) Federal Highway Administration (2013, pp. 7–8) describes the shortening process accordingly: “As the bar is heated it tries to expand. However the fixture prevents expansion in the longitudinal direction. - - Since the bar is prevented from longitudinal expansion, it is forced to expand a greater amount laterally and transversely through it’s thickness - -. When the heating source is removed, the material will cool and contract three-dimensionally. The clamp cannot prevent the bar from contracting longitudinally. As cooling progresses the bar shortens - -.” When the bar shortens, redistribution of material (plastic deformations) happens (Federal Highway Administration, 2013, p. 8). When the bar is not fixed with a clamp the surrounding structure that remains somewhat cool will obstruct the expansion to some extend causing the same effects.

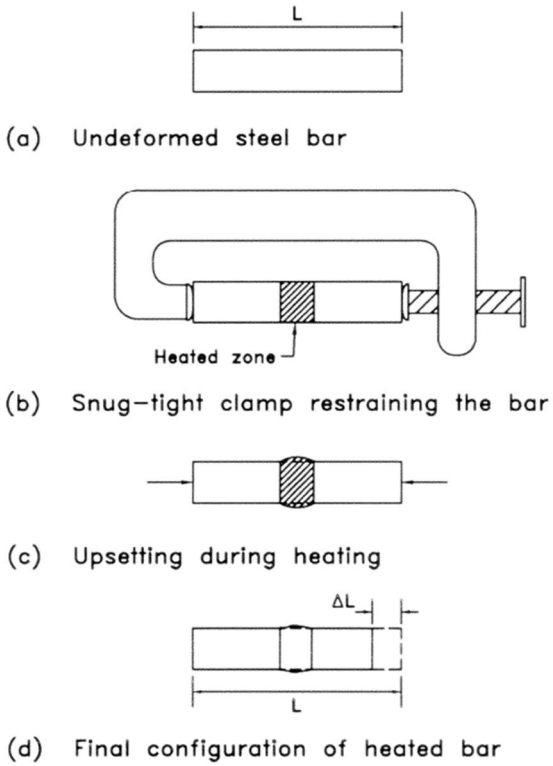

Figure 10. Idea behind shortening of a steel bar with heating (Federal Highway Administration, 2013, p. 8).

The vee-shaped heat is fundamentally used in straightening strong axis bends. In heat straightening the beam is heated partially from an area in the shape of vee (Figure 11). (Federal Highway Administration, 2013, p. 9.) According to Federal Highway Administration (2013, p. 9): "- - a typical vee heat starts with a very small spot heat applied at the apex of the vee-shaped area - -, the torch is advanced progressively in a serpentine motion towards the base of the vee. - - The plate will initially move upward - - as a result of longitudinal expansion of material above the neutral axis producing negative bending. - - At the completion of the heat, the entire heated area is at a high and relatively uniform temperature. At this point the plate has moved downward - - due to longitudinal expansion of material below the neutral axis producing positive bending." The cool material surrounding the heat affected zone (HAZ) obstructs the expansion in the longitudinal direction causing the material to upset through its thickness creating redistribution of material. Cooling of the beam causes it to start straightening, counteracting with the initial distortion caused by the shape of heat distribution (Figure 11c). (Federal Highway Administration, 2013, p. 9.)

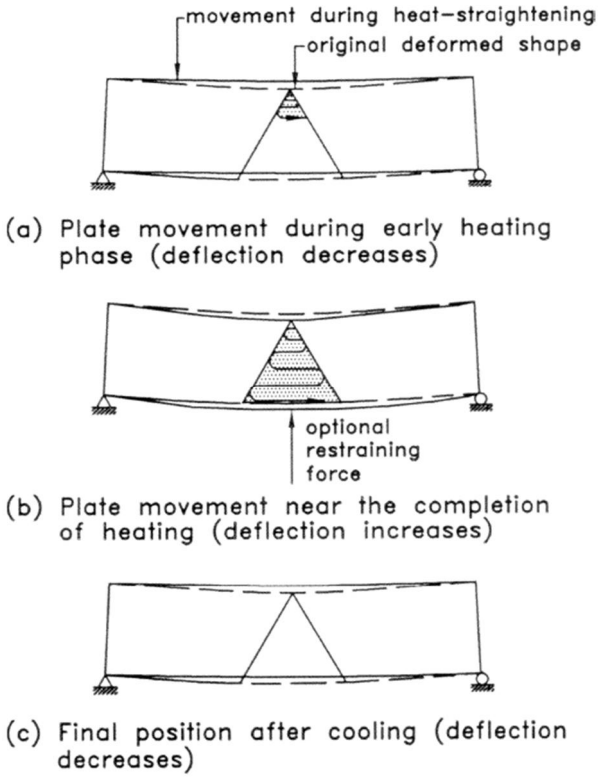

Figure 11. Idea behind straightening of a steel plate with a vee heat (Federal Highway Administration, 2013, p. 9).

The uneven heating of a part develops stresses and the hot regions pursue to expand as the cold regions pursue to obstruct the expansion. In that phase, compression forms to the hot regions and tensile to the cold regions. When heating with a torch, the heat affected zone in a part is small compared to the zone not affected by the heat. Reduction of yield strength on the HAZ causes upsetting, while the cold regions retain their elasticity. In the cooling phase, the hot upset regions pursue to shrink shorter than their original size, while the cold elastic regions pursue to obstruct the shrinking. When the temperature has settled by the HAZ there is a longitudinal tensile stress of the amount of yield strength. Elsewhere in the surroundings there is a compressive stress that keeps the part in balance. (Niemi & Kemppi, 1993, pp. 167–168.) According to Federal Highway Administration (2013, p. 40): "- - residual stresses are self-equilibrating, large compressive stresses at one location on a cross section are balanced by tensile stresses at another location."

The deformations that happen when heating an arc are explained using a small part of a ring (Figure 12). In Figure 13 the deformations of an arc that is heated with a torch in the outer rim are illustrated. With an arc, the heating process goes as explained above causing tensile stress to the HAZ and compressive stress elsewhere. When the outer element is heated it pursues to expand (Figure 13a) the inner element resist the expansion causing compressive stress to the outer element and tensile stress to the inner element (Figure 13b). The compressive stress in the outer rim and the happening upsetting from the outer rim's resist of the expansion causes the outer element to yield. As a result of the compressive yielding while cooling, the outer element shrinks in height and widens in width from its original dimensions (Figure 13c). Cooling causes tension on the outer rim and compression on the inner rim (Figure 13d). (Towfighi, 2011, pp. 37–39.) The same phenomenon that happens as an arc is heated can be applied to a whole ring. In the entire ring the geometry constraints only allow radial movement, so cooling of the ring results in an overall shrinkage (Mousivand, 2015).

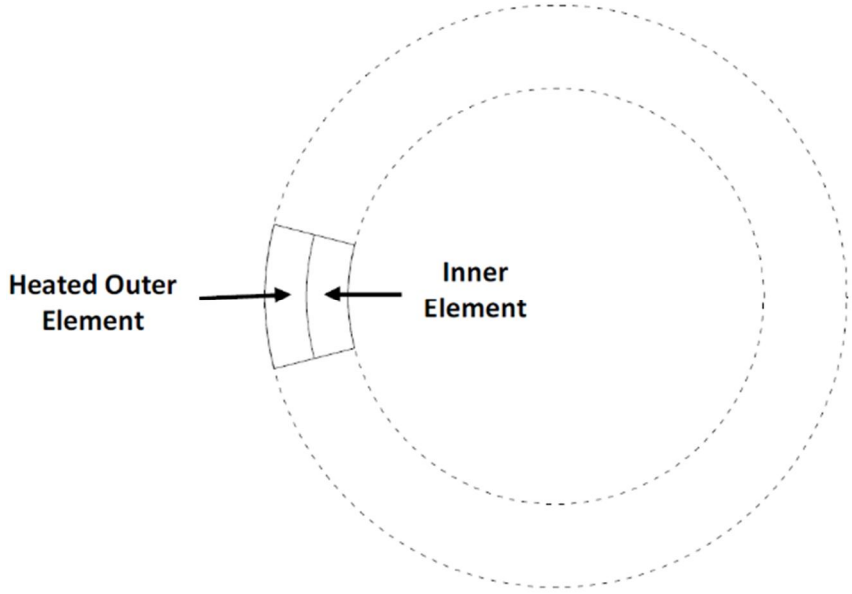

Figure 12. A small part of a ring (Towfighi, 2011, p. 37).

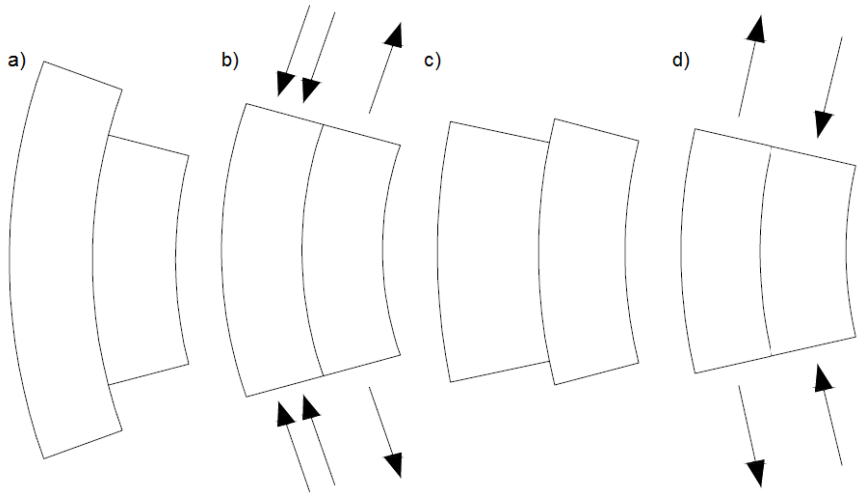

Figure 13. Heat affected changes in a small part of a ring, a) free expansion of the outer rim b) stress state during heating c) free contraction of the outer element d) stress state after cooling (Towfighi, 2011, pp. 38–39).

To achieve plastic deformations on the HAZ, the yield limit of the material has to be reached. The yield limit is slightly above the elastic limit. To reach the yield limit a force is needed to accumulate a stress in relation to the component contour. The stress build-up causes the flow process to exceed the elastic limit. These interconnections are illustrated with a stress-strain curve for mild steel in Figure 14. (Flame Straightening, 2013, p. 5.)

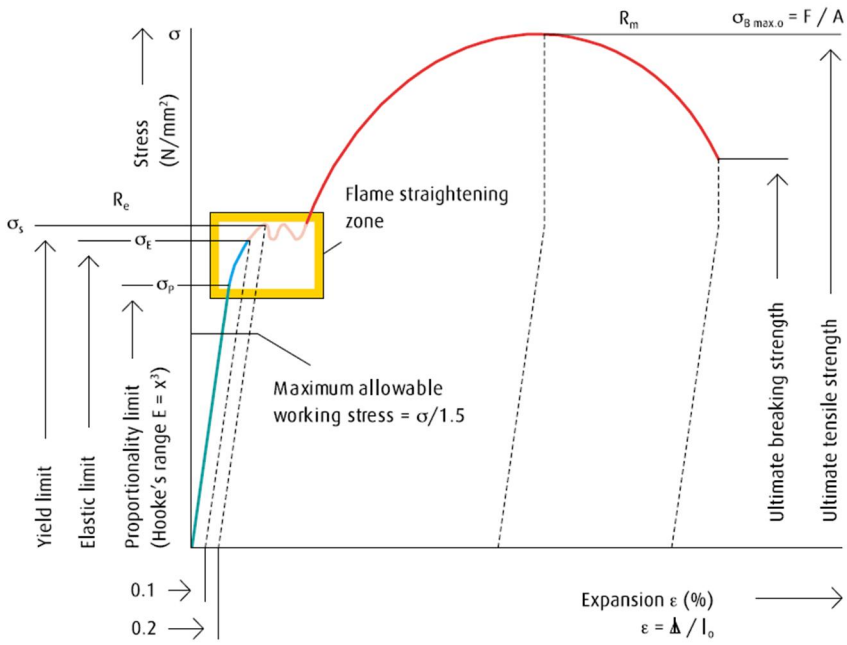

Figure 14. Stress-strain curve for mild steel (Flame Straightening, 2013, p. 5).

Components that do not distort after the welding joints have cooled down are exposed to larger residual stresses causing from shrinkage stresses not leading to deformations. During welding as well as flame heating, four shrinkage stresses occur that affect the deformations. These are longitudinal, transverse, thickness and angular shrinkages (Figure 15). (Flame Straightening, 2013, p. 6.)

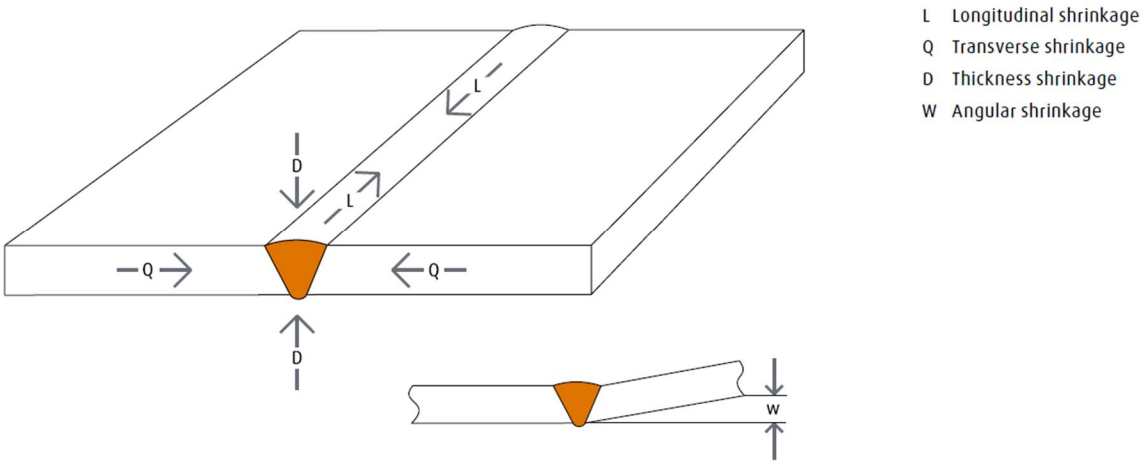

Figure 15. Types of shrinkage during welding (Flame Straightening, 2013, p. 6).

How materials behave during heat straightening depend on their properties and in particular their thermal expansion and thermal conductivity behavior. Materials with high

expansion coefficients expand more during heating. When this expansion is obstructed, the shrinkage is larger. (Flame Straightening, 2013, p. 7.) Thermal conductivity represents the materials ability to transfer heat. Materials with high thermal conductivity cool faster than materials with low thermal conductivity. With the case of heating a ring lower thermal conductivity is better. (Callister, 2007, p. 728.) Different materials also require different heat straightening temperatures (Flame Straightening, 2013, p. 10). Expansion behaviors of different materials can be found from Appendix I, the thermal conductivity of different materials from Appendix II and the heat straightening temperatures of different materials from Appendix III. The expansion coefficient α is 0.016–0.019 mm/mK and the corresponding shrinkage is 14 mm for stainless steel. The thermal conductivity k is 15.9 W/mK for stainless steel. The heat straightening temperature for stainless steel is 650–800 °C. If one compares these values to the fine-grain structural steel expansion coefficient of 0.012–0.015 mm/mK, shrinkage 10.2 mm and temperature 550–700 °C or to the 1025 steel thermal conductivity of 51.9 W/mK, for example, it can be stated that stainless steel provides better shrinking properties.

3.1.2 Heat flux

Heat straightening using a torch is still considered more of an art than a science because it is so dependent on the worker's experience (Federal Highway Administration, 2013, p. 1). Temperature has been identified as an important parameter in heat straightening. The temperature is also the most difficult parameter to control. (Federal Highway Administration, 2013, p. 19.) The main factors influencing temperature are according to Federal Highway Administration (2013, p. 19): "- - size and type of the torch orifice, intensity of the flame, speed of torch movement, and thickness and configuration of the member." Various methods are used to monitor temperature during heating, these are as stated by Federal Highway Administration (2013, p. 20): "- - visual observation of color of the steel - -; use of special temperature sensing crayons or pyrometers; and infrared electronic temperature sensing devices." The torch heat flux constructs of according to Federal Highway Administration (2013, p. 22): "- - the type of fuel, the number and size of the orifices, the fuel pressure and resulting heat output at the nozzle tip."

Federal Highway Administration (2013, p. 18) states: "The heat source is typically an oxygen-fuel mixture. Typical fuels include acetylene, propane, and natural gas." Acetylene

differs from slow-burning gases; propane and natural gas. The heat flux densities of these three fuel gases are illustrated in Figure 16, where λ is the oxidation ratio. The oxygen acetylene mixture has an intensive combustion that offers a much higher heat flux density than propane and natural gas as a fuel gas which can be seen from Figure 16. Thus the oxy-acetylene gas mixture is preferred by many. Raising the oxy-acetylene ratio increases the heat flux density even more. Figure 17 illustrates heat flux densities with different acetylene ratios. The optimum flame setting is consequently important in heat straightening. (Flame Straightening, 2013, p. 12.)

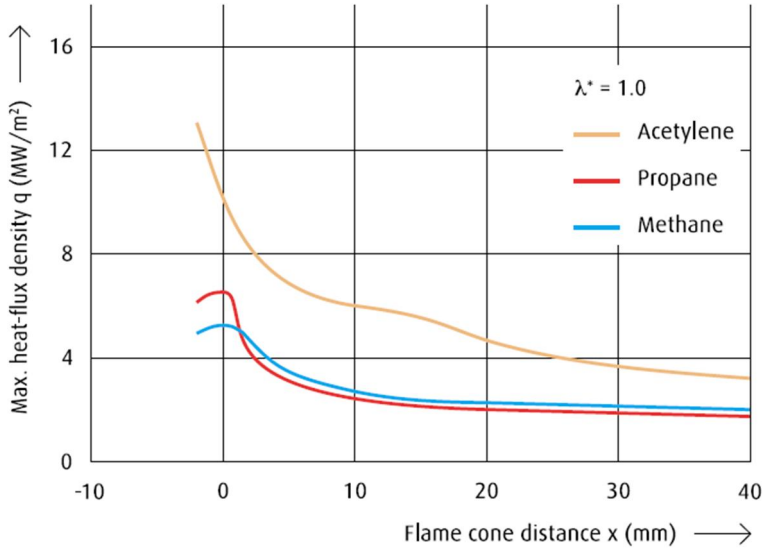

Figure 16. Heat flux density of different fuel gases (Flame Straightening, 2013, p. 13).

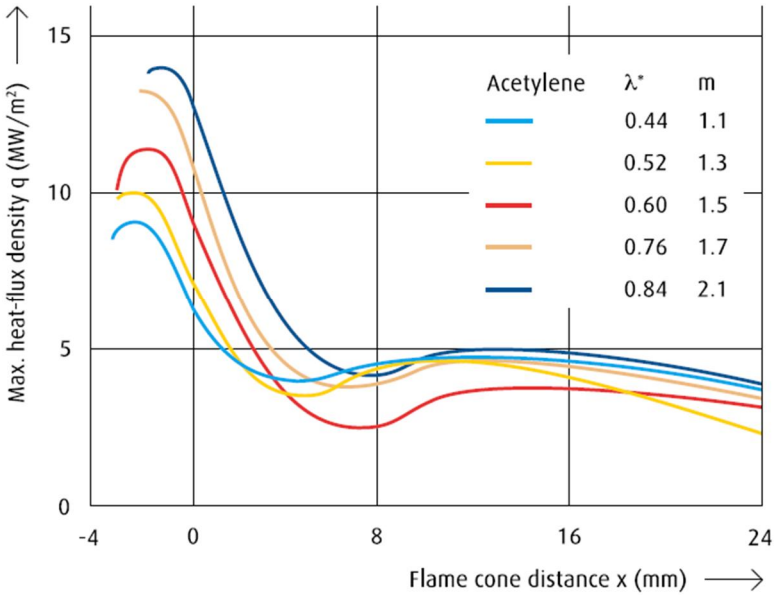

Figure 17. Heat flux density of acetylene (Flame Straightening, 2013, p. 13).

The classical torch used in heat straightening is an oxy-acetylene single flame torch. Other types of torches are also used in heat straightening such as the multi-flame torch and the multi-nozzle torch (Figure 18). (Flame Straightening, 2013, p. 14.) Sizing the heating torch/nozzle tips can be challenging because manufacturers mark tips by numbers that might have no relationship to bore size, material thickness or any other variable (Uccellini, 2003, p. 20). BOC Industrial Gases UK has characterized the suitable torch/nozzle sizes depending on the work piece thickness and on the material. Figure 19 illustrates their selection method of torches for heat straightening. For austenitic stainless steels that have low thermal conduction, the same nozzle size or one size smaller is used. As can be seen from Figure 19, for stainless steel of 4 mm thickness the nozzle size is thus 2–4 or 1–2. (Flame Straightening, 2013, p. 14.) The nozzle size indicates a nozzle with what the heat straightening can be accomplished. The goal of heat straightening is to bring the steel rapidly to the specified temperature through-out the thickness of the component. (Federal Highway Administration, 2013, p. 22.) Once this is achieved the torch is moved along a path with as described by Federal Highway Administration (2013, p. 22): "- - a rate that brings successive sections of steel to the specified temperature." Too small tip results in insufficient heat input and too large tip has a tendency to input heat quickly making the temperature and distortion difficult to control (Federal Highway Administration, 2013, p. 22).

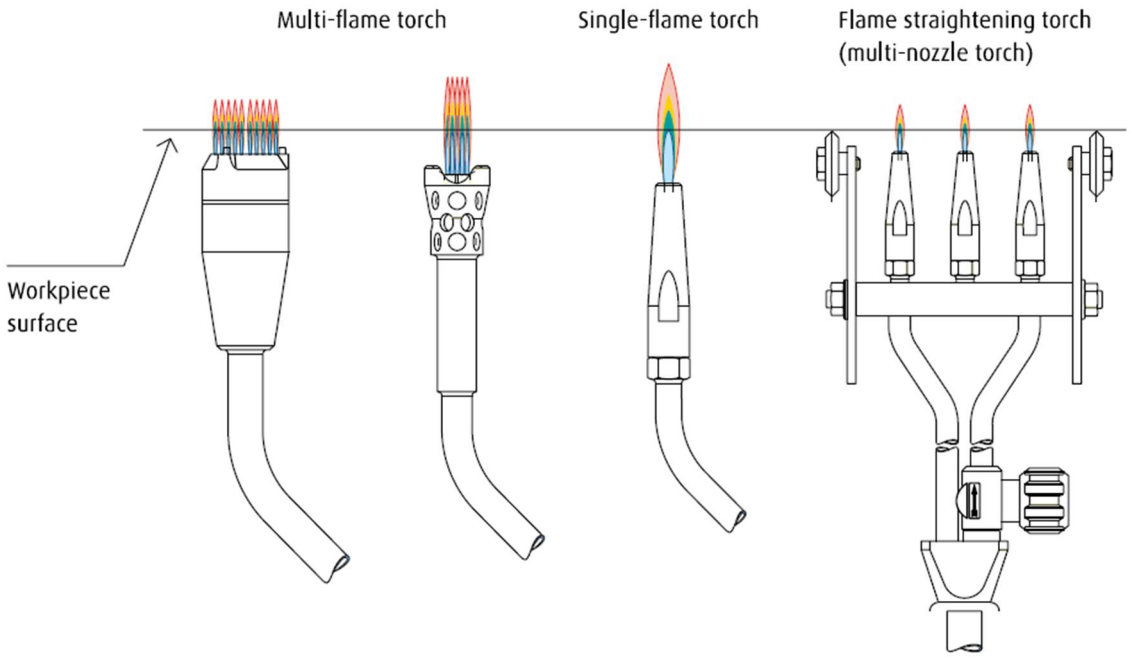

Figure 18. Torch types for heat straightening (Flame Straightening, 2013, p. 14).

Workpiece thickness			Nozzle size for flame straightening	Gas consumption	
Mild steel	Stainless steel	Aluminium and its alloys		Acetylene	Oxygen
mm	mm	mm		l/min	l/min
1–2	2–3	1–2	1–2	2.5	2.8
2–4	3–4	2–3	2–4	5.0	5.5
2–5	5–8	2–4	4–6	8.3	9.2
4–6	7–12	3–5	6–9	12.5	13.8
5–7	10–18	4–8	9–14	19.2	21.1
6–12	15–30	5–10	14–20	28.3	31.2
10–16	25–50	8–15	20–30	41.7	45.8
15–25	> 50	10–20	30–50	66.7	73.3
20–40	> 50	15–30	50–100	125.0	137.5
Multi-nozzle torch (3 nozzles)					
5–15	8–20	5–10	2–4	15.0	16.5
10–30	15–40	8–25	4–6	25.0	27.5
15–40	20–50	12–35	6–9	37.5	41.3
1–300	1–300	1–300	Specialised torch	2–333	2.2–366.3

Figure 19. One selection method of torches for heat straightening (Flame Straightening, 2013, p. 15).

The resulting heat output at the nozzle tip is given as a heat flux variable consists of the distance and angle between the torch and the heated surface as well as the intensity of the flame. The distance and the angle between the torch and surface of the ring impact significantly to the temperature profile on the surface. When heating an entire section of the component completely through, the flame cone should be somewhat standoff type (Figure 20, left). A contact flame (Figure 20, center) is used by experienced heat straighteners with the tip of the flame cone touching the heated surface. An impinging flame cone (Figure 20, right) is used when only the surface needs to be heated. With an impinging flame, the heat transfer is improved compared to the contact flame. The risk of surface damage is higher with impinging flame so it is necessary to work rapidly. (Flame Straightening, 2013, p. 16.)

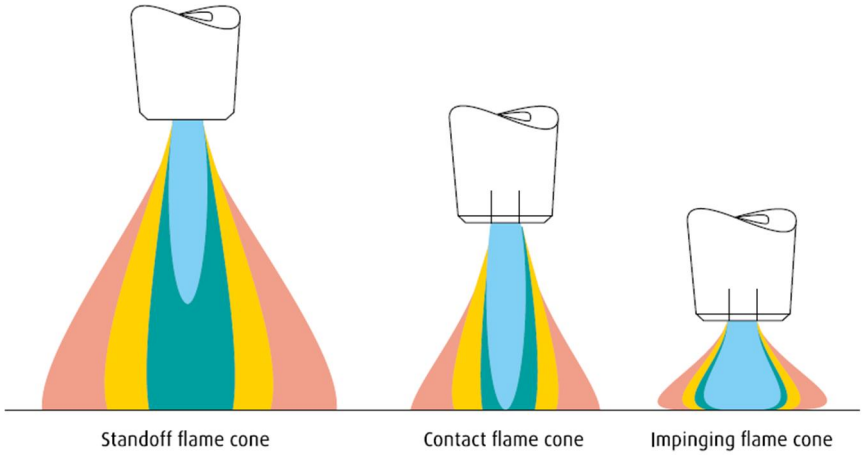

Figure 20. Flame cone distance and formation (Flame Straightening, 2013, p. 16).

In heat straightening there are three different flame settings that are used with the different distances between the nozzle and the heated surface. These flame settings are reducing flame, neutral flame and oxidizing flame (Figure 21). The flame setting and guidance selection guidelines for heat straightening are illustrated in Appendix IV. From Appendix IV can be seen that for stainless steel, a 50 % oxidizing flame usage with standoff flame cone is suggested. (Flame Straightening, 2013, p. 16.)

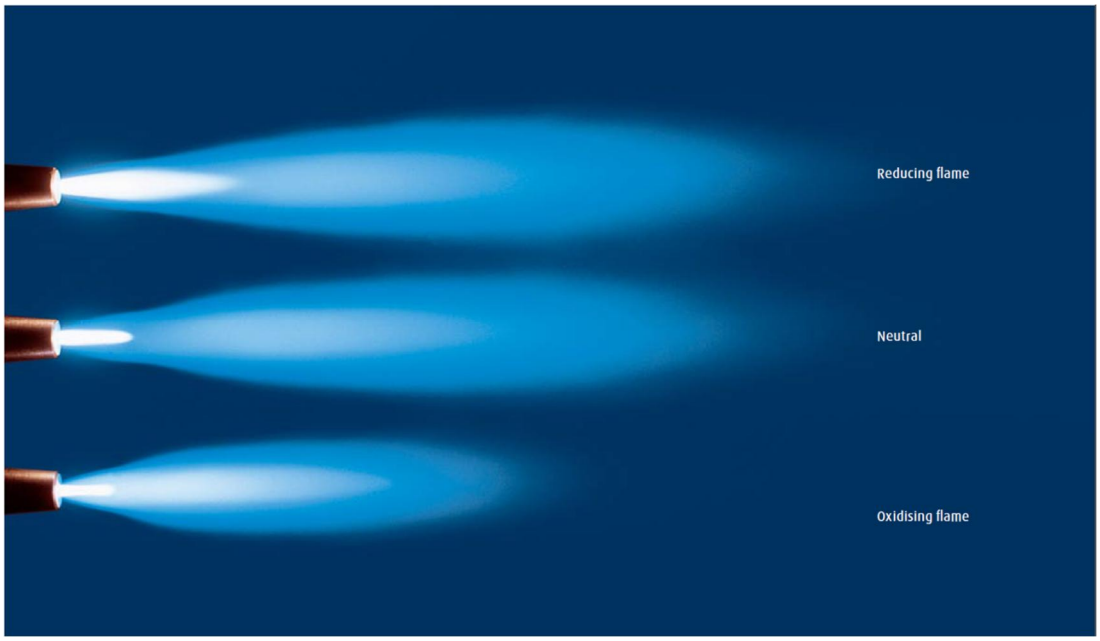

Figure 21. Three different flame settings (Flame Straightening, 2013, 17).

The rotation speed of the torch impacts the overall distortion. Effects of welding speed on the temperature distribution are illustrated in Appendix V. The faster the torch movement, the smaller the heat affected area. The target rotational speed is varied for each heating pass according to the needed shrinkage.

3.2 Manufacturing with heat

Working procedures for heating go the same as for heat straightening. Working procedures can be divided into steps; pre-measuring, determination of where to heat, restriction of thermal expansion, choosing the fuel gas and the torch, precise local heat build-up, upsetting by means of plastic deformation, allowing to shrink until ambient temperature is reached and measuring of plastic deformations. Precise local heat build-up is more effective when it is performed with several small heating patterns than one large figure. It

is essential to allow the component to shrink until ambient temperature or temperature balance between HAZ and adjacent structure is reached. The success of the heating operation can only be measured after the component has cooled down. (Flame Straightening, 2013, p. 29.)

Heating of the support rings in a screen cylinder may be done by applying controlled heat in different sequences with repetitive heating and cooling cycles to get the desired diameter and roundness. So the most important requirement for the ring under study is that the ring should be as round as possible and the deformations should only occur as overall shrinkage in the ring diameter.

Heating a ring as explained above was in an ideal situation where any out of plane deformations were ignored. There are two distinct ways buckling may happen in a heated ring: vertical (Figure 22) and radial (Figure 23). In radial buckling, the ring's outer regions experience tension and inner regions compression (Figure 24) which is contrary to the stress state in ideal situation discussed above. Buckling allows the ring to maintain the expanded length acquired during heating causing less compressive yielding. (Towfighi, 2011, p. 44–46.)

Figure 22. Vertical out of plane buckling (Towfighi, 2011, p. 44).

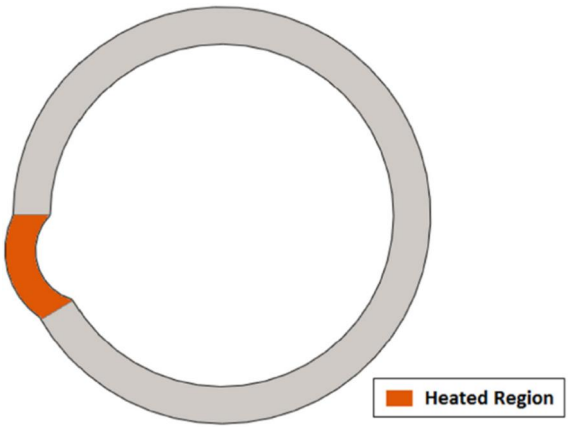

Figure 23. Radial out of plane buckling (Towfighi, 2011, p. 44).

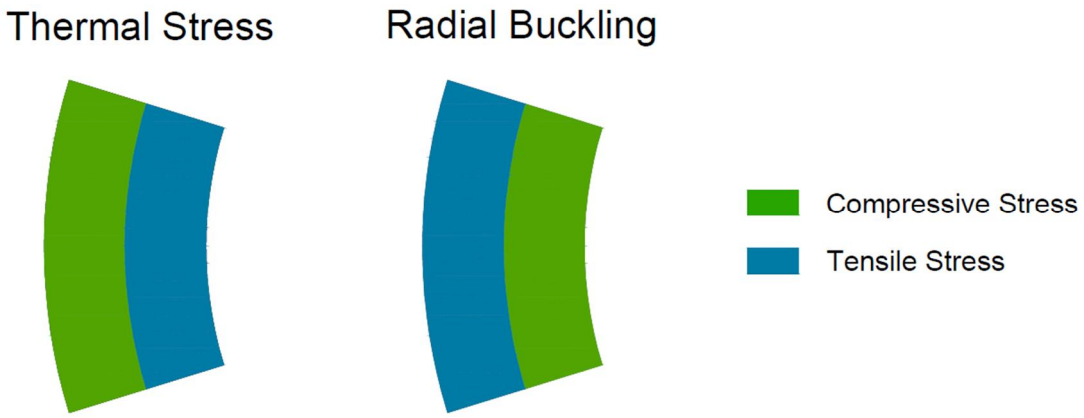

Figure 24. Stress states in ideal thermal stress situation and in radial buckling (Towfighi, 2011, p. 47).

The three main factors that influence the deformations in a ring have been identified as the heating sequence, torch heat flux and the dimensions of the ring. An optimum heating sequence maximizes the shrinkage in ring diameter and minimizes any other distortions like buckling. Torch heating can be performed with single heating, multiple-torch heating (progressive, back-stepping and jump-heating) as well as multiple-cycle heating. Single heating, multiple-cycle heating and ring structure are examined next.

3.2.1 Single heating

Teng, Chang and Tseng (2003, p. 273) analyzed the residual stresses in circular patch welds. The welding sequences they used in circular patch welds are illustrated in Figure 25. From the results conclusions were made: 1) Teng et al. (2003, p. 285) states: “In circumferential residual stress - -, the weldment has a uniform tensile stress field in the patch’s central region, and then decreases to compressive, finally becoming zero as distance from the weld bead.” The circumferential residual stress distribution is illustrated in Figure 26. 2) Teng et al. (2003, p. 285) states: “In radial residual stress - -, the weldment has a uniform tensile stress field in the patch’s central region, and the residual stresses do not markedly differ away from the weld bead.” The radial residual stress distribution is illustrated in Figure 27. 3) Between various weld sequences the circumferential stresses do not significantly differ (Teng et al., 2003, p. 283). 4) Teng et al. (2003, pp. 283–284) states: “The radial residual stress σ_r, of the backstep welding is smaller than the other welding sequences because the post-weld heat treatment and preheating effect in backstep welding are better than the other welding sequences.”

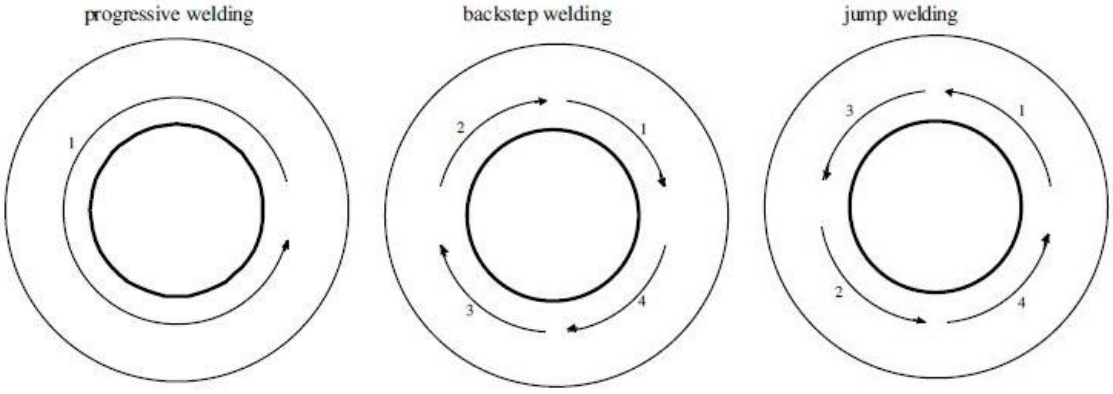

Figure 25. The welding sequence in circular patch welds (Teng et al., 2003, p. 285).

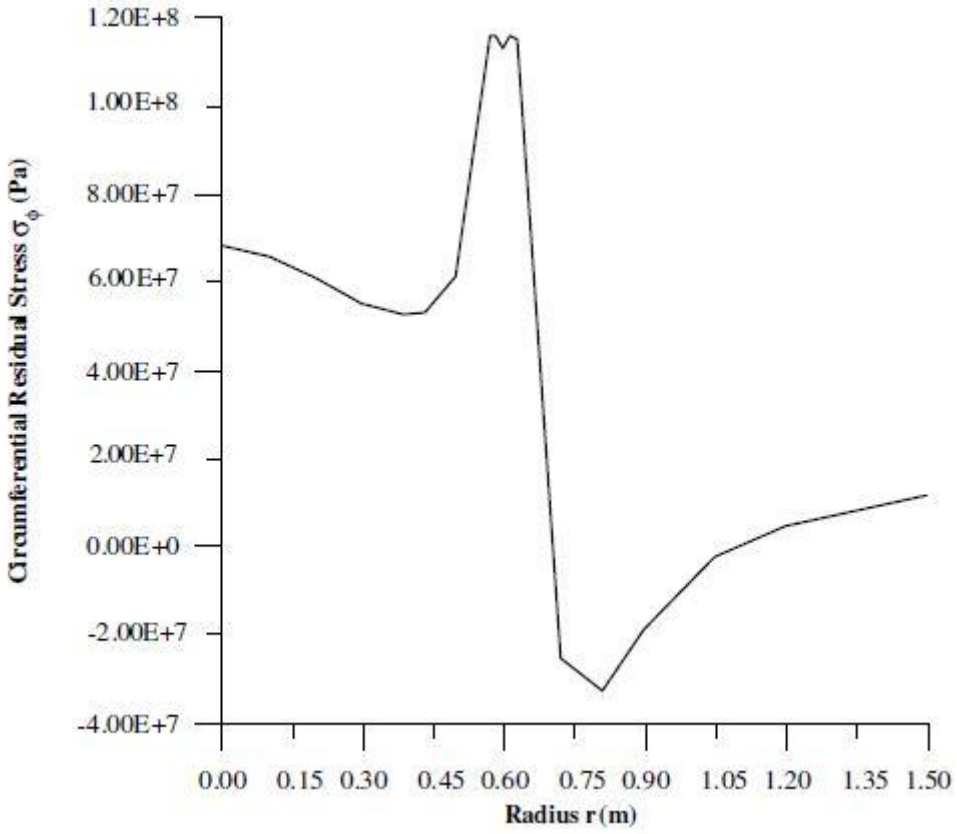

Figure 26. Circumferential residual stress distribution (Teng et al., 2003, p. 285).

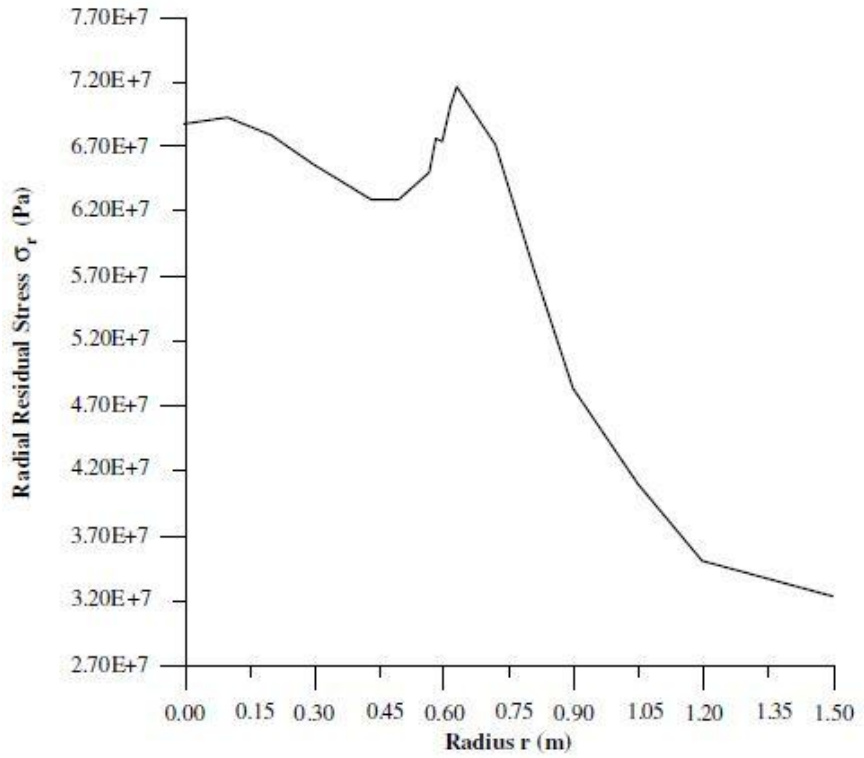

Figure 27. Radial residual stress distribution (Teng et al., 2003, p. 285).

Zeng, Wang, Du and Li (2010, p. 543) studied: "- - the residual stresses and distortion on fillet welds of aluminum cylinder structure in the discontinuous welding." Figure 28 illustrates residual stresses caused by discontinuous welding. They came to conclusions; discontinuous welding increases the residual stresses and decreases the distortions as well as the temperature gradient through thickness generates angular distortion. In the case of the cylinder ring, the temperature gradient through thickness is assumed to be small to minimize out of plane distortion. (Zeng et al., 2010, p. 543.)

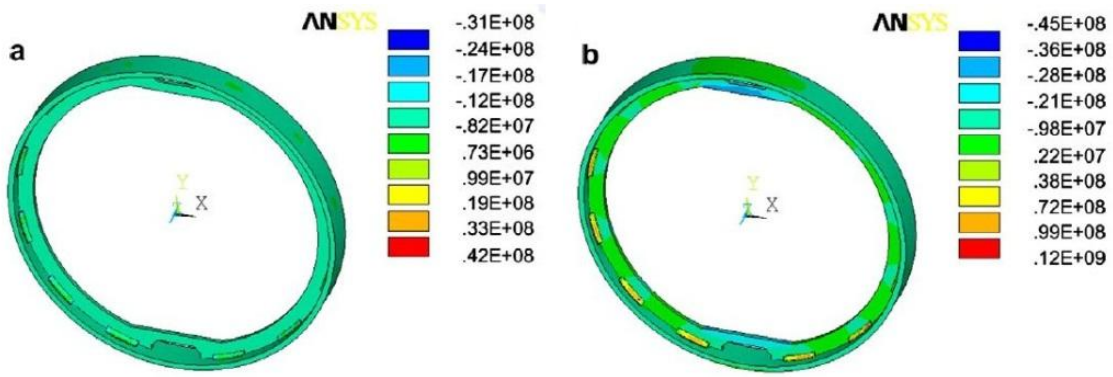

Figure 28. Residual stresses in discontinuous welding (a) radial stress and (b) circumferential stress (Zeng et al., 2010, p. 537).

Teng, Chang and Ko (2000, p. 650) studied the distribution of residual stresses in circular patch welds. The following conclusions were made: 1) Teng et al. (2000, p. 650) states: "- - the weld line experiences shrinkage. This leads to a circumferential residual stress close to the material's yield strength." 2) Teng et al. (2000, p. 650) states: "In the center of the patch is a region where residual circumferential and radial stresses are similar." 3) Teng et al. (2000, p. 650) states: "If the patch size is smaller, there is a higher residual stress in the patch center."

The natural shrinkage strains caused by heating are uniform along the weld length, except for the starting and ending points (Feng, 2005, p. 7). Peak temperature has a key role in the final shrinkage. With modified torch speed, a gradual increase of heat flux through the course of heating can be accomplished to provide a more uniform shrinkage. Heating a ring with a faster speed before the actual starting point will help with getting the peak temperature to become stable from the starting point on. Heating with a faster speed over the ending point also aids in getting the temperature to rise in the start/end region.

3.2.2 Multiple cycle heating

In heat straightening according to Federal Highway Administration (2013, p. 23) "- - re-heating before the material has cooled interrupts the contraction process." This is why the heating and cooling of support rings are done in turns. Repeated heating and cooling cycles increases ring shrinkage (Towfighi, 2011, p. 35). The heating cycle's purpose in manufacturing is to get the ring as near to the wanted dimensions with as few heating times as possible.

Deng and Kiyoshima (2010, p. 620) researched the start/end region offset and the pass location offset procedures in a girth-welded SUS304 pipe. Figure 29 illustrates the weld start/end positions and welding direction of each pass. Figure 30 shows the weld pass locations in the groove they studied. The results of Deng and Kiyoshima (2010, p. 621) were: "- - the hoop and axial stresses sharply change with central angle - -. - - both the maximum tensile axial stress and the maximum tensile hoop stress appear near the location with 350° central angle. Both the hoop and axial stresses strongly varies with weld pass. - - final weld pass has a largest contribution to the final residual stress distribution."

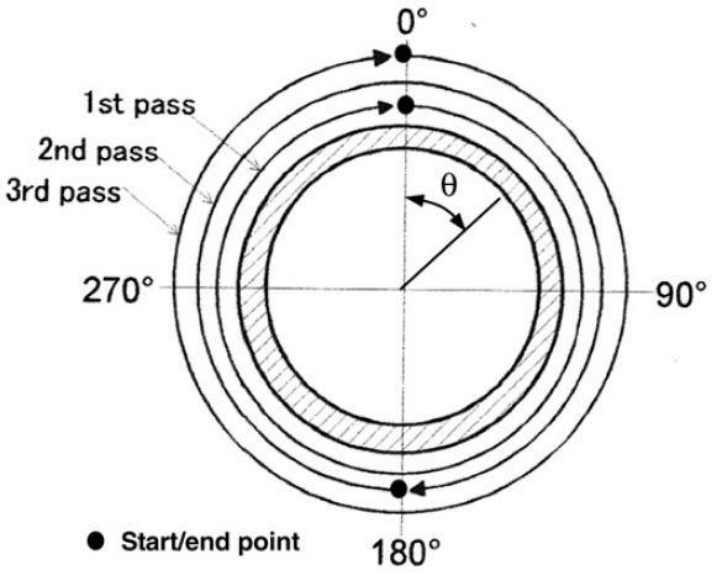

Figure 29. The weld start/end positions and welding direction of each pass (Deng & Kiyoshima, 2010, p. 613).

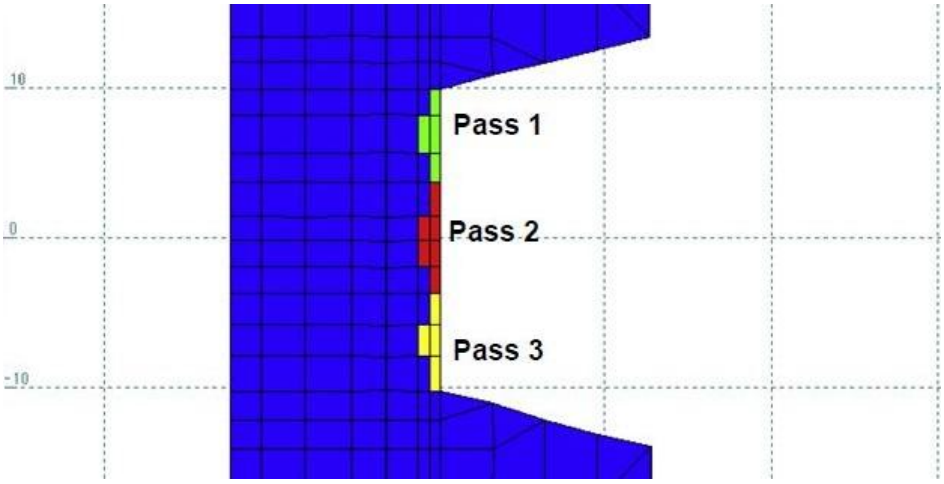

Figure 30. The welding pass locations in the studied groove (Deng & Kiyoshima, 2010, p. 614).

A significant problem with one weld pass, which is comparable to single progressive heating, is the uneven residual stress distribution in start/end region. The finite element model of the pipe and the definition of middle section are illustrated in Appendix VI. Figure 31 illustrates the final hoop stress distribution of the middle section. (Deng & Kiyoshima, 2010, p. 618.) This problem can be solved with dividing the start/end regions in different locations of the ring in multiple heating. Higher temperatures aggravate the out of plane buckling. With multiple heating cycles the heat flux, the temperature and the

speed of the torch can be chosen for each cycle so that out of plane buckling is prevented still reaching wanted dimensions. Heating from both sides of the ring should be considered, thus it also prevents out of plane buckling.

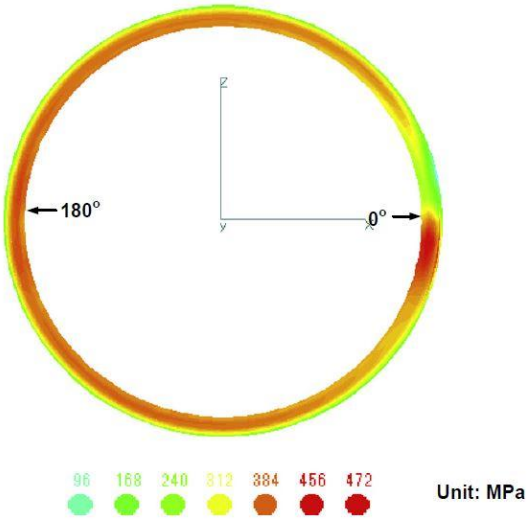

Figure 31. Final hoop stress distribution of the middle section (Deng & Kiyoshima, 2010, p. 619).

3.2.3 Ring structure

The ring structure will naturally affect the heat induced shrinkage. The affecting factors are assumed to be: the diameter of the ring, thickness of the ring, height of the ring and number of wires. To ensure the needed clamping force between the notches in the rings and the wires, the rings must be shrunk by a certain percentage.

It is assumed, without any supporting data or analysis, that in heating the rings with a torch the heat affected zone is on the surface and the effective depth of penetration is small. If this is true, the inside of the ring will not be affected by the heat so much as the surface and will obstruct expansion, causing upsetting in a way. Because of the upsetting, the ring would contract to a smaller diameter. The same would happen with the ring height also, when the height is bigger there are more cool regions obstructing the expansion. The ring height may also affect the variations in heating location along ring height in multiple-cycle heating with an offset; with smaller ring heights the cool parts have to be left to obstruct expansion so no need to change the heating location and with bigger heights there can be multiple different heating locations.

As the thickness and height of the ring affect the shrinkage by obstructing the expansion so does the wires. All these factors may also decrease the out of plane deformation. The number of wires and the associated wire width and slot width were discussed in Chapter 2.1. Wire width and slot width in their cooperative action affect the amount of constructing wires in a ring. When the studied structure consists of multiple heated rings also the effects of the spacing between adjacent rings should be studied because the wires connect the rings as one structure.

4 MEASUREMENT, REDUCTION AND REMOVAL OF DEFORMATION

The direct measurement of the deformations in the kind of ring talked about presents challenges due to small wire sizes and complex interface between wires and the ring. Factors such as manufacturing situations and fluctuations in the torch power can compromise the accuracy, precision and repeatability of measurements.

The goal of the shrinking process with heating the rings is to attain a strong hold between the wires and ring. In one ring there can be depending on the ring diameter 400–1000 wire ring connections. In this thesis direct measurement of that joint is not done, but it can be characterized with average ring shrinkage, roundness of the ring and buckling of the ring. It has been studied and stated that if a certain percentage shrinkage is attained the clamping force between wires and ring is accomplished. This requires that the roundness of the ring is as good as possible to guarantee equal clamping force to each wire and the deformations are directed toward shrinkage in the diameter instead of buckling.

Carrolo (2010, p. 1) studied different reduction and removal methods to decrease the distortions caused by a welding process in a water jacket production at Carr's Welding Technologies. He game to the end result that forging did not produce any measurable results, clamping alone was not very effective, pre-bending was effective in reducing the distortions and the best option was to combine pre-bending and clamping. (Carrolo, 2010, s. 9.) In this study the goal is to obtain deformations and control them so the result is as uniform as possible. In this case pre-bending doesn't really work but with clamping the ring expansion may be further prevented which increases the shrinkage. Clamping should be considered, however the execution might be problematic cause of the heating is done circling around the whole ring.

The out of plane buckling is quite under control because the affecting factors have been identified during manufacturing. The affecting factors are as discussed before the amount of cool structures and the temperature not being too high. Still the rings need to be inspected to ensure the best screening ability possible.

5 MODELING

Welding residual stresses and deformations analyses using finite elements in space and time, simulating thermal and mechanical material and component behavior during welding, remain still insoluble. These following features of the finite element analyses help understand the difficulty and effort involved:

1) The model ought to be designed three-dimensionally to project accordingly the cooling conditions.
2) The process is transient, with position and time dependent field gradients caused by the rapid heating-up and cooling-down events.
3) The process is non-linear and temperature-dependent.
4) Local material behavior is dependent on the stress and strain prehistory.
5) Changes in state and microstructure.
6) Defects and cracks make the continuum concept doubtful.

The features presented above affiliate only to simulating the complex reality with the maximum possible detail. The features don't apply if the problem is reduced to its central issue and only the influencing parameters are presented in the finite element model. (Radaj, 1992, pp. 148–149.)

Simplifications to the above mentioned features may be:

1) Reduction of the three-dimensional model to a two-dimensional or to a one-dimensional model.
2) Simplification of geometry, support and load conditions.
3) Symmetrization or periodization of the model.
4) Reduction of the non-linear thermoelastic-viscoplastic model to a linear thermoelastic model.
5) Reduction of the transient process to a quasi-stationary process.
6) Decoupling of the thermal and mechanical processes.
7) Ignoring defect or crack formation.
8) Omitting the fusion, solidification and transformation processes.
9) Registering the transformation at lower temperature only globally.
10) Ignoring creep and hardening as well as introducing simplifications in yield laws.

11) Simplification of groove shape and layers structure.
12) Replacement of heat source movement by momentary application of total heat quantity.
13) Replacement of the temperature-dependent material characteristic values by temperature-constant averaged values.
14) Modelling of the formation of residual stresses as a pure cooling process.

The simplifications depend on the questions posed to the central issue. The situation in practice is facilitated by the fact that analyses are primarily expected to provide relative statements to specific problems. The number of parameter combinations and process variants is almost unlimited in practice. Finite element analysis can be performed only for a very limited number of cases if the expenditure is limited. (Radaj, 1992, s. 149–151.)

Simplifications had to be used to the model made for studying the deformations on a ring due to heating with a torch. Next the models used by Towfighi (2011) and Mousivand (2015) are examined more detailed as well as the model used constructing the studies in this thesis.

5.1 Model developments

Towfighi (2011, p. ii) created a finite element model using LS-DYNA and C++ code to examine plastic deformations in AISI 304L rings after welding. Towfighi (2011, p. 28) captured the deformational effects, bending, buckling and high temperature gradients, with a three-dimensional nonlinear transient thermo-structural model. Material parameters to the model were acquired from compression tests using a Gleeble 3500 testing machine. Compression tests were done ranging the temperature from 20 °C to 1227 °C and loading at low strain rates. The Gleeble 3500 test machine was used to determine true stress-strain curves in elevated temperatures. (Towfighi, 2011, p. 14.) The low strain rates were used to make the material response curves suitable for deformations caused by heating and constraining a structure (Towfighi, 2011, p. 25).

The results got from the compression tests were compared to the coefficient of thermal expansion and modulus of elasticity found from literature. The results, the coefficient of thermal expansion and modulus of elasticity were observed to be in reasonable agreement. The material’s yield strength acquired from the tests differed significantly compared to the

values found from literature. (Towfighi, 2011, p. 25.) Towfighi (2011, p. 21) states that the experimental yield strength seems more reliable and is used in the model. With a bilinear model of the stress-strain curves were approximated to ease the input of material properties to the finite element modeling software. The approximation was constructed with the modulus of elasticity, the yield strength and the tangent modulus. Sample bilinear model and the true stress-strain curve are illustrated in Figure 32. (Towfighi, 2011, p. 21.) The material properties with incorporated experimental properties are illustrated in Figure 33 (Towfighi, 2011, p. 29).

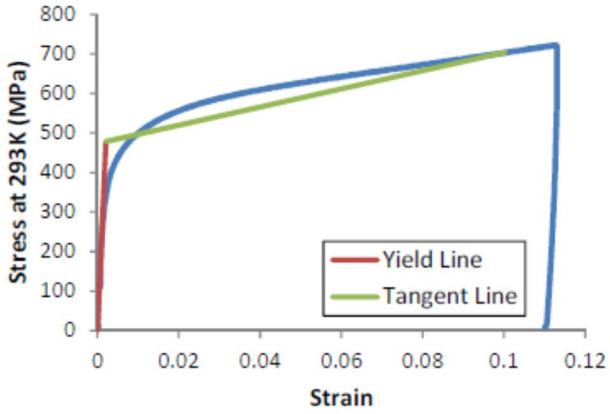

Figure 32. Sample bilinear model (red and green) and true stress-strain curve (blue) at 20 °C (Towfighi, 2011, p. 22).

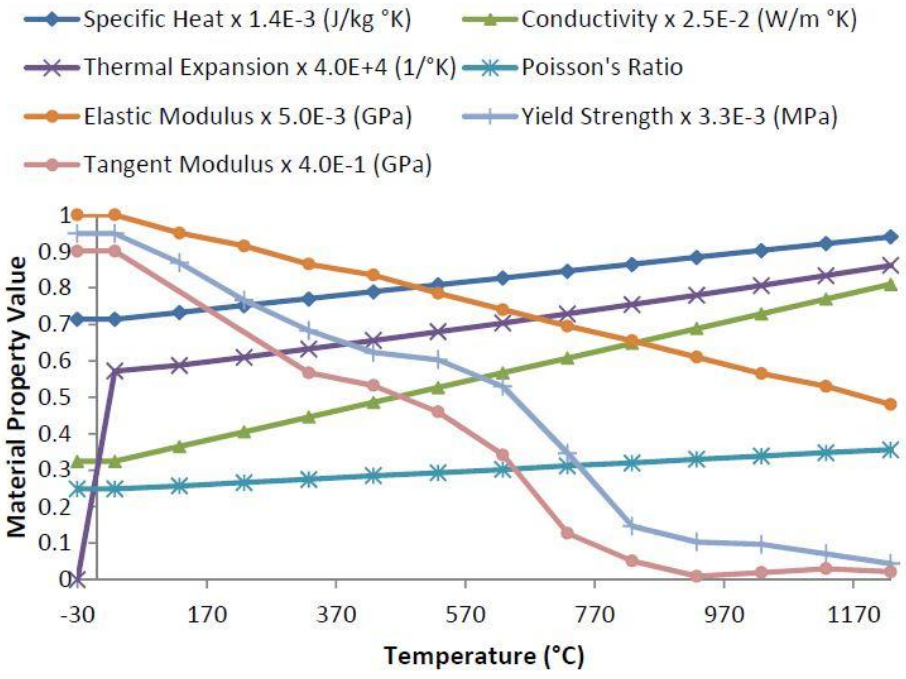

Figure 33. Material properties of AISI 304L stainless steel (Towfighi, 2011, p. 29).

Convection and radiation cooling boundary conditions were incorporated into the model. The convection coefficients for a plate surface in air with different orientations are presented in Figure 34 assuming an ambient temperature of 27 °C. Surfaces that were not completely vertical or horizontal were assumed to be vertical for convection. (Towfighi, 2011, p. 29.) Towfighi (2011, p. 29) described: “Radiation cooling was applied using an emissivity of 0.17.”

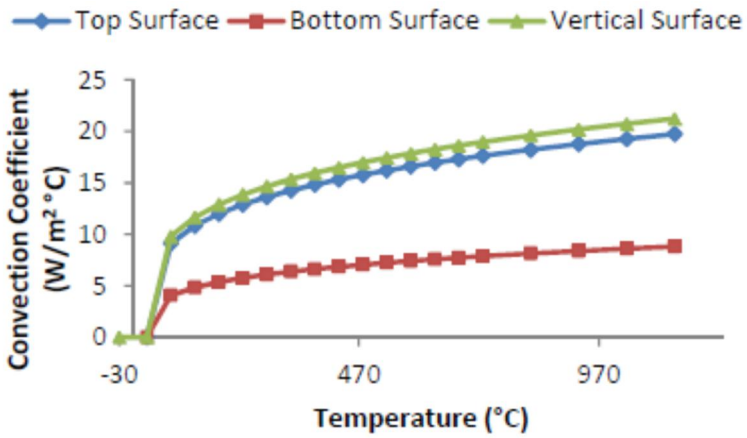

Figure 34. Convection coefficients for surfaces of a plate in air (Towfighi, 2011, p. 30).

Pavelic et al. (1969, p. 295) found in their study a practical method of predicting the temperature distribution in welding. A disk model was introduced to replace the earlier simplified model with a line or point heat source (Pavelic et al., 1969, p. 295). This new disk model was more realistic for it distributed the heat input over a source area (Goldak & Akhlaghi, 2005, p. 25). Goldak and Akhlaghi (2005, p. 25) states: “- - for a preheat torch that causes no melting this may be a very accurate model indeed.” Goldak and Akhlaghi (2005, p. 30) specifies the previous statement: “For welding situations, where the effective depth of penetration is small, the surface heat model - - has been quite successful.” The preheat torch can be compared to the heating method of the studied rings which make the disk model suitable for studying the heating of a ring. If the source is normal and circular, the distribution of specific heat flux may be approximated by (Pavelic et al., 1969, p. 300):

$$q(r) = q(0)e^{-Cr^2}, \quad (1)$$

where *q(r)* is surface flux at radius, *q(0)* is maximum flux at the center of the heat source, *C* is distribution width coefficient and *r* is radial distance from the center of the heat source (Figure 35). The coefficient *C* is determined by the heat distribution on the heated surface

as can be seen from the Figure 35, therefore it's related to the heat source width. (Goldak & Akhlaghi, 2005, p. 26–27.)

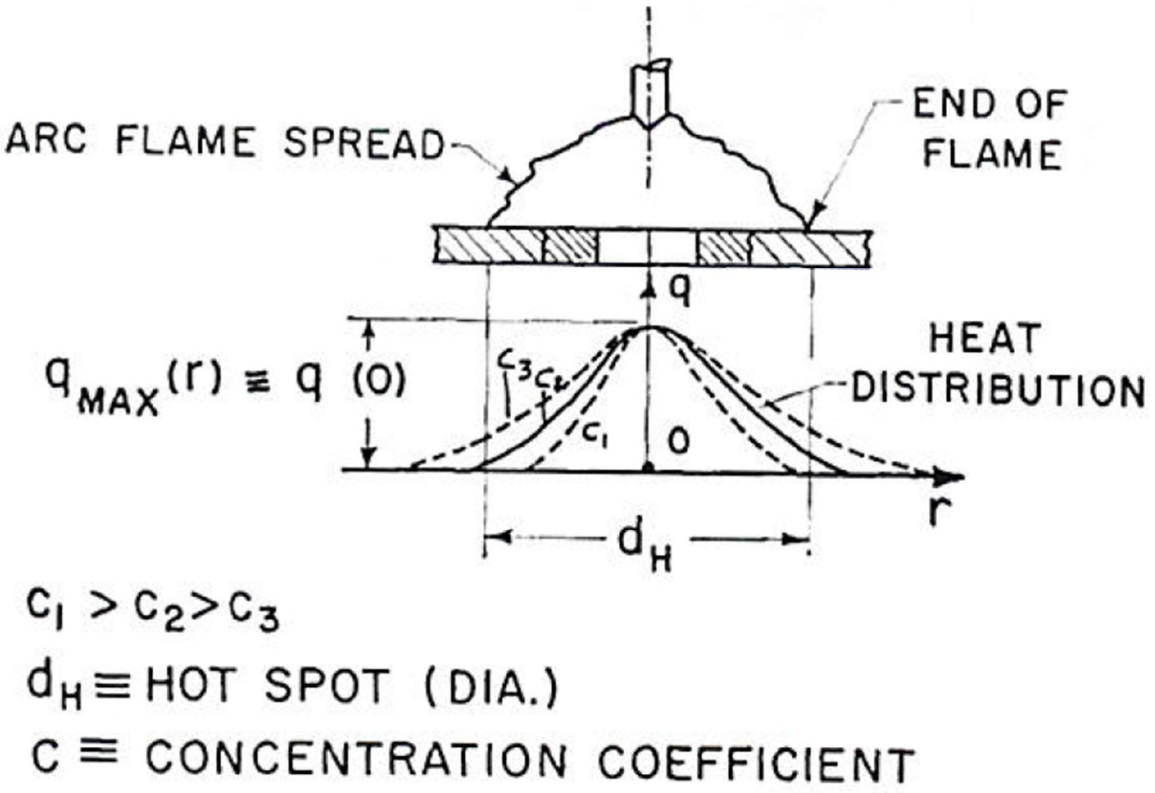

Figure 35. Normal circular heat source (Pavelic et al., 1969, p. 300).

Friedman (1975) and Krutz and Segerlind (1978) gave a different form to the disk model of Pavelic et al. (1969) suggesting it to be a function of location and time. The heat source in a coordinate system that moves takes the form:

$$q(x_m, \xi) = \frac{3Q}{\pi c^2} e^{-3x_m^2/c^2} e^{-3\xi^2/c^2}, \quad (2)$$

where Q is energy input rate and c is the characteristic radius of heat flux distribution. (Goldak & Akhlaghi, 2005, p. 28.) With (x_m, ξ) the moving coordinate system is presented (Goldak & Akhlaghi, 2005, p. 29). The equation for this flux distribution used in modeling the torch heating of a screen cylinder support ring can be written as:

$$q(x, y) = \frac{3Q}{\pi c^2} e^{-3(x-x_0)^2/c^2} e^{-3(y-y_0)^2/c^2}, \quad (3)$$

where x_0 and y_0 are the coordinates for the center of the torch (Towfighi, 2011, p. 30).

Towfighi (2011, p. 30) used a C++ code to apply the Gaussian heat flux value, discussed above, to each element exposed to the torch in his model. From the model, the temperature

profile was generated to represent the torch heat input. Another temperature profile was generated from testing AISI 304L stainless steel plates heated with an oxy-acetylene torch. From the test the temperature was measured with K-type thermocouples. (Towfighi, 2011, pp. 30–31.) Towfighi (2011, pp. 35–36) states that the temperature profiles acquired from experiments and simulations were in reasonable agreement.

Towfighi (2011, p. 47) added discrete nonlinear elastic spring elements to his model to represent the restraints produced by the wires. With spring elements he wanted to avoid adding remarkable amount of additional solid elements to the model. He performed a thermo-structural finite element simulation for a longitudinal strip that illustrated a wire. From these results the force displacement behavior was determined. (Towfighi, 2011, p. 47.)

The model Towfighi created has since been modified further in a thesis that is still under work. The LS-DYNA model was found deficient with resulting excessive out of plane buckling after cooling that isn't realistic. To improve the accuracy of the model it was transferred to Abaqus. Figure 36 illustrates the difference between deformed shapes of two identical models (the same geometry, material properties, loading and boundary conditions) made using Abaqus and LS-DYNA softwares. Abaqus provided more uniform structural elements that model stress concentrations more accurately. (Mousivand, 2015.)

Figure 36. Deformed shape of rings after heating in LS-DYNA (red) and Abaqus (blue) (Mousivand, 2015).

Towfighi (2011) modeled the wires as springs in a Cartesian coordinate system with one end of the springs attached to the node nearest inside the ring and other end fixed on the ground (Figure 37). The buckling that occurred with the LS-DYNA model was at least partially caused by a small out of plane force due to the reaction force in z-direction not being constrained. To get more accurate results a connector element that models the wire force resembling a beam element. Each wire is assigned at its center to an independent

cylindrical coordination system where the reaction force in z-direction is modeled as friction (Figure 38). (Mousivand, 2015.)

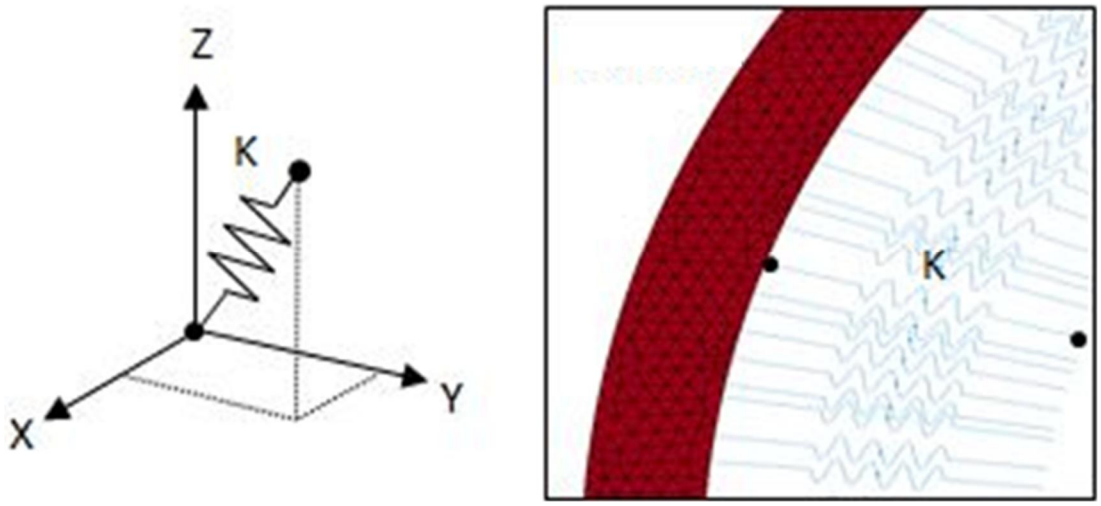

Figure 37. Wire forces in LS-DYNA model (Mousivand, 2015).

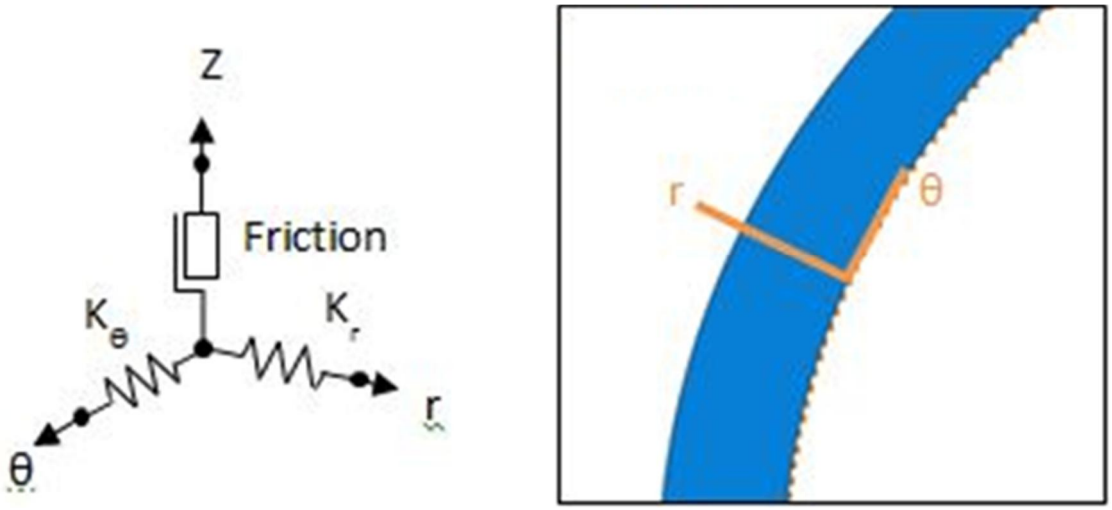

Figure 38. Wire forces in Abaqus model (Mousivand, 2015).

In Abaqus, the modeling is done as a sequential thermal-displacement model so the heat transfer analysis is done separately from the displacement and stress analysis. The main idea behind sequential modeling technique is to incorporate the independently gathered temperature field to the stress/deformation field. This modeling way saves time in error diagnosis as the decoupling thermal and displacement models are done separately and allows the thermal analysis to be done with independent time increment that is then interpolated to the displacement analysis. (Mousivand, 2015.)

The meshing is improved in the Abaqus model compared to the LS-DYNA model. In Abaqus model more uniform structural elements are used that improve the accuracy significantly compared to the triangular elements used in LS-DYNA model. Towfighi (2011) used C++ to apply the Gaussian heat flux value to each element with Abaqus Fortran was deployed for the same purpose. (Mousivand, 2015.)

5.2 Own model contributions

The modified Towfighi's model is transferred to a Python code. The Python code enabled certain factors to be modified easily without having to otherwise construct the model again from scratch. These easily varied factors for the Python code are the location of the wires (inside or outside), the heated surface (one side or both), the diameter of the ring, the height of the ring, the thickness of the ring and the number of wires.

The Fortran code used to apply the Gaussian heat flux value to each element was modified by the same mentality as the Abaqus model to enable certain factors to be modified easily. Two modified Fortran codes were made to conduct the studies: one with only one heating cycle and a Fortran code with three heating cycles. In Fortran code the same factors are the amount of heating cycles (one or three), the Gaussian heat flux parameters (energy input rate and the characteristic radius of heat flux distribution), the heating speed, the speed for the speeded portions, the angle for the speeded portions, the location of the heated region along ring height and the location of starting point.

Some of the values are assumed constant and so they are the same in every model. The heating is modeled to the top surface of the ring. The heating is assumed to be done with an oxy-acetylene torch thus the constant values that represent the heat flux influenced by the torch are the energy input rate Q 5500 W and characteristic radius of heat flux distribution c 50 mm (Mousivand, 2015).

Default values are defined to the Fortran code and to the Python code to ease conducting the studies and comparing the results. These default values are:

- Ring diameter: 646 mm
- Ring height: 30 mm
- Ring thickness: 4 mm

- Number of wires: 525
- The wires are located on the outer rim of the ring
- Heating speed: 0,1 °/s
- Location of the heated region along ring height 0,1*height calculated from the outer rim
- Location of the starting point 0°

The default factors are varied according to different studied cases. With varying factors, the effects of the heating on the shrinkage and its uniformity can be studied.

6 STUDIED CASES AND RESULTS

A variety of different cases are chosen to be studied with the model constructed. The studied cases provide directional knowledge about the effects of these studied variables on the shrinkage and its distribution. The studied cases illustrated in Figure 39 can be divided into three main categories; torch flux (speed, speeded start/end), location of the wires, heating location (variation along ring height) and structural factors (diameter, height, thickness, number of wires).

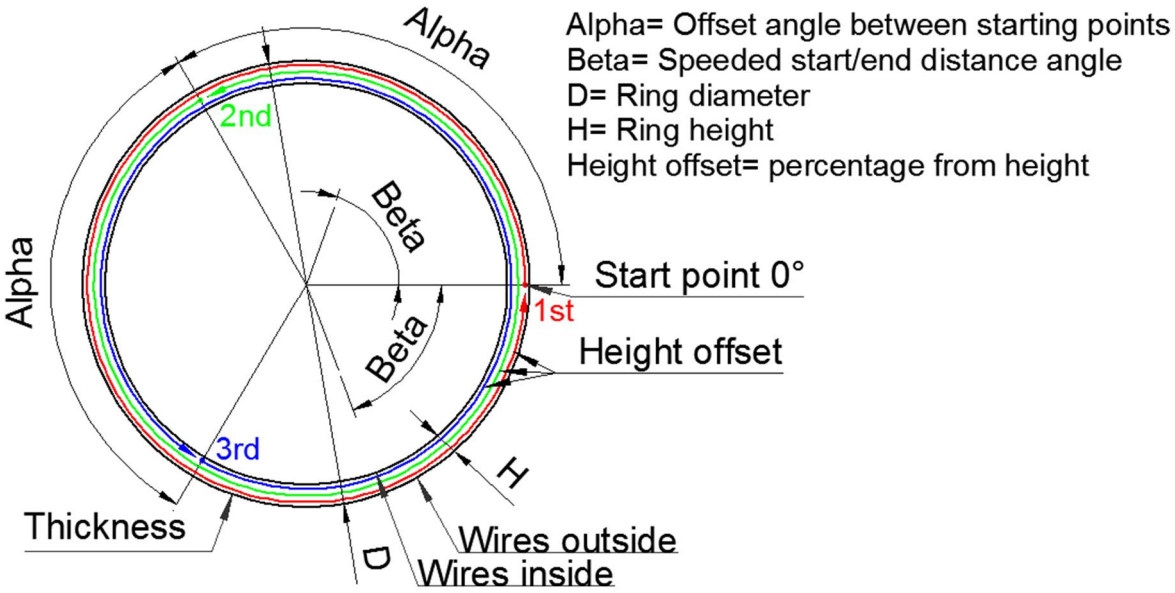

Figure 39. Studied cases.

6.1 Torch heat flux

The torch heat flux constructs of according to Federal Highway Administration (2013, p. 22): "- - the type of fuel, the number and size of the orifices, the fuel pressure and resulting heat output at the nozzle tip." The main factors influencing temperature are according to Federal Highway Administration (2013, p. 19): "- - size and type of the torch orifice, intensity of the flame, speed of torch movement, and thickness and configuration of the member."

Conducting these studies the heating is supposed to be done with an oxy-acetylene single nozzle torch. The constant heat flux value calculated with the Gaussian heat flux equation

(3) include the energy input rate *Q*, that contains the information about fuel pressure and the resulting heat output at the nozzle tip, and the characteristic radius of heat flux distribution *c*, that contains the information about the size of the orifice and the intensity of the flame. The configuration of the member, diameter, height and thickness, are kept constant in the torch heat flux studies to get better comparable results. The torch heat flux is varied with the torch speed. Next the effects from different torch speeds are studied with modeling and the results are processed.

6.1.1 Speed

The torch speed studies are conducted with four different torch speeds; 0.1 °/s, 0.125 °/s, 0.15 °/s and 0.175 °/s. The local radial displacement values are taken from four different locations from both the heated upper surface and the bottom surface. These four different locations are shown in Figure 40; A is 0 °, B is 90 °, C is 180 ° and D is 240 °. The eight nodes are approximately chosen from both ring surfaces at the outer rim from the mentioned angle areas; 0 °, 90 °, 180 ° and 240 °. The overall displacements on the top surface for the speed 0.1 °/s are illustrated in Figure 41 from where the local radial displacements in those four points also have been gathered. For the other three speeds (0.125 °/s, 0.15 °/s and 0.175 °/s) the overall displacements are shown in Appendix VII. These local radial displacements are gathered from the top surface to Table 1 and from the bottom surface to Table 2.

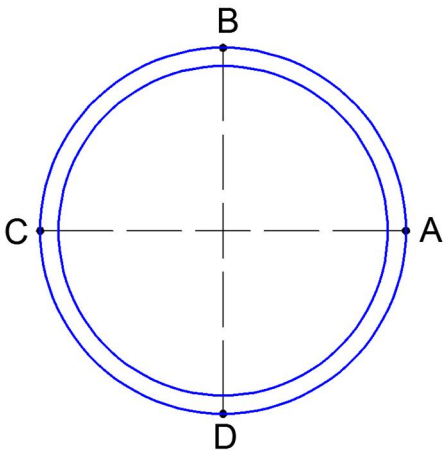

Figure 40. Four different locations along the ring circumference.

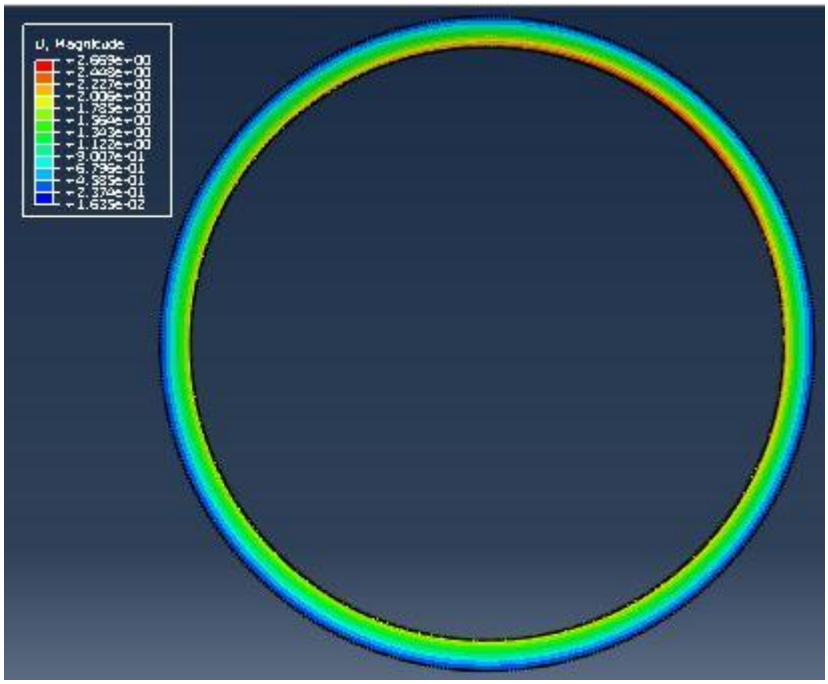

Figure 41. Overall displacement distribution on the top surface after heating with the speed 0.1 °/s.

Table 1. Local radial displacements [mm] on the top surface for four different speeds.

	A	B	C	D
0,1 °/s	0,307455	0,343467	0,306186	0,287546
0,125 °/s	0,199024	0,262807	0,252817	0,231777
0,15 °/s	0,0200453	0,0192683	0,0245531	0,0256985
0,175 °/s	0,00644069	0,00602211	0,00687785	0,00734789

Table 2. Local radial displacements [mm] on the bottom surface for four different speeds.

	A	B	C	D
0,1 °/s	0,12005	0,0425754	0,0754587	0,0315787
0,125 °/s	0,0260297	0,0434665	0,0415096	0,0345389
0,15 °/s	0,049768	0,058023	0,0675828	0,0665473
0,175 °/s	0,00141329	0,00160025	0,000314444	0,00131092

If Table 1 is investigated it can be seen where approximately the maximal displacement is attained with each of the speeds: for speed 0.1 °/s the biggest displacement is around point B, for speed 0.125 °/s the biggest displacement is also around point B as well as for the speed 0.175 °/s but for the speed 0.15 °/s the peak temperature is acquired around point C. From the overall distributions of displacement Figure 41 and Appendix VII can be seen the

exact locations of the biggest displacements. From Table 1 and Table 2, figures are made to illustrate the relation between the heating speed and the affected displacement on the top (Figure 42) and the bottom (Figure 43) surfaces. The figures illustrate well how the speed affects the displacement; the faster the speed the smaller the displacements. This applies better to the heated top surface than the bottom surface that is not heated. The cooling convection and radiation boundary conditions causes most of the displacements on the bottom surface (Figure 43). From Figure 42, it can be seen that on the heated top surface the speed influences greatly to the happening displacement.

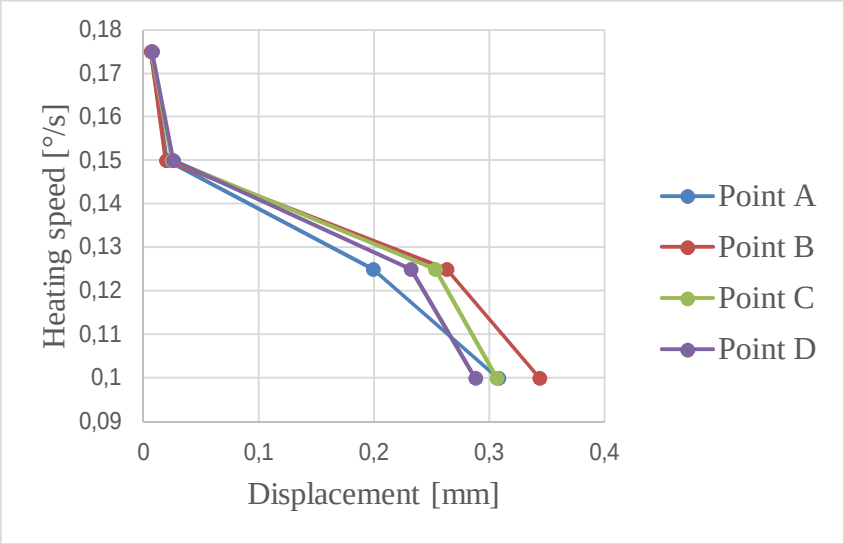

Figure 42. Relation between the heating speed and the displacement on the top surface.

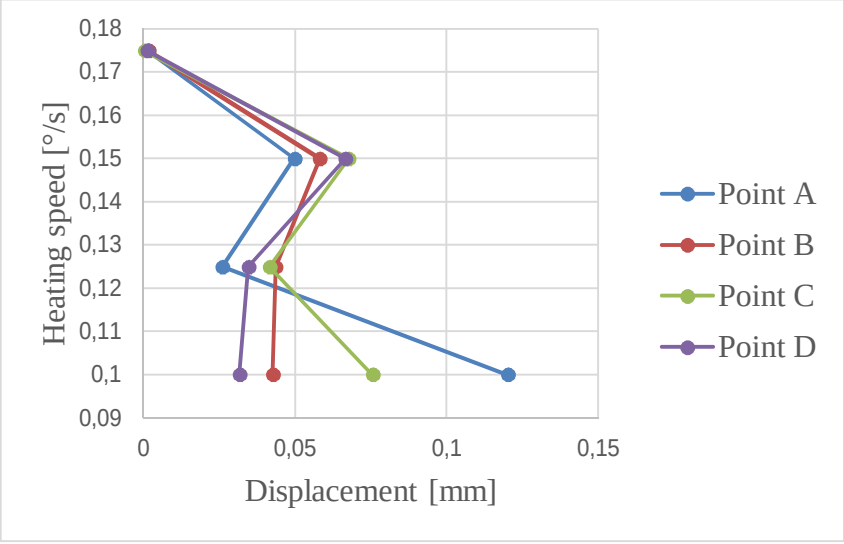

Figure 43. Relation between the heating speed and the displacement on the bottom surface.

Heat input is the main factor that causes the slower speeds to result in bigger displacements. The heat input can be evaluated with temperature. The relation between the temperature and the speed is illustrated in Figure 44. In Appendix VIII, the effects of the speed on the temperature distributions are shown. These temperature distributions are in good agreement with the temperature distributions discussed in Chapter 3.1.2. The difference in temperatures in time at those before mentioned four points (A, B, C and D) when heating with speed 0.1 °/s are illustrated in Figure 45, with showing also the temperature differences between the inner rim and the outer rim. From Figure 45 can be seen that the starting point A experiences two heating cycles: one at the beginning and another at the end of heating. The temperature in point A does not rise as high as in the other points B, C and D. This causes uneven shrinkage to the starting region. This happening uneven shrinkage in the starting region is further examined.

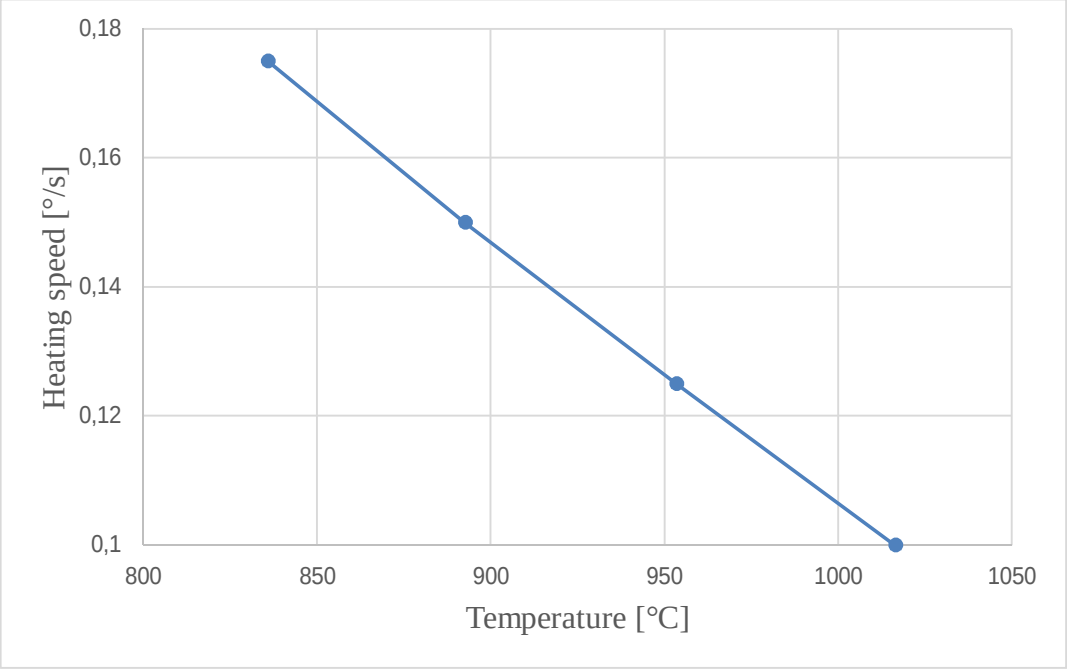

Figure 44. Relation between temperatures and heating speeds.

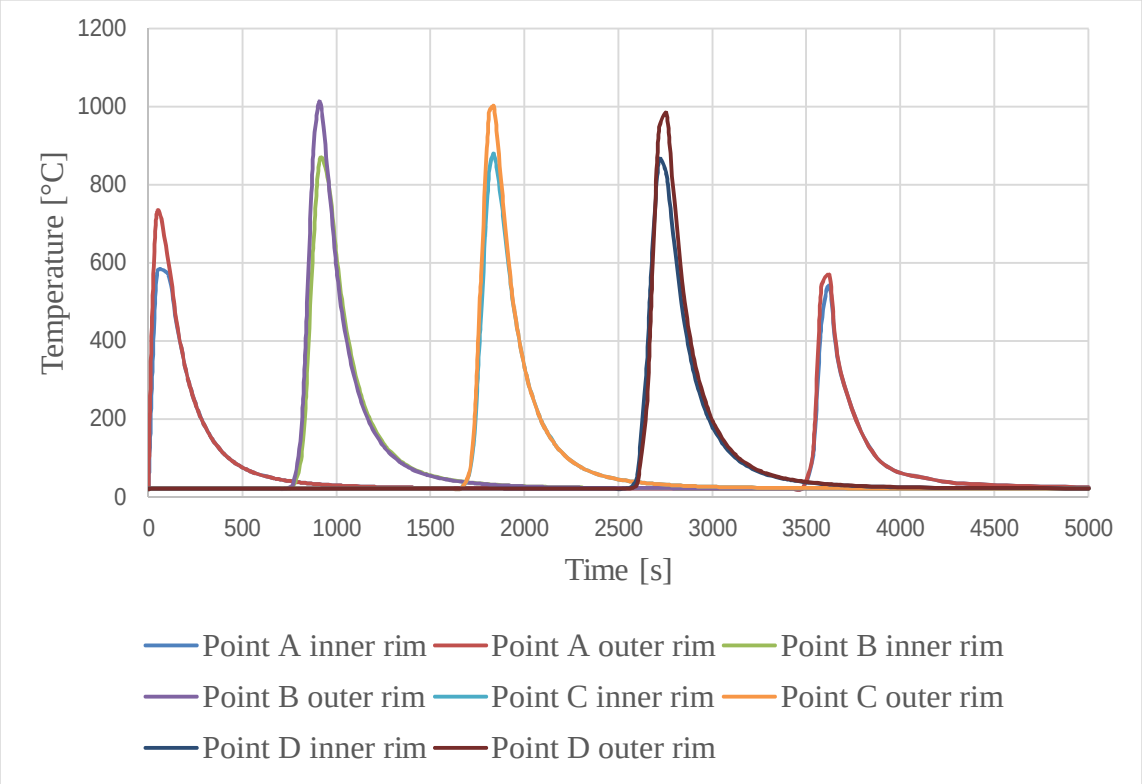

Figure 45. The difference in temperatures.

The temperature reaches its peak after the torch has passed 30 ° to 45 ° from the starting point of heating. The peak temperature location varies with different heat source powers and speeds. When the peak temperature is acquired it becomes more stable which makes the plastic deformations greater at that point. The overall distribution of the displacements and residual stresses are examined in more detail for the speed 0.1 °/s.

For the studied ring heated with the speed 0.1 °/s the plastic deformations become more stable after the torch has passed almost a quarter of the ring. Figure 46 illustrates the distribution of plastic strains in the ring. From Figure 46 can be seen that clearly the distribution of plastic strain is inconsistent which leads to smaller shrinkage in certain regions

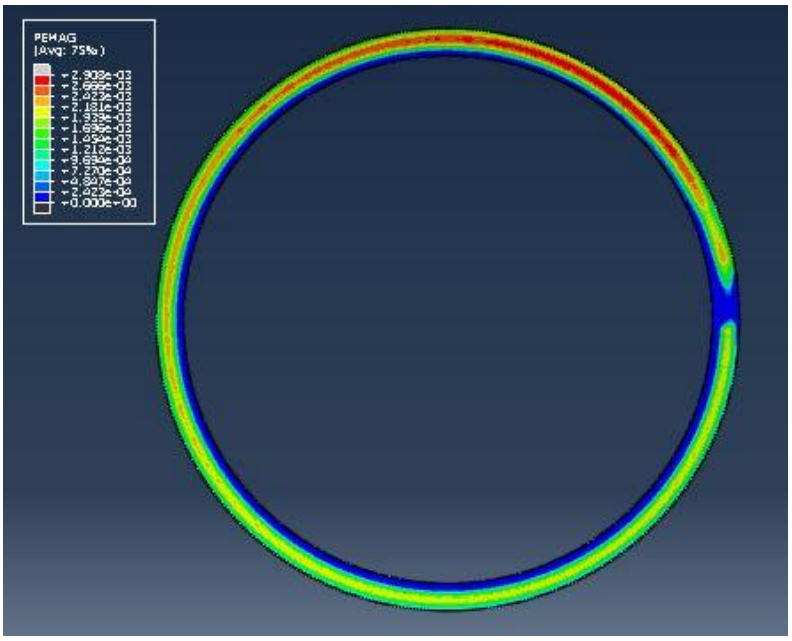

Figure 46. Distribution of plastic strains for heating speed of 0.1 °/s.

The distribution of residual stresses is shown in Figure 47. From Figure 47, fluctuations in the start/end region can be seen while otherwise the distribution is somewhat uniform. The fluctuations of stress in the start/end region are the main reason of asymmetrical contractions which may cause problems in the future since there are regions with less shrinkage. These regions affect the clamping force of the wires in that region and overall roundness of the cylinder.

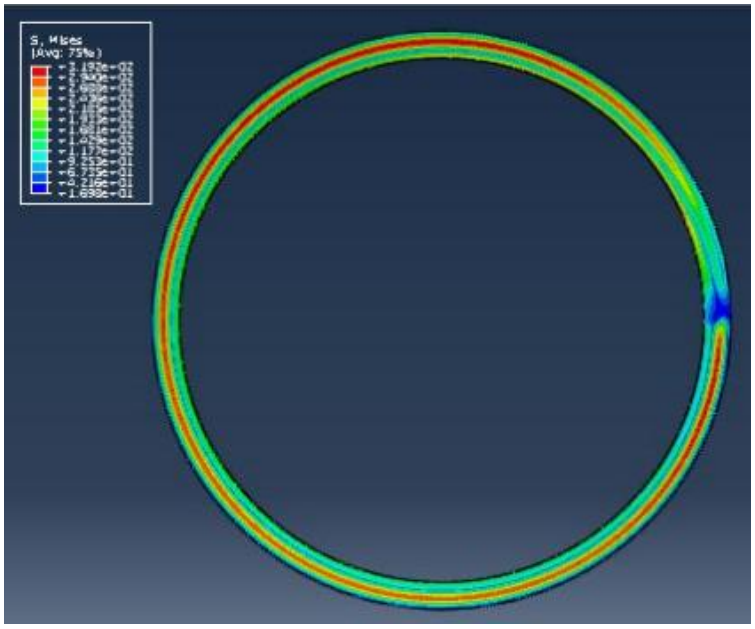

Figure 47. The residual stress distribution for heating speed of 0.1 °/s.

With the heat flux values and the higher speeds (0.125 °/s, 0.15 °/s and 0.175 °/s) used, the stainless steel AISI 304L does not necessarily have any plastic deformations and residual stresses. The distribution of plastic strains for the other three studied speeds are in Appendix IX and the distribution of residual stresses in Appendix X. Also the nonexistent plastic deformations and residual stresses can be caused by some errors in the model.

If the support ring is heated just once with the speed 0.1 °/s, there is a need to find a way to produce the same uniform shrinkage in the first quarter as well as in the remaining ring in all the temperature ranges. A gradual increase of heat flux through the course of heating could solve this problem. The gradual increase of heat flux is done with adding speeded heating portions before and after the actual heating cycle.

6.1.2 Speeded start/end

The speeded start/end is studied with adding a speeded heating portion of 5 times faster speed and 45 ° distance to the initial heating cycle of speed 1.0 °/s. The distance of 45 ° means that the heating is started with a faster speed from point 45 ° before the starting point 0 °, when the starting point is reached the speed is dropped to the initial and the whole ring is ones heated around, when the ending point 0 ° is reached the heating continues speeded to the point of 45 °. The speeded heating cycles displacements and residual stresses are compared to the initial heating cycle.

The local radial displacement values are taken from four different locations (A, B, C and D) as mentioned above from the overall distribution of displacements (Figure 48) on the heated upper surface along with the peak temperature and the results are compared to the corresponding results of the initial heating cycle studied above. These results are shown in Table 3. Table 3 shows that there either is some faults in the model or the speeded heating even with the same peak temperature as in the initial heating does not increase the displacements.

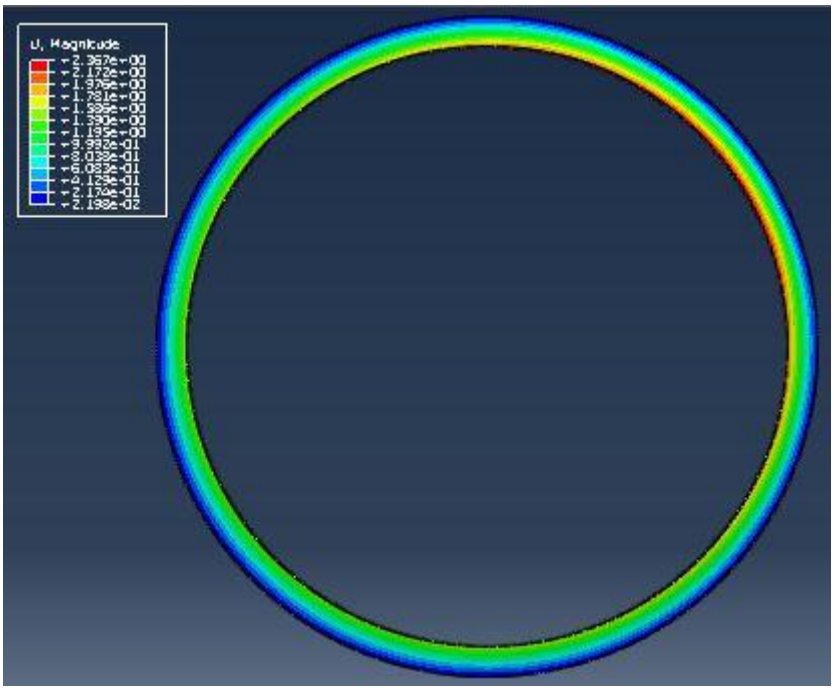

Figure 48. Overall distribution of displacements from the top surface of the ring in speeded heating.

Table 3. Local radial displacements [mm] and peak temperature [°C] of a speeded heating cycle and initial heating cycle.

	Peak temp.	A	B	C	D
Initial heating	1016,26	0,307455	0,343467	0,306186	0,287546
Speeded heating	1016,36	0,143826	0,0547246	0,0792221	0,0414291

Even if there is some faults in the model the distributions of plastic strains and residual stresses as well as the difference in temperatures in time may still give information about the uniformity of the ring. Figure 49 illustrates the distribution of plastic strains in speeded heating. If only the first quarter of the Figure 49 is considered, the distribution is more uniform in that region and the peak temperature is reached near the starting point. From the distribution of the plastic strains the advantage of the speeded heating to the distribution on the starting region can be improved.

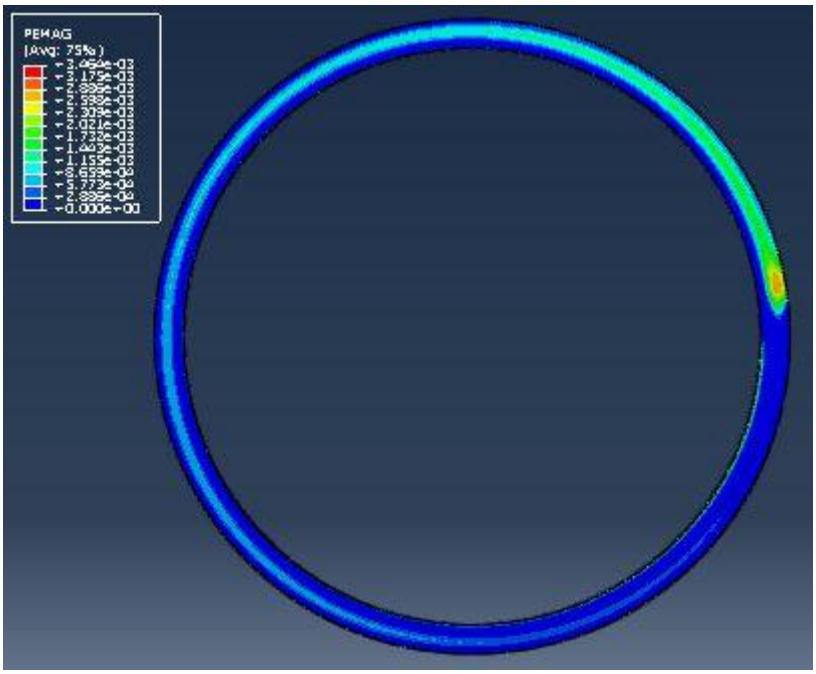

Figure 49. Distribution of plastic strains in speeded heating.

Figure 50 shows the distribution of the residual stresses in speeded heating. The same advantages that were seen from the distribution of plastic strains can be seen from the distribution of residual stresses. In the first quarter the residual stresses are more uniform when using speeded heating than with the initial single progressive heating.

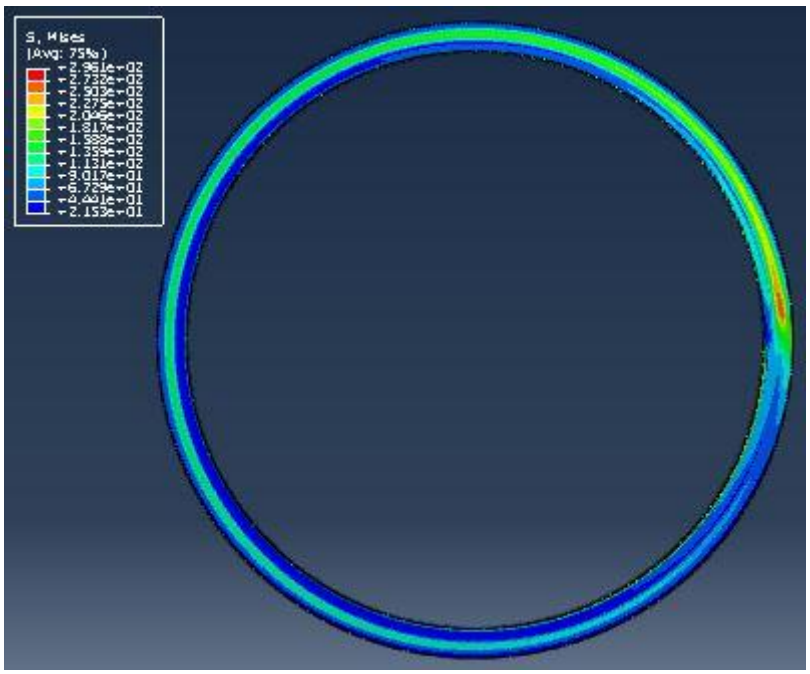

Figure 50. Distribution of residual stresses in speeded heating.

The differences in temperatures in time at the same points as before (A, B, C and D) are in Figure 51. The temperatures in points B, C and D are not influenced with using the speeded heating when compared to the same values in initial heating. The temperature in point A however increases. The temperature of the first pass on point A is lower in speeded heating but the second pass is higher compared to the initial heating. The higher second pass temperature is likely the cause to the more uniform distributions of displacements and residual stresses in the start/end region.

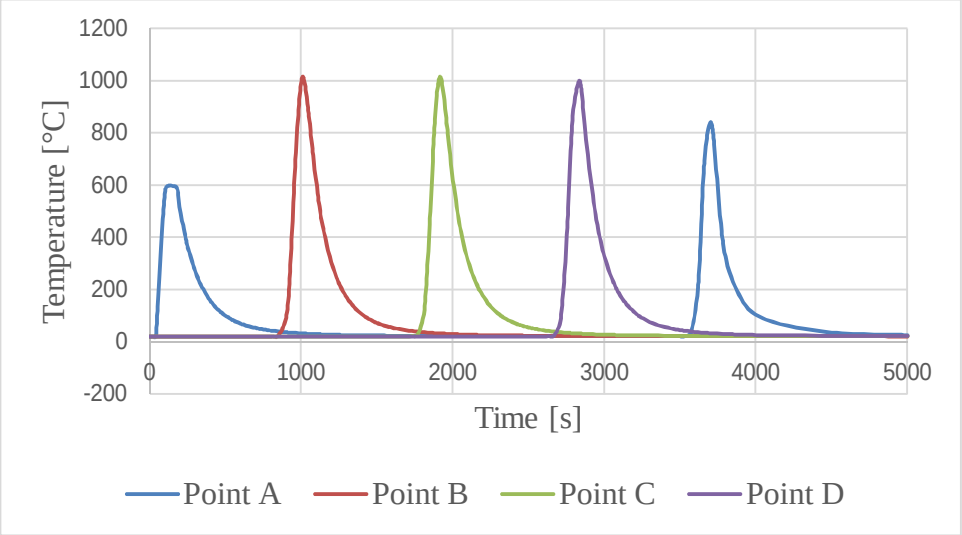

Figure 51. Difference in temperatures in speeded heating.

6.2 Location of the wires

Location of the wires is studied with keeping the other factors the same in two different models; one with wires located on the inner rim of the ring (outflow-type) and another with wires located on the outer rim of the ring (inflow-type). The inflow-type ring case is the same as the initial single progressive heating case with the heating speed of 0.1 °/s.

The local radial displacements are taken from the same four points (A, B, C and D) from the overall distribution of displacements (Figure 52) on the top surface as previously. The local radial displacements and the peak temperatures for the two different wire locations are displayed in Table 4. When both of the types outflow and inflow are heated from the same location 0.1*height the peak temperature is equal in both cases but the local radial displacements are about two times larger with outflow types. This can be explained with

the wires being closer to the heating point in inflow type rings and farther away in outflow type rings.

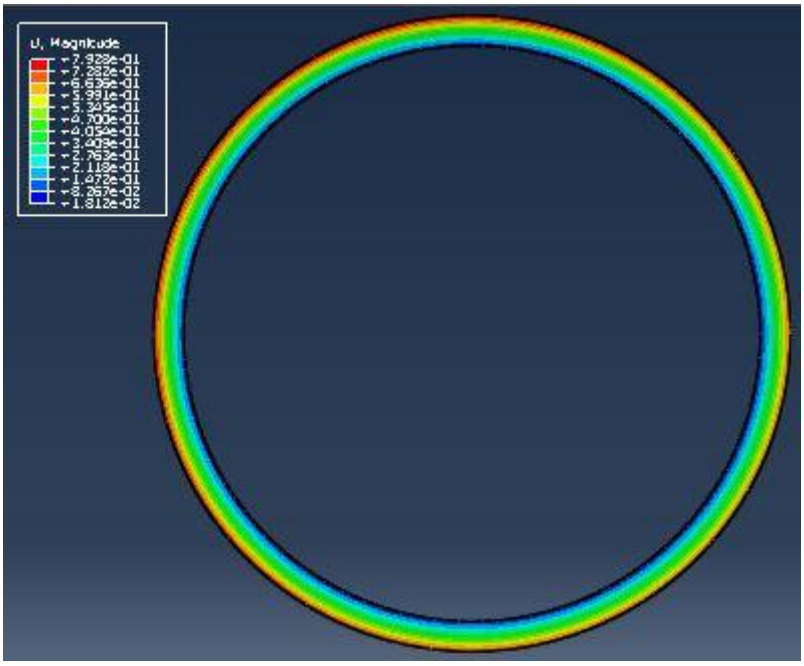

Figure 52. Overall distribution of displacements on the top surface in outflow type cylinder.

Table 4. Local radial displacements [mm] and peak temperature [°C] for two wire locations.

	Peak temp.	A	B	C	D
Inflow	1016,26	0,307455	0,343467	0,306186	0,287546
Outflow	1016,26	0,734023	0,702077	0,744793	0,782107

As can be seen from Figure 52 the overall distribution of displacements are for the outflow type ring much more uniform than for the inflow type. As are the distributions of the plastic strains and the residual stresses also more uniform in heating the outflow type ring than in heating the inflow type ring. The distribution of plastic strains is shown in Figure 53. The temperature becomes stable earlier and the uneven distribution near the starting region is not so severe than compared to the heating of the inflow type. Figure 54 illustrates the distribution of residual stresses. The same can be stated from the distribution of the residual stresses; the uneven starting region is smaller compared to the inflow type ring.

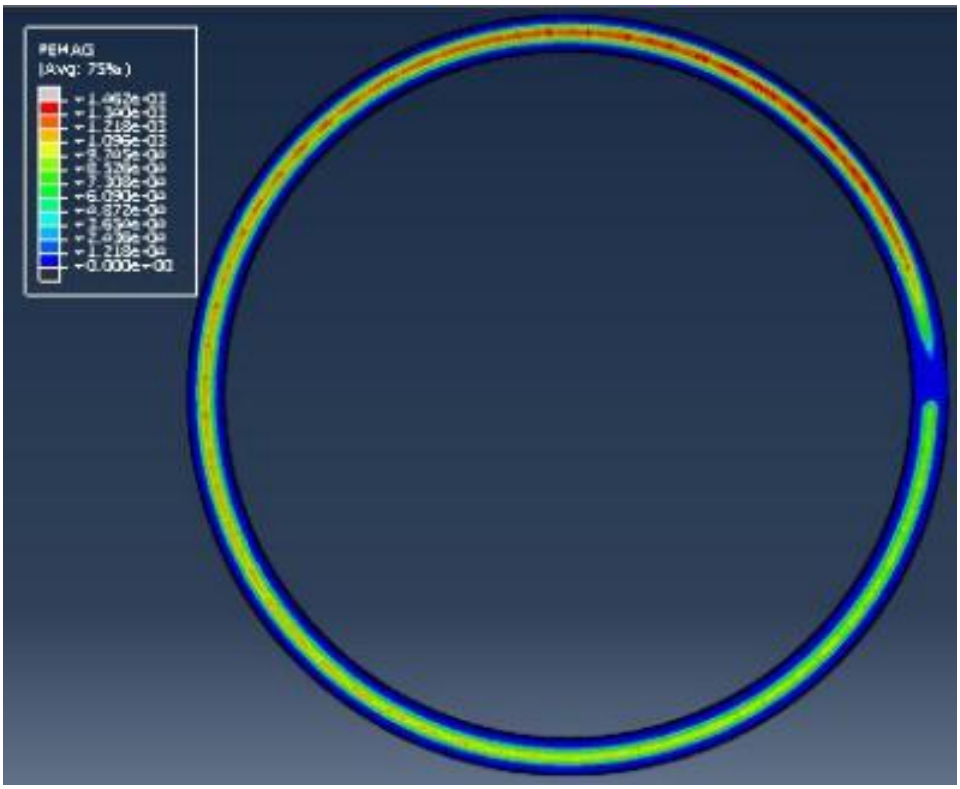

Figure 53. Distribution of plastic strains in outflow ring.

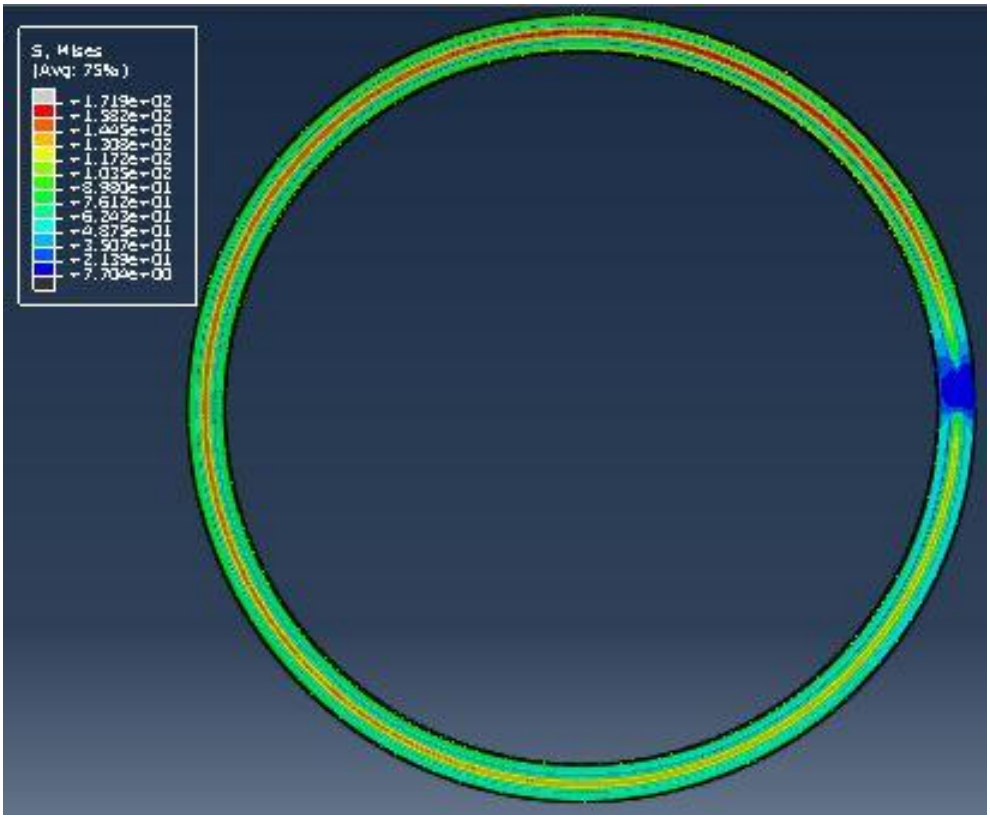

Figure 54. Distribution of residual stresses in outflow ring.

6.3 Heating location

As was noticed in the previous case the outflow ring when heated from the opposite edge away from the wires produces larger shrinkage. Thus the placement of the heat is studied with comparing the inflow ring heated near the wires 0.1*height and away from the wires 0.9*height. The local radial displacements are taken from the same four points (A, B, C and D) from the overall distribution of displacements (Figure 55) on the top surfaces outer rim as previously. The local radial displacements and the peak temperatures for the two different heating locations are displayed in Table 5. Even when the peak temperature is almost the same in both heating's directed to different locations there are deviations in the results that do not correlate with the results from comparing the inflow and outflow rings.

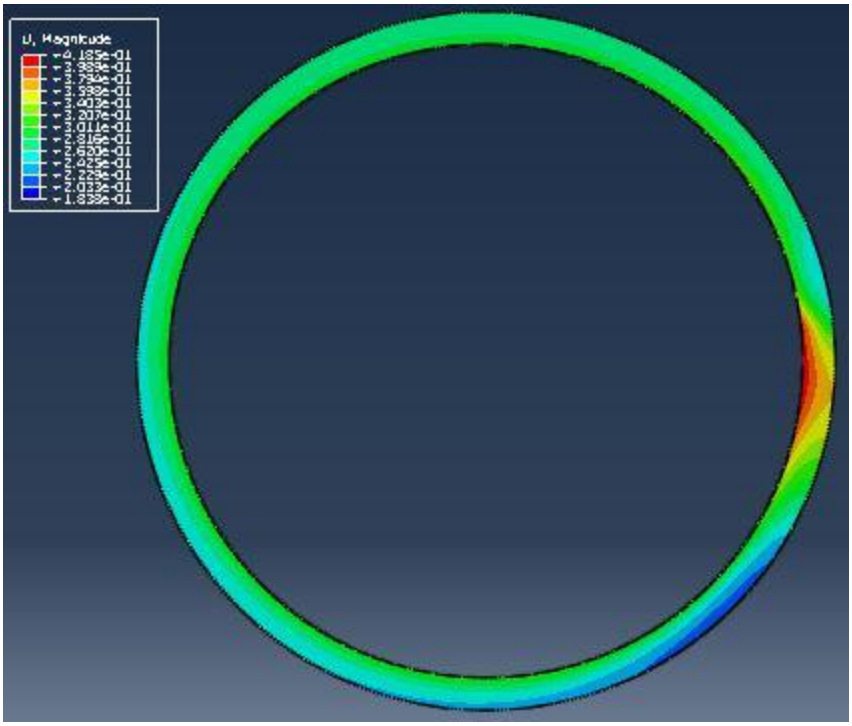

Figure 55. Overall distribution of displacements on the top surface for heating away from the wires.

Table 5. Local radial displacements [mm] and peak temperature [°C] for two different heating locations.

	Peak temp.	A	B	C	D
0.1*height	1016,26	0,307455	0,343467	0,306186	0,287546
0.9*height	1024,14	0,345793	0,263131	0,255932	0,237653

For the heating location of 0.9*height the peak temperature location after heating is near point A where it starts to weaken as it continues towards the end. This can be seen from the distribution of plastic strains (Figure 56). The distribution of plastic strains were expected to be more like in the case of the outflow ring. Thus the placement of the wires effect the shrinkage more than the location of the heat.

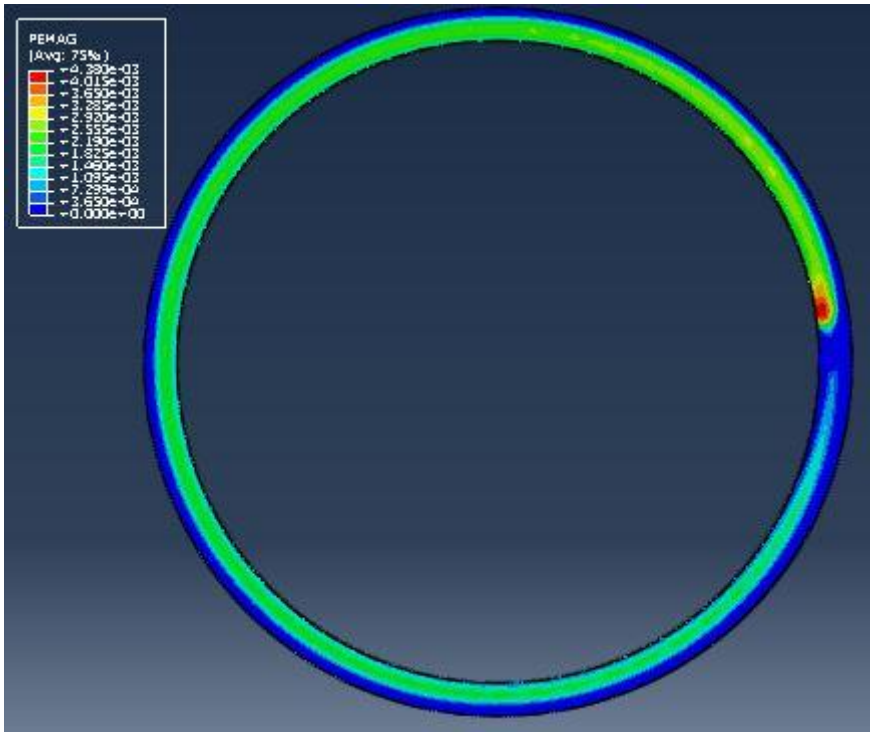

Figure 56. Distribution of plastic strains for a heating location of 0.9*height.

The distribution of residual stresses (Figure 57) seem more similar to the distribution of residual stresses for the heating location of 0.1*height. The main difference between the distributions of plastic strains and residual stresses of the two different heating locations are the distributions on the start region. Heating location 0.9*height reaches the peak temperature right after the start and so there is not so big uneven region in that area but the uneven area occurs more near the ending region.

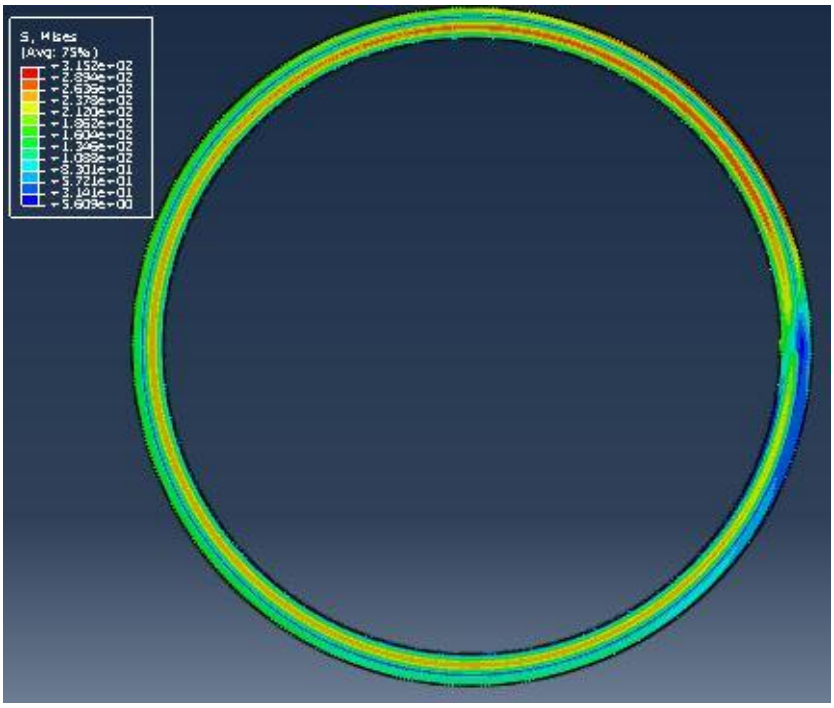

Figure 57. Distribution of residual stresses for heating location of 0.9*height.

6.4 Structural factors

The effects of the structural factors of the ring are studied with varying the ring diameter, height, thickness and the number of wires. The main effect of the different structural factors in the shrinkage is the remaining cool obstructing structure while some regions are heated.

6.4.1 Ring diameter

Ring diameter is studied with three different diameters 500, 600 and 700 mm. When comparing just the effects of the diameter, the number of wires and the heating speed have to be adjusted accordingly. With 500 mm diameter ring, the number of wires is 500 and the heating speed is 0.16 °/s while with 600 mm diameter, there is 600 wires and 0.133 °/s speed. For the 700 mm diameter ring, the number of wires is 700 and the heating speed is 0.114 °/s. The heating speed was adjusted so that the heated distance in one second is about 0.7 mm for all of the three different diameters.

Local radial displacements are taken from the four different points (A, B, C and D) on the top surface from the overall distribution of displacements (Figure 58). The local radial displacements and the peak temperatures are illustrated in Table 6. The heating speed were

adjusted to get the peak temperature as equal as possible to all the diameter ring cases. The peak temperature is equal enough to get good comparable shrinkage results. From the local radial displacements can be seen that with higher peak temperature and smaller diameter the displacements are larger. However Figure 58 illustrates that there are regions with larger displacements with all the ring diameters even if those are not seen in Table 6. Also deviation between the different diameter cases can be seen at the location where the largest displacements are (Figure 58); with 500 mm diameter the peak temperature is around point C, with 600 mm diameter the peak temperature is around point B and with 700 mm diameter the peak temperature is between the points A and B.

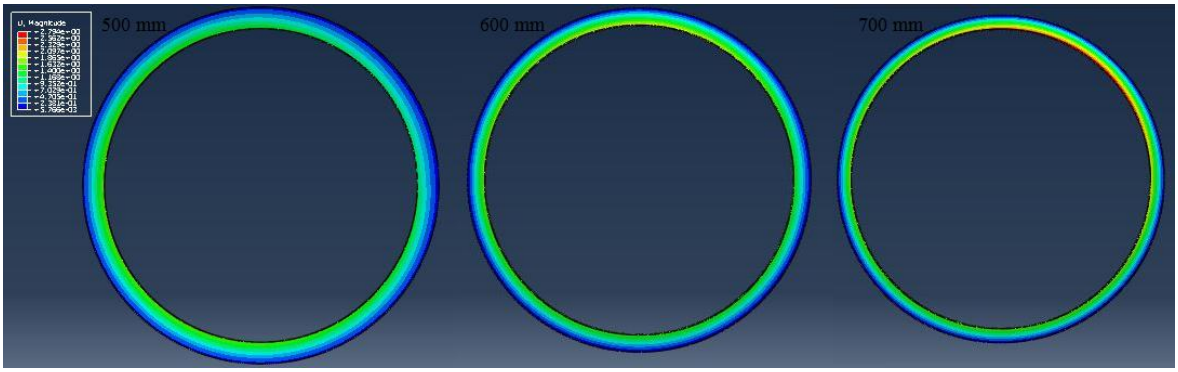

Figure 58. Overall distribution of displacements on the top surface for different ring diameters.

Table 6. Local radial displacements [mm] and peak temperature [°C] for three different diameters.

	Peak temp.	A	B	C	D
500 mm	959	0,147153	0,180644	0,202445	0,194151
600 mm	957,866	0,046718	0,103314	0,0416176	0,0210668
700 mm	956,235	0,110485	0,0402982	0,0600958	0,0123411

The differences in the peak temperature locations are better illustrated with the distributions of plastic strains (Figure 59). Figure 59 shows the entity of the difference in shrinkage between the 500 mm diameter and the 600 as well as 700 mm diameters. The 600 mm diameter ring and 700 mm diameter ring have similar distributions where the much lower strains can be seen. With different ring diameters the amount of shrinkage needed differs because it defined as a percentage from the diameter. So to get bigger

shrinkage the speed has to be slower. The uniformity of the displacements are correlated to the distributions of the residual stresses that are illustrated in Figure 60.

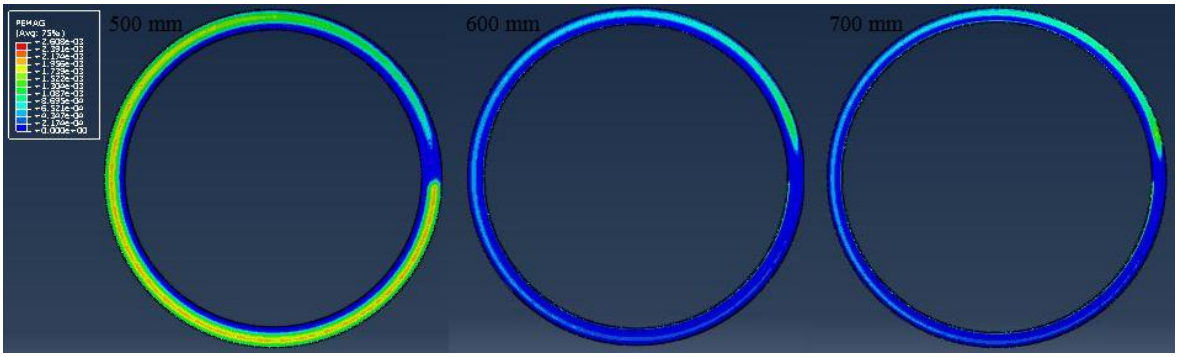

Figure 59. Distributions of plastic strains with three different diameters.

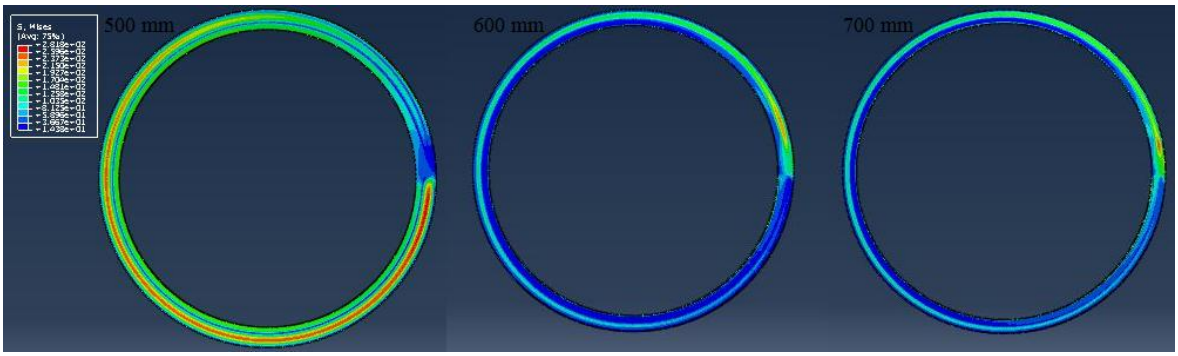

Figure 60. Distribution of residual stresses for three different diameters.

6.4.2 Ring height

The effects of different ring heights on the heat induced shrinkage are studied with comparing three different ring heights: 25, 30 and 35 mm. The outer diameter is kept the same in spite of different ring heights. Thus the ring inner diameter deviates in the different ring height cases. The ring height 30 mm case is the same as the basic case with the default values.

Local radial displacements are taken from the four different points (A, B, C and D) on the heated top surfaces outer rim from the overall distribution of displacements (Figure 61). The local radial displacements and the peak temperatures are illustrated in Table 7. The overall distributions of displacements (Figure 61) show that in ring height 25 mm the distribution is really evenly distributed compared to the heights 30 and 35 mm. The displacements increase with increasing the ring height, but from Table 7 is seen that with

degreasing the ring height the peak temperature rises. The location of the peak temperature is for the 30 and 35 mm ring heights around point B but for the 25 mm ring height around point A.

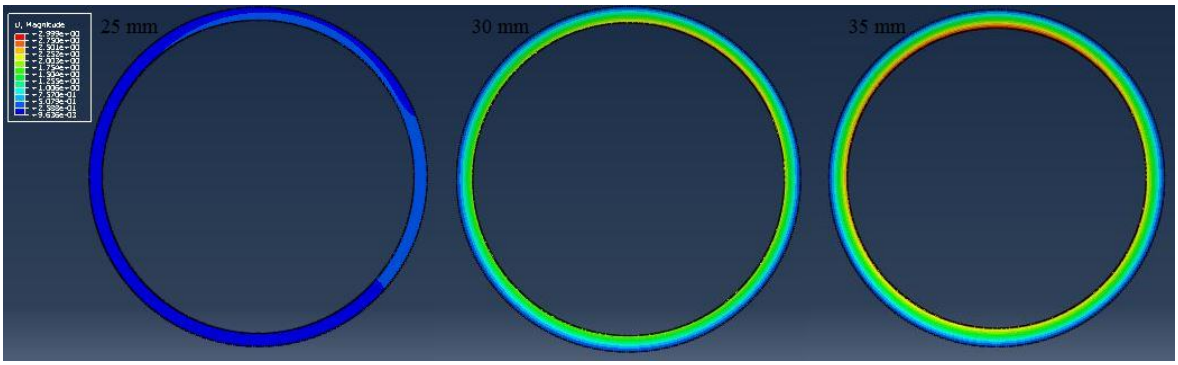

Figure 61. Overall distribution of displacements on the top surface for three different ring heights.

Table 7. Local radial displacements [mm] and peak temperature [°C] for three different ring heights.

	Peak temp.	A	B	C	D
25 mm	1033,11	0,442803	0,249976	0,211103	0,178491
30 mm	1016,26	0,307455	0,343467	0,306186	0,287546
35 mm	1004,78	0,279054	0,344142	0,318641	0,294136

The really even distribution of displacements can be explained by comparing the distributions of temperatures during heating with the different ring heights (Appendix XI). From Appendix XI, can be seen that the entire rings top surface is heated when the ring height is 25 mm causing of the peak temperature zone from the flame covers an area that reaches the whole height of the ring while with the ring heights 30 and 35 mm the peak temperature zone does not cover the whole height.

The differences in temperature in time for the 25 mm ring height in those familiarized four points (A, B, C and D) (Figure 62) shows that there aren't notable changes in points B, C and D as well as the first pass while starting of point A but the real difference can be seen in the second pass while ending the cycle at point A. The second pass at point A rises the temperature to about 900 °C when the corresponding temperature for the 30 mm ring height with a single progressive heating is only about 600 °C and with speeded heating is a

bit over 800 °C. So it can be stated that with heating at the entire ring height the deformations are more uniform than with speeded heating.

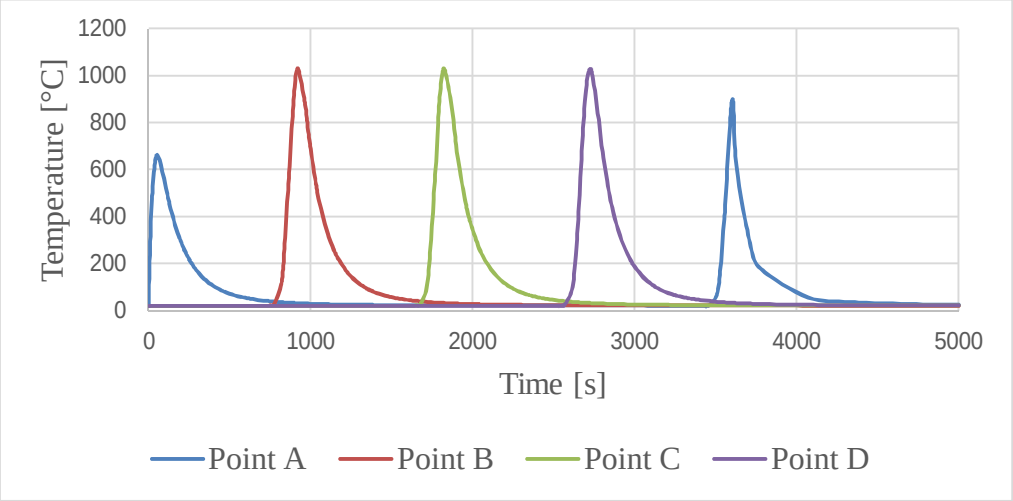

Figure 62. Difference in temperature in time for ring height 25 mm.

The differences in the peak temperature locations are better illustrated with the distributions of plastic strains (Figure 63). Figure 63 shows the entity of the difference in shrinkage between 25 mm ring height as well as 30 and 35 mm ring heights. The peak temperature locations are: with 25 mm ring height near the point A, with ring height 30 mm between points A and B and with 35 mm ring height near point B. It can be stated that the peak temperature location moves farther from the starting point when the ring height is increased. The difference of the distribution of temperature during heating with ring height 25 mm causes deviating distribution of plastic strains compared to the distribution of plastic strains with ring heights 30 and 35 mm that are more similar looking.

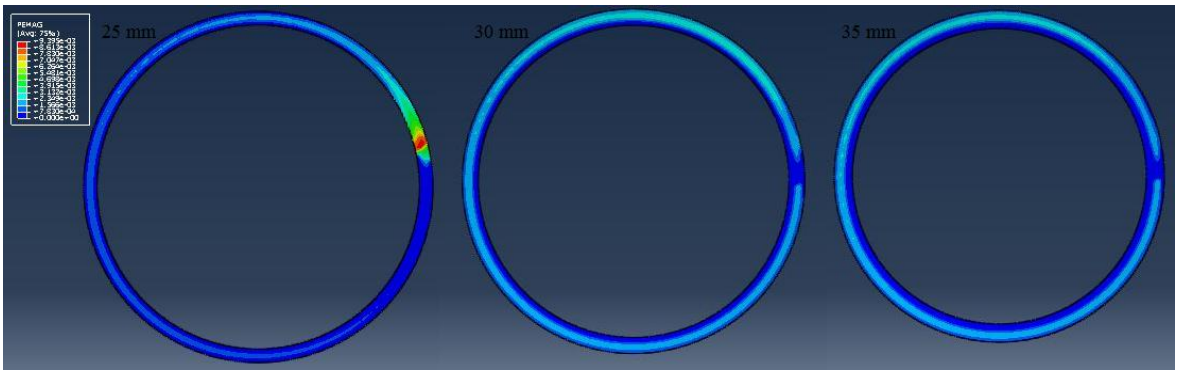

Figure 63. Distributions of plastic strains with three different ring heights.

The uniformity of the displacements are correlated to the distributions of the residual stresses that are illustrated in Figure 64. The residual stress distributions show that with ring height 25 mm the uneven residual stress region is more in the ending area between points D and A while with ring heights 30 and 35 mm the corresponding region is between points A and B. Also a big difference can be seen in the amount of residual stresses: with ring heights 30 and 35 mm there are larger residual stresses than with ring height 25 mm.

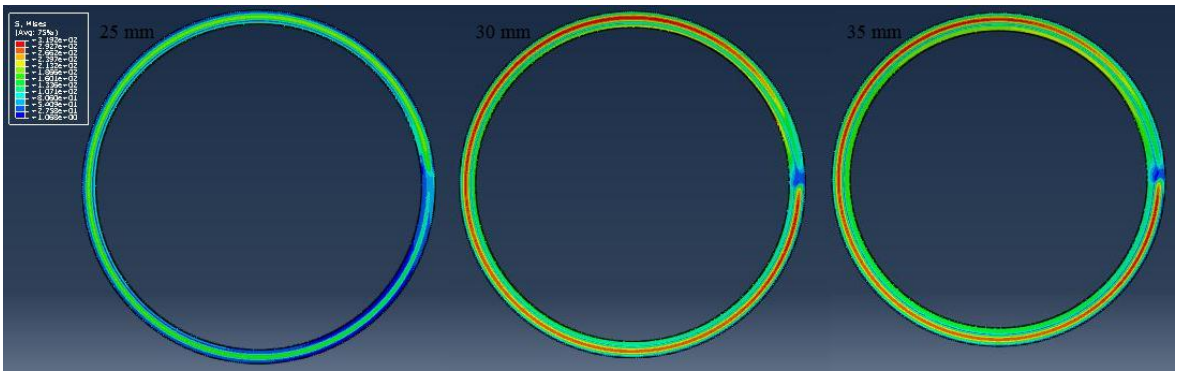

Figure 64. Distribution of residual stresses for three different ring heights.

Heating the entire ring height decreases the amount of obstructing structure around the heat affected zone. Thus the ring is more vulnerable towards out of plane buckling. However during the modeling it was noted that with the heat flux values and speeds used the ring does not tend to distort. The amount the ring when heated the entire ring height 25 mm with speed 0.1 °/s distorted is in point A approximately 3.9 E-5 mm.

6.4.3 Ring thickness

The ring thickness is studied with four different ring thicknesses 4, 6, 8 and 10 mm. The ring thickness 4 mm case is the same as the basic case with the default values. When only the top surface of the ring is heated the local radial displacements are taken from the four different points (A, B, C and D) on both the heated top surfaces and bottom surfaces outer rim. The overall distribution of displacements on the top surfaces for the 4 and 6 mm ring thicknesses are illustrated in Figure 65. The local radial displacements and the peak temperatures are illustrated from the top surface in Table 8 and from the bottom surface in Table 9. From Figure 65 can be seen that the displacements are almost nonexistent with ring thicknesses 6 mm as well as with 8 and 10 mm thicknesses compared to the displacements with 4 mm ring thickness.

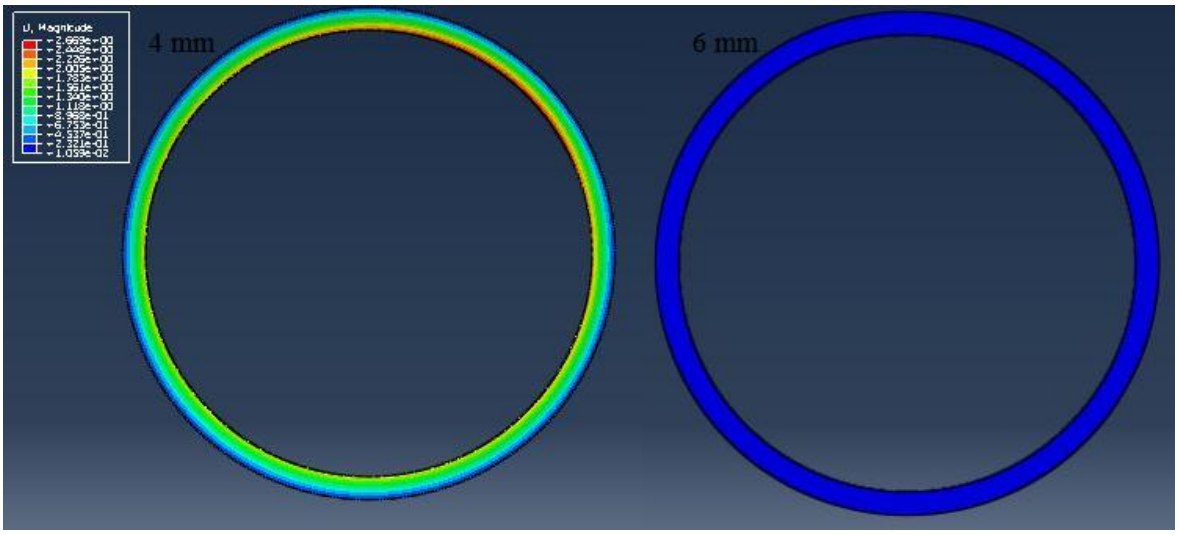

Figure 65. Overall distribution of displacements on the top surface for three different ring thicknesses.

Table 8. Local radial displacements [mm] and peak temperature [°C] on the top surface of the ring for different ring thicknesses.

	Peak temp.	A	B	C	D
4 mm	1016,26	0,307455	0,343467	0,306186	0,287546
6 mm	862,524	0,0178399	0,0133034	0,0124448	0,0171744
8 mm	750,324	0,0337133	0,0234416	0,0224571	0,0318533
10 mm	667,555	0,0516616	0,0345045	0,034625	0,0477231

Table 9. Local radial displacements [mm] and peak temperature [°C] on the bottom surface of the ring for different ring thicknesses.

	Peak temp.	A	B	C	D
4 mm	1016,26	0,12005	0,0425754	0,0754587	0,0315787
6 mm	862,524	0,0180793	0,0135619	0,0127569	0,0174606
8 mm	750,324	0,0339681	0,0236501	0,0226791	0,0320898
10 mm	667,555	0,0520525	0,0347984	0,0349445	0,0481102

Local radial displacements with ring thickness 4 mm from the heated top surface and the bottom surface differ greatly, but with ring thicknesses 6, 8 and 10 mm the displacements do not differ that much on the different surfaces. If you count out the ring thickness 4 mm, the displacement increase when the thickness increases on both top and bottom surfaces.

The peak temperature decreases when the ring thickness increases. However while the peak temperature is the same on both the top surface and the bottom surface during heating the distribution of the temperatures are different. In Appendix XII the compared distributions of temperatures on the top and bottom surfaces for different ring thicknesses during heating are illustrated. From Appendix XII is seen that the bigger the ring thickness, the smaller the highest temperature area.

The differences in the peak temperature locations after the heating illustrated with the distributions of plastic strains are almost nonexistent like in the overall distributions of displacements. Thus there are only small elastic deformations in the rings when using these heat flux parameters and rings with larger thickness. As there are not plastic deformations, there either is not notable residual stresses.

6.4.4 The number of wires

The effects the wires have on the shrinkage are studied with five different ring amounts: 475, 500, 525, 550 and 575 wires. 525 wires case is same as the basic case with default values. Local radial displacements are taken from the four different points (A, B, C and D) on the heated top surfaces outer rim. The overall distribution of displacements on the top surfaces for the 475 wires are illustrated in Figure 66. The overall distribution of displacements for the 525 wires is in Chapter 6.1.1 and for the 500, 550 and 575 wires are in Appendix XIII.

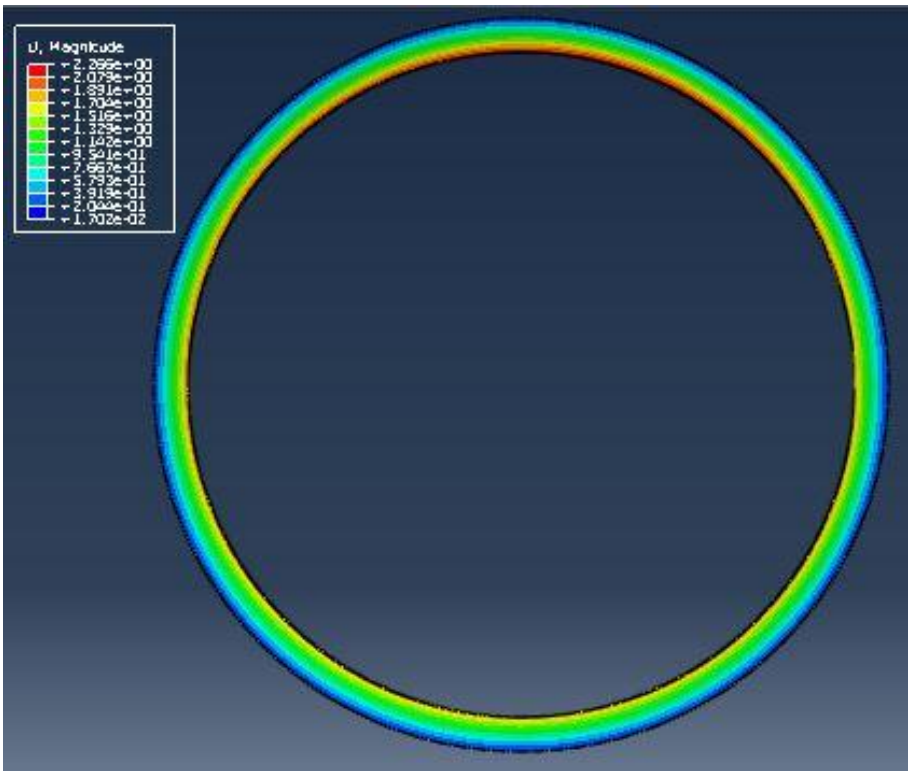

Figure 66. Distribution of displacements on the top surface for 475 wires.

From the distributions of the displacements on the top surface the locations of the largest deformations can be seen. The largest displacements for the fewer wires are around point B and start nearing point A when increasing the number of wires. The local radial displacements after the heating that are gathered from the distribution of displacements and the peak temperatures during heating are illustrated from the top surface in Table 10. The heating temperature is the same despite different numbers of wires. Interestingly the displacements get larger with increasing the number of wires from 475 to 525 but then with 550 and 575 wires the displacements drop notably. However when you compare the maximum local radial displacements shown in the overall distribution of displacements in Appendix XIII and Figure 66 that occur at the inner rim the differences are not so great. These are as graded from smallest to largest 475 wires with 2.27 mm displacement, 550 wires with 2.33 mm displacement, 500 wires with 2.48 mm displacement, 575 wires with 2.52 mm displacement and 525 wires with 3.92 mm displacement.

Table 10. Local radial displacements [mm] and peak temperature [°C] for the five different numbers of wires.

	Peak temp.	A	B	C	D
475 wires	1016,33	0,25737	0,310101	0,285381	0,264448
500 wires	1016,62	0,282584	0,329208	0,297495	0,277212
525 wires	1016,26	0,307455	0,343467	0,306186	0,287546
550 wires	1016,5	0,137278	0,0552606	0,0894892	0,0525892
575 wires	1016,51	0,154431	0,0673526	0,0947749	0,0529372

The differences in the peak temperature locations are better illustrated with the distributions of plastic strains (Appendix XIV). From the distributions of plastic strains can be seen that there are some flaws in the 550 and 575 wire models that cause the distribution to differ greatly from the distributions of 475, 500 and 525 wires. With 550 and 575 wires the peak temperature is right after starting as a point strain as in 475, 500 and 525 wires the peak temperature is reach around 45° after the starting point as a line strain going the same route as the heat source. The uniformity of the displacements are correlated to the distributions of the residual stresses that are illustrated for the 475, 500, 550 and 575 wires in Appendix XV. The distribution of residual stresses go the same way as the distributions of plastic strains.

7 DISCUSSION AND CONCLUSIONS

In this chapter the models and the results are discussed and analyzed for all the studied cases as well as recommendations are given and possible future research subjects are suggested. Also the making of the thesis, the hardships and successes are discussed.

Utilizing a ready-made model itself causes troubles starting with understanding what has been done. A model this complex has so many different properties that need to be just right for the results to be reliable. Thus during the modeling a lot of troubles were encountered. Tweaking the model took a lot time and effort. The computing times were extensive, without the use of CSC supercomputer to admit multiple jobs to be calculated simultaneously, there would not be any results. At the end the results are what they are.

The main idea of this thesis was to study how different factors affect the heat-induced deformations and their uniformity when heating a stainless steel ring with a torch. The studied factors lived all the way throughout the conducting of the thesis. All the factors that were aimed to be studied were not possible with the timeframe given. The multiple heating cycle study had to be left out because there were some sort of troubles with the model that were not solved in the given time.

7.1 Main findings

Main finding about the studied factors effects on the shrinkage are:

- Increase in speed decreases the deformations. Increases in speed equal smaller heat flux value which means smaller temperature so obviously smaller deformations.
- Temperature reaches its peak in single progressive heating after the torch has passed 30 ° to 45 °.
- Temperature not reaching its peak right from the start causes fluctuations of stress to the start end region that causes asymmetrical contraction to that region. So when heated starting from 0 ° and ending to the 0 ° an uneven displacement distribution zone is created to the start/end region.
- With speeded heating the heat flux is gradually increased to the starting zone getting more even distribution.

- With speeded heating the temperature near the ending point A is risen which gives better distribution to the start/end region.
- Location of the wires on the inner rim causes two times larger deformations and smaller uneven start/end region.
- Changing the heating location did not give the results that were hoped and did not affect notably.
- With smaller diameter higher peak temperature is achieved and so larger displacements occur.
- Increased ring height causes more displacement however with smaller ring height the peak temperature zone of the torch covers the whole ring height that evens out the distribution of displacements.
- Thicker ring causes less shrinkage however with thicker rings the difference in displacements on the top and the bottom surfaces do not deviate as much as with smaller thickness.
- More wires increase displacement.

7.2 Evaluation of the results

The easiest way to evaluate the results from the modeling is to compare the distribution figures. With the same default base values even with little deviations for each study the distributions of displacements and residual stresses should mainly look alike. The different model variations gave controversial results. Thus there probably is some faults in some of the studies or the different used models.

When all the cases are heated the same way the overall distributions of displacements should look the same with getting stronger going towards the center like in the case of different speeds. With the speeded start/end study the heating cycle is mainly the same as with the 0.1 °/s speed case, the only difference being the added speeded portions, but the figures are totally different looking.

Some of the models were successful giving plausible displacement distribution figures while others with using almost the same computing values gave implausible figures. The number of wires study case produced comparable realistic distribution figures for the 475, 500 and 525 wires but for the 550 and 575 the figures were unrealistic and deviated greatly

from the figures of 475, 500 and 525 wires. The figures from the study of heating location should at least create results alike from the study of the wire location but this did not happen either.

7.3 Recommendations and future research

To really know if the results are realistic experiments need to be made and the results compared. A calibration test with thermo-elements and strain gauges could be made to confirm the functionality of the model. The model used also needs some more work and examination to find possible malfunctions discussed above. Comparing local radial displacements might not be the best way to get comprehensive and usable results. Alternative method of comparing results should be found.

Future research could be directed to studying the use of multiple heating cycles and cooperative action of the studied factors. Different heating methods should also be studied using multiple torches. To get more reliable results the whole cylinder structure should be included to the studies because in the same cylinder there is multiple rings that may not all behave the same way even when heated similarly. The optimal heating parameters for different types of cylinders and the optimal cylinder structure should be defined to attain the wanted shrinkage as easily as possible. Also evaluation of the stability of the residual stress state should be studied to guarantee a lasting clamping between wires and rings.

8 SUMMARY

Both the chemical and mechanical pulping processes include the screening process. Screening is used to remove oversize contaminants from the desired pulp fibers. The pulp screen constitutes of two basic mechanical elements as mentioned above that control the separation, the screen and the rotor. Commonly the screen is a cylindrical cylinder that is fixed to the screen housing. The design of the wedge-wire cylinder consists of vertical, parallel wires arranged in a circle forming a cylinder and metal rings that hold the wires in place.

Various means are used to create wedge-wire cylinders, and in particular the means to join the wires to the support structure. These means include riveting, welding, clamping, gluing and heat-induced shrinkage. When heating with a torch, the heat affected zone in a part is small compared to the zone not affected by the heat. Reduction of yield strength on the HAZ causes upsetting, while the cold regions retain their elasticity. In the cooling phase, the hot upset regions pursue to shrink shorter than their original size, while the cold elastic regions pursue to obstruct the shrinking. This way the heat-induced shrinkage is obtained.

Heating of the support rings in a screen cylinder may be done by applying controlled heat in different sequences with repetitive heating and cooling cycles to get the desired diameter and roundness. So the most important requirement for the ring under study is that the ring should be as round as possible and the deformations should only occur as overall shrinkage in the ring diameter.

A variety of different cases are chosen to be studied with the model constructed. Measurement, reduction and removal of deformations are discussed as well as the model used is explained. The studied cases are torch flux by means of speed, location of the wires, heating location and structural factors. The studied cases provide directional knowledge about the effects of the studied variables on the shrinkage and its distribution.

REFERENCES

ASM International. 1993. ASM handbook volume 6: welding, bracing and soldering. 10. ed. USA: ASM International. 1299 p.

Callister, W. D. 2007. Materials science and engineering: an introduction. 7. Ed. New York: John Wiley & Sons, Inc. 832 p.

Cannell, E. 1999. Pulp screening advancements reduce shives, boost quality. Pulp & Paper, 73: 7. pp. 76–78.

Carrolo, V. S. 2010. Laser welding distortions on thin plates. [Article of a master's thesis] Technical university of Lisbon, department of mechanical engineering. [retrieved 24.03.2015]. 9 p. From as pdf-file: https://fenix.tecnico.ulisboa.pt/downloadFile/395142134403/Paper%20Laser%20welding%20heat%20distortion.pdf

Deng, D. & Kiyoshima, S. 2010. FEM prediction of welding residual stresses in a SUS304 girth-welded pipe with emphasis on stress distribution near weld start/end location. Computational Materials Science, 50: 2. pp. 612–621.

Federal Highway Administration. 2013. Guide for heat-straightening of damaged steel bridge members. [PDF in U.S. Department of Transportation Federal Highway Administration www-pages]. Updated 23.7.2013 [retrieved 17.3.2015]. 77 p. From: http://www.fhwa.dot.gov/bridge/steel/

Feng, Z. 2005. Processes and mechanisms of welding residual stress and distortion. Boca Raton, Florida. Woodhead Publishing Limited. 364 p.

Flame Straightening. 2013. Fundamentals of flame straightening. [PDF in The Linde Group www-pages]. Updated 3.9.2013 [retrieved 29.4.2015]. 32 p. From:http://www.linde-gas.com/en/processes/cutting_joining_and_heating/lindoflamm_flame_solutions/heating-process/flame-straightening/index.html

Friedman, E. 1975. Thermo-mechanical analysis of the welding process using the finite element method. Journal Pressure Vessel Technology, 97:3. pp. 206–213.

Goldak, J. A. & Akhlaghi, M. 2005. Computational welding mechanics. USA, New York: Springer Science+Business Media. 321 p.

Kaila, P. 2014. Control of distortions and residual stresses when heating. Bachelor's thesis. Lappeenranta University of Technology, Faculty of Technology. Lappeenranta. 42 p.

Krutz, G. W. & Segerlind, L. J. 1978. Finite element analysis of welded structures. Welding Journal Research Supplement, 54: 7. pp. 211–216.

Metla. 2012. Forest industry in Finland [In Natural Resources Institute Finland www-page]. Updated 21.03.2012 [retrieved 20.03.2015]. From: http://www.metla.fi/metinfo/sustainability/SF-1-forest-industry.htm

Mousivand, R. 2015. Re: VS: Hi [Private communication]. Email to: Pia Kaila (pia.kaila@lut.fi). Sent 9.2.2015 at 16:41 pm (GTM +0200).

Niemi, E. & Kemppi, J. 1993. Hitsatun rakenteen suunnittelun perusteet. Helsinki: Painatuskeskus Osakeyhtiö. 337 p.

Pat. US 4634521. 1987. Screening apparatus with light reject removal. Ahlsröm Corp; Oy Wilh, Schauman AB. (Simola M. & Haapoja V.) Publ. 6.1.1987. 5 p.

Pavelic, V., Tanbakuchi, R., Uyehara, O. A. & Myers, P. S. 1969. Experimental and computed temperature histories in gas tungsten-arc welding of thin plates. Welding Journal Research Supplement, 48: 7. pp. 295–305.

Pulp and Paper Applications. 2008. [PDF in Yokogawa Corporation of America www-pages]. Updated 30.3.2009 [retrieved 16.3.2015]. 6 p. From: http://www.yokogawa.com/us/technical-library/application-notes/pulp-and-paper-applications.htm

Radaj, D. 1992. Heat effects of welding. New York: Springer-Verlag Berlin Heidelberg. 348 p.

Seppälä, M. J. (Editor), Klemetti, U., Kortelainen, V.-A., Lyytikäinen, J., Siitonen, H. & Sironen, R. 1999. Kemiallinen metsäteollisuus 1. Paperimassan valmistus. Helsinki: Hakapaino oy. 201 p.

Sixta, H. (Editor) 2006. Handbook of pulp. Weinheim: WILEY-VCH Verlag GmbH & Co. KGaA. 1316 p.

Teng, T. L., Chang P. H. & Ko, H. C. 2000. Finite element analysis of circular patch welds. International Journal of Pressure Vessels and Piping, 77: 11. pp. 643–650.

Teng, T. L., Chang, P. H. & Tseng, W. C. 2003. Effect of welding sequences on residual stresses. Computers & Structures, 81: 5. pp. 273–286.

The Institute for Industrial Productivity. 2015. Mechanical pulping. [In Industrial Efficiency Technology Database www-pages]. [Retrieved 20.03.2015]. From: http://ietd.iipnetwork.org/content/mechanical-pulping

Towfighi, S. 2011. An investigation of deformations in stainless steel rings by heating. Master's thesis. The University of British Columbia, The Faculty of Graduate Studies, Department of Mechanical Engineering. Vancouver. 77 p.

Uccellini, J. 2003. Identifying the right cutting and welding tips. Practical Welding Today, 7: 5. Pp. 18–20.

Weckroth, R., Marshall, L., Tuomela, P. & Gooding, R. 2002. Enhanced pulp screening using high-performance screen components and process simulation. In: African Pulp and Paper Week: Proceedings of Technical Association of the Pulp and Paper industry of Southern Africa's international conference, held at Durban, South Africa 8–11 October, 2002. 14 p.

Zeng, Z., Wang, L., Du, P. & Li, X. 2010. Determination of welding stress and distortion in discontinuous welding by means of numerical simulation and comparison with experimental measurements. Computational Materials Science, 49: 3. pp. 535–543.

Appendix I

Expansion behavior of different materials (Flame Straightening, 2013, p. 8).

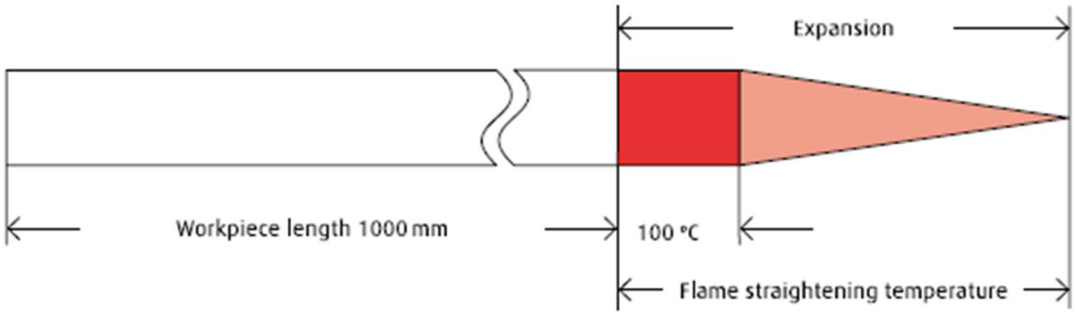

Table 1: Expansion behaviour of different materials

Material		Example		Expansion coefficient α (mm/m K)	Expansion (mm)
Mild steel Boiler steel Rail steel		S235JR S355JO P265GH 16Mo3 13CrMo4-5		0.011 – 0.014	1.3 9.1
Fine-grain structural steel TM steel		S355N S890QL S355M S460M		0.012 – 0.015	1.4 8,8
Nickel-based materials		2.4360 [NiCu30Fe] 2.4602 [NiCr21Mo14W] 2.4856 [NiCr22Mo9Nb]		0.010 – 0.014	1.2 8.7
Austenitic stainless steel		1.4404 [X2CrNiMo17-22-2] 1.4301 [X5CrNi18-10] 1.4541 [X6CrNiTi18-10]		0.016 – 0.019	1.7 12.3
Aluminium	Pure aluminium			0.020 – 0.024	2.6 7.8
	Non-age-hardening wrought alloys suitable for welding	EN AW-3103 [Al Mn1]	Soft		2.6 9.8
		EN AW-5754 [Al Mg3]			
		EN AW-5083 [Al Mg4,5Mn0,7]	Hard		2.6 6.5
	Age-hardening wrought alloys suitable for welding	EN AW-6005A [Al SiMg(A)]			2.6 4.6
		EN AW-6082 [Al Si1MgMn]			
		EN AW-7072 [Al Zn1]			2.6 6.5
		EN AW-7020 [Al Zn4,5Mg1]			
Copper				0.018 – 0.019	1.8 12.6

Appendix II

Thermal properties of different materials (Callister, 2007, p. 726).

Material	c_p *(J/kg-K)*[a]	α_l *[(°C)$^{-1}$ × 10^{-6}]*[b]	*k (W/m-K)*[c]	*L* *[Ω-W/(K)^2 × 10^{-8}]*
		Metals		
Aluminum	900	23.6	247	2.20
Copper	386	17.0	398	2.25
Gold	128	14.2	315	2.50
Iron	448	11.8	80	2.71
Nickel	443	13.3	90	2.08
Silver	235	19.7	428	2.13
Tungsten	138	4.5	178	3.20
1025 Steel	486	12.0	51.9	—
316 Stainless steel	502	16.0	15.9	—
Brass (70Cu–30Zn)	375	20.0	120	—
Kovar (54Fe–29Ni–17Co)	460	5.1	17	2.80
Invar (64Fe–36Ni)	500	1.6	10	2.75
Super Invar (63Fe–32Ni–5Co)	500	0.72	10	2.68
		Ceramics		
Alumina (Al_2O_3)	775	7.6	39	—
Magnesia (MgO)	940	13.5[d]	37.7	—
Spinel ($MgAl_2O_4$)	790	7.6[d]	15.0[e]	—
Fused silica (SiO_2)	740	0.4	1.4	—
Soda–lime glass	840	9.0	1.7	—
Borosilicate (Pyrex™) glass	850	3.3	1.4	—
		Polymers		
Polyethylene (high density)	1850	106–198	0.46–0.50	—
Polypropylene	1925	145–180	0.12	—
Polystyrene	1170	90–150	0.13	—
Polytetrafluoroethylene (Teflon™)	1050	126–216	0.25	—
Phenol-formaldehyde, phenolic	1590–1760	122	0.15	—
Nylon 6,6	1670	144	0.24	—
Polyisoprene	—	220	0.14	—

[a] To convert to cal/g-K, multiply by 2.39×10^{-4}; to convert to Btu/lb$_m$-°F, multiply by 2.39×10^{-4}.

[b] To convert to (°F)$^{-1}$, multiply by 0.56.

[c] To convert to cal/s-cm-K, multiply by 2.39×10^{-3}; to convert to Btu/ft-h-°F, multiply by 0.578.

[d] Value measured at 100°C.

[e] Mean value taken over the temperature range 0–1000°C.

Appendix III

Flame straightening temperatures of different materials (Flame Straightening, 2013 p. 11).

Table 2: Flame straightening temperatures of different materials

Materials		Specification	Alternative specification	Flame straightening temperature [°C]
Mild steel		S235JR		
		S355JO		600 ... 800
Boiler steel		P265GH		
		16Mo3		
		13CrMo4-5		
Fine-grain structural steel		S355N		550 ... 700
		S890QL		
TM steel		S355M		
		S460M		
Nickel material		2.4360	NiCu30Fe	650 ... 800
		2.4602	NiCr21Mo14W	
		2.4856	NiCr22Mo9Nb	
Austenitic stainless steel		1.4404	X2CrNiMo17-12-2	650 ... 800
		1.4301	X5CrNi18-10	
		1.4541	X6CrNiTi18-10	
Aluminium	Pure aluminium			150 ... 450
	Non-age-hardening wrought alloys suitable for welding	EN AW-3103	AlMn1	300 ... 450
		EN AW-5754	AlMg3	
		EN AW-5083	AlMg4,5Mn0,7	150 ... 350
	Age-hardening wrought alloys suitable for welding	EN AW-6005A	AlSiMg(A)	
		EN AW-6082	AlSi1MgMn	150 ... 200
		EN AW-7072	AlZn1	150 ... 350
		EN AW-7020	AlZn4,5Mg1	
Copper				600 ... 800

Appendix IV

Flame setting and guidance for heat straightening (Flame Straightening, 2013, p. 17).

– Unsuitable – – Impermissible • Possible + Acceptable + + Correct

Material	Flame setting				Flame guidance Distance flame cone to workpiece			
	Excess				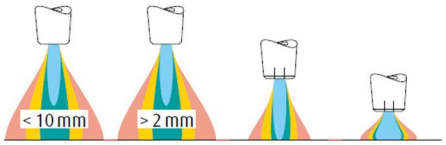			
	C_2H_2 0 < 1 %	Neutral	O_2 30 %	O_2 50 %				
Mild steel	–	•	+	+ +	Heating of edge zone*			
Fine-grain structural steel	–	•	+	+ +	– –	–	+	+ +
TM steel	–	•	+	+ +				
Boiler sheet metal	–	•	+	+ +	Heating of lower-lying zones*			
Rail steel	–	•	+	+ +	+ +	+ +	–	– –
Austenitic stainless steel	– –	–	•	+ +	+	+ +	–	– –
Duplex steel	– –	–	•	+ +	+	+ +	–	– –
Aluminium	+ +	–	– –	– –	+ +	+	–	– –
Aluminium alloys	+ +	–	– –	– –	+ +	+	–	– –

*Box highlighted in blue refers to mild steel, fine-grain structural steel, TM steel, boiler sheet metal and rail steel.

Appendix V

Effects of welding speed on the temperature distribution (ASM International, 1993, p. 50).

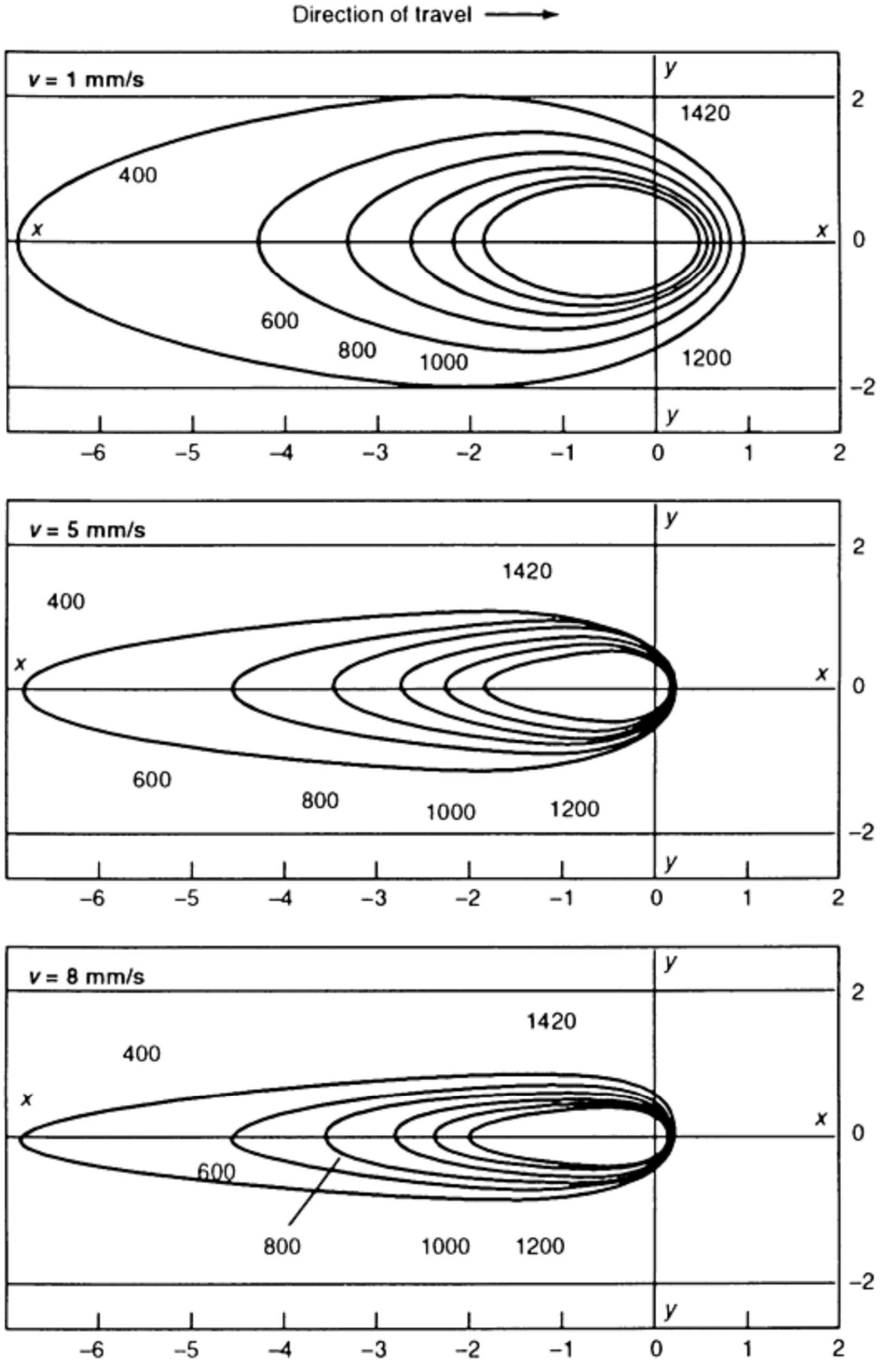

Appendix VI

Pipe's finite element model (on top, Deng & Kiyoshima, 2010, p. 614) and definition of middle section (underneath, Deng & Kiyoshima, 2010, p. 618).

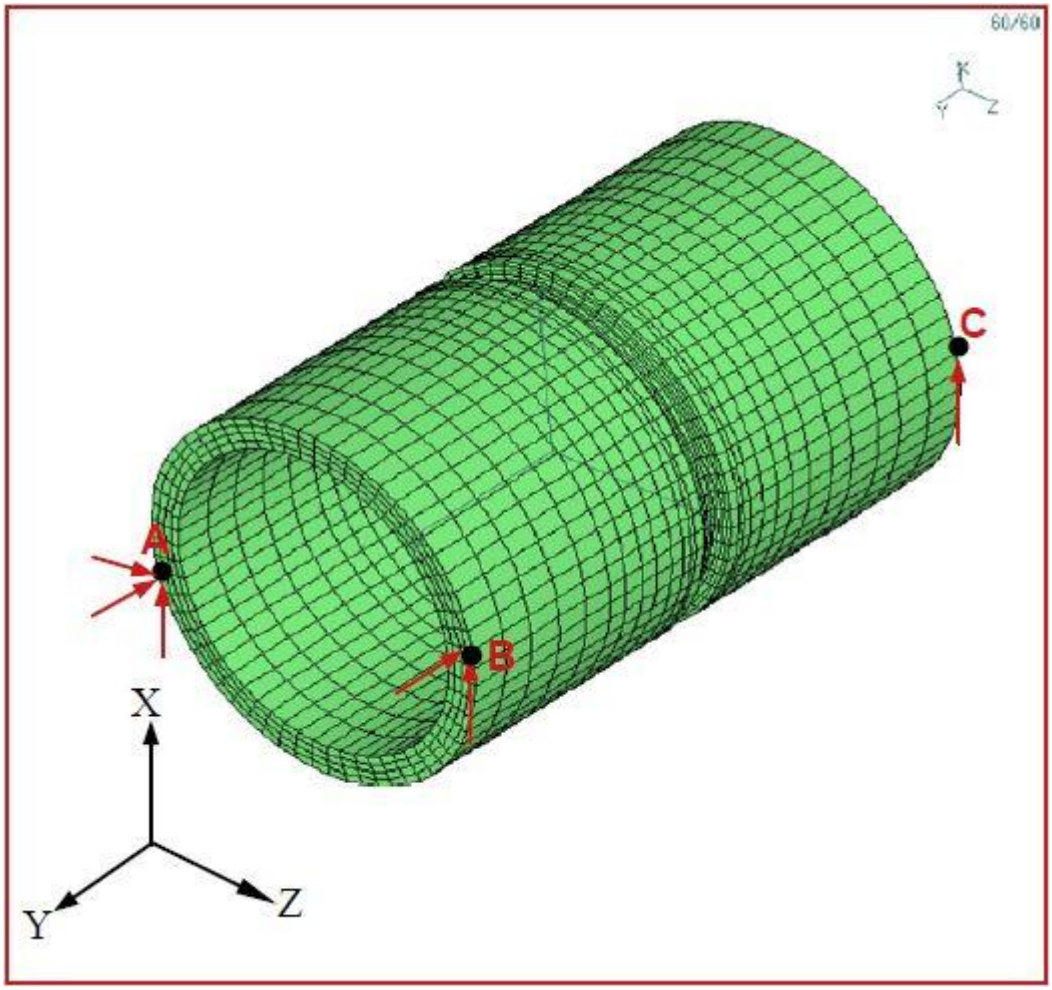

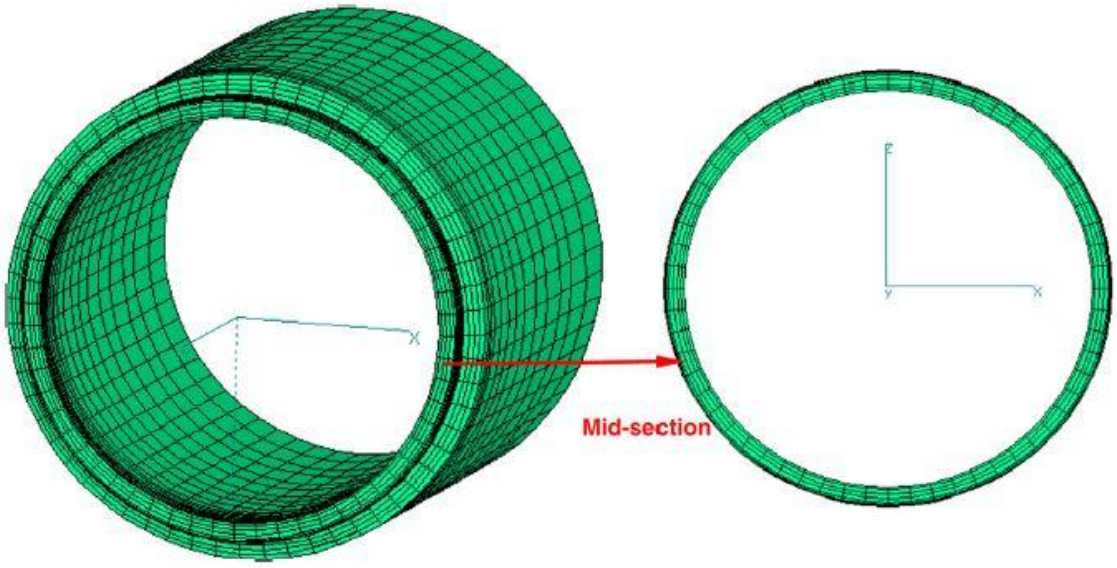

Appendix VII, 1

Overall distribution of displacements for speeds 0.125, 0.15 and 0.175 °/s.

0.125 °/s

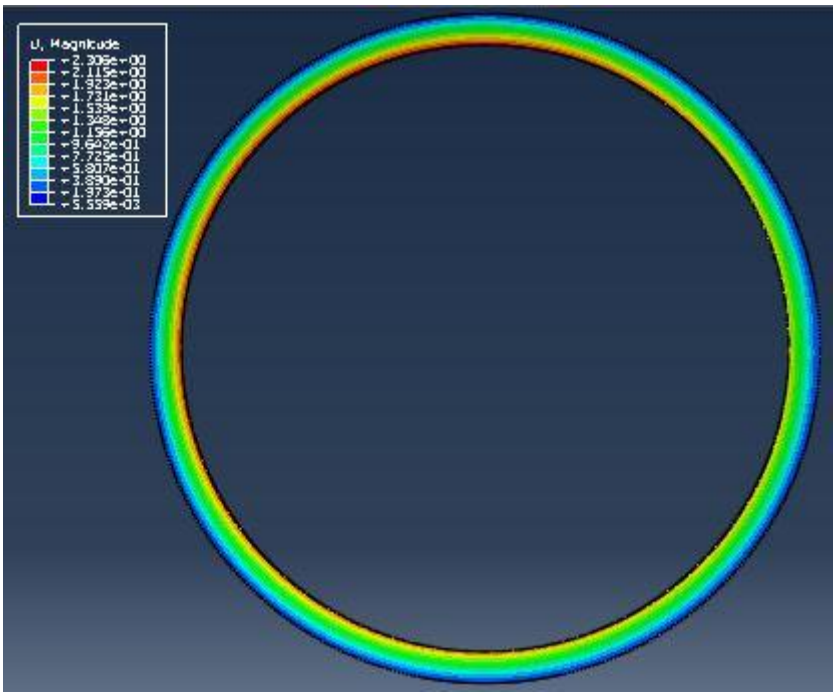

0.15 °/s

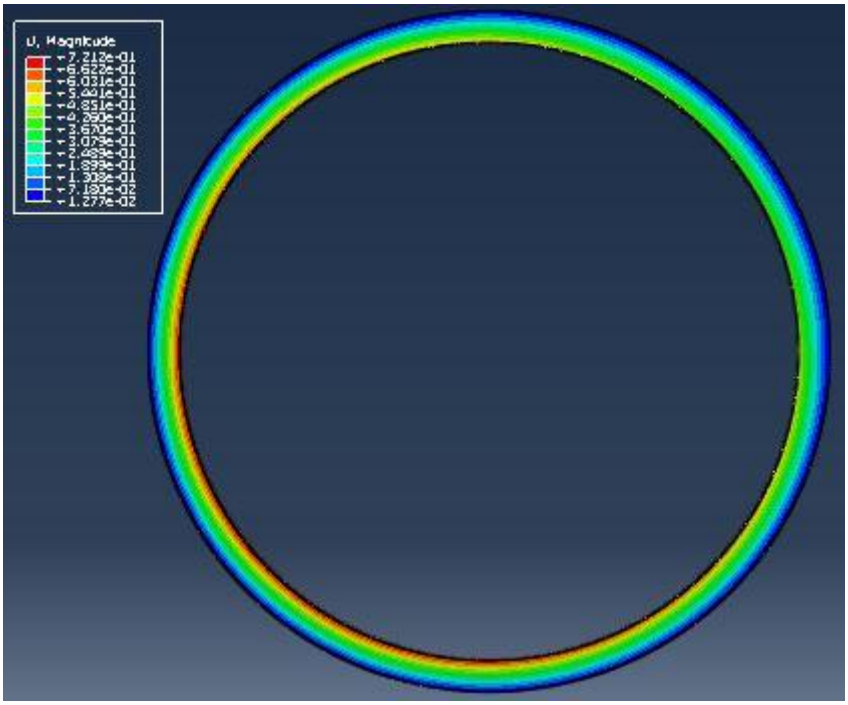

Appendix VII, 2

0.175 °/s

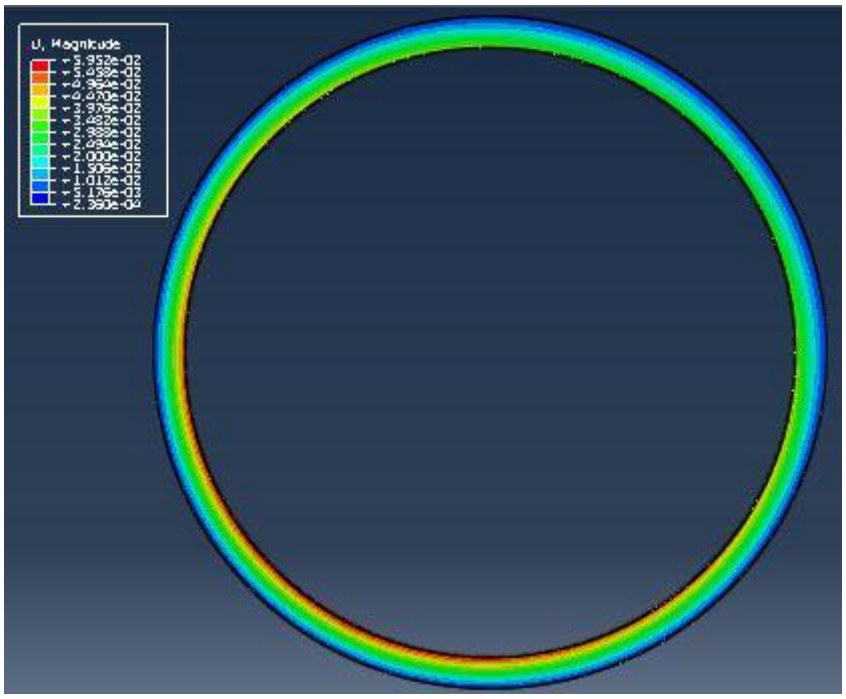

Appendix VIII

Temperature distribution for speeds 0.1, 0.125, 0.15 and 0.175 °/s.

0.1 °/s

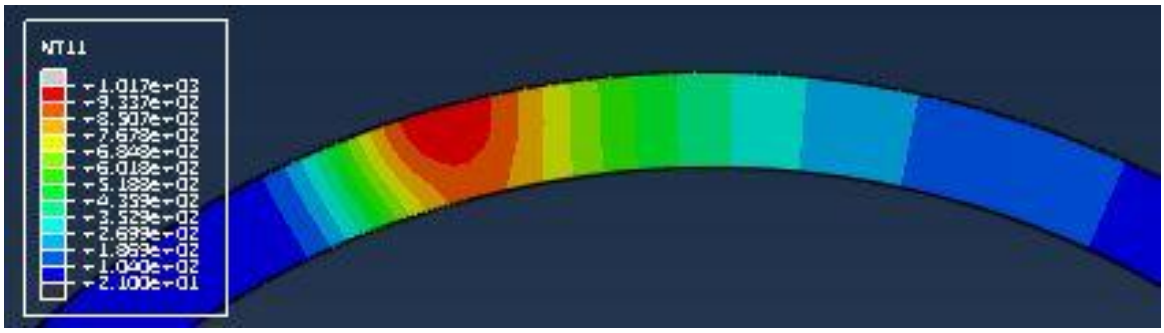

0.125 °/s

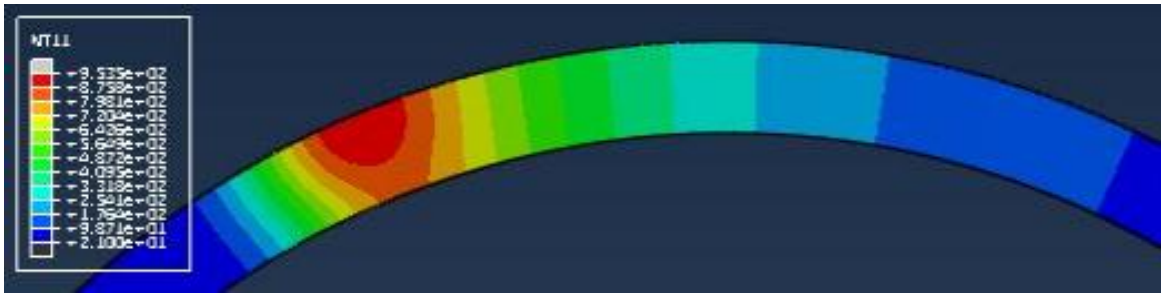

0.15 °/s

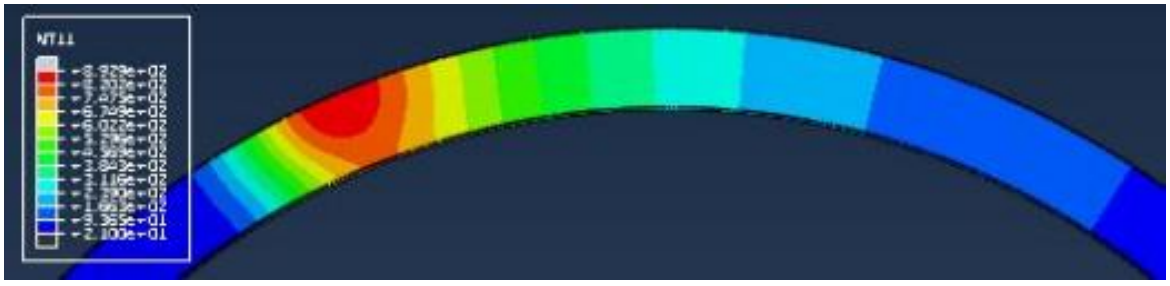

0.175 °/s

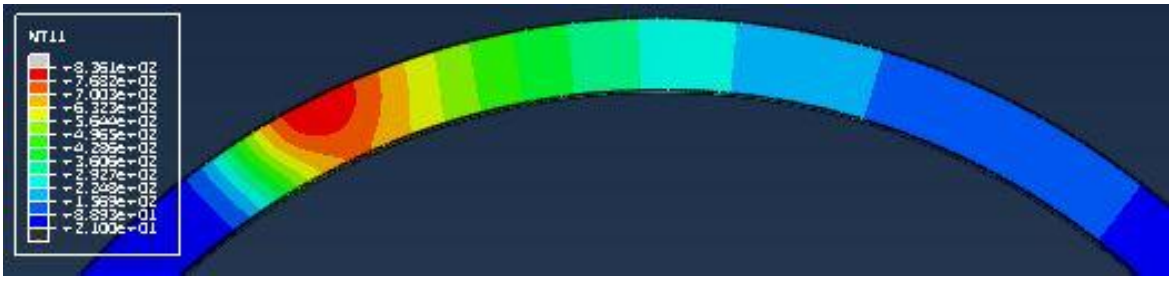

Appendix IX, 1

Distribution of plastic strains for speeds 0.125, 0.15 and 0.175 °/s.

0.125 °/s

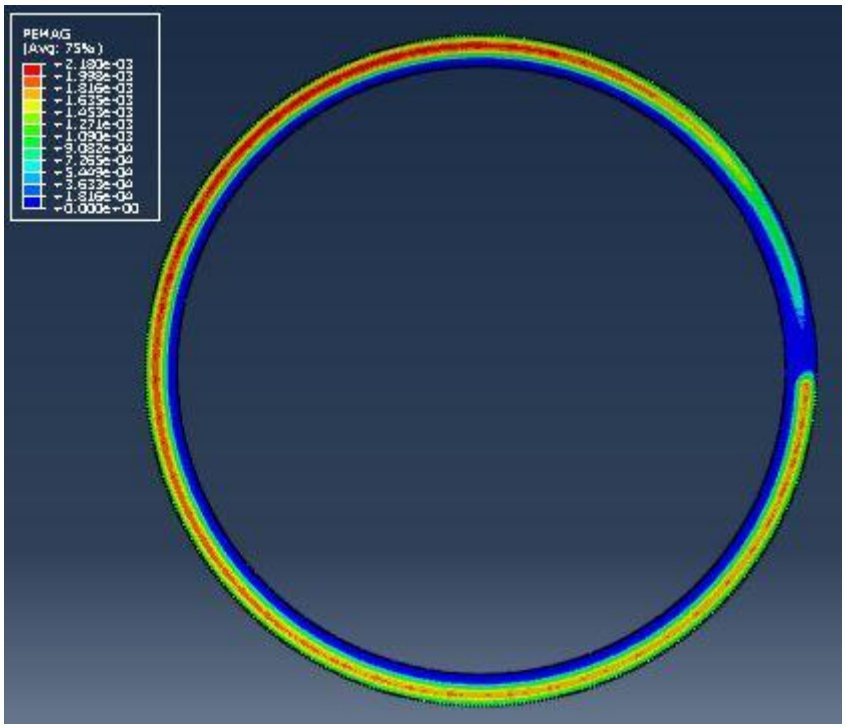

0.15 °/s

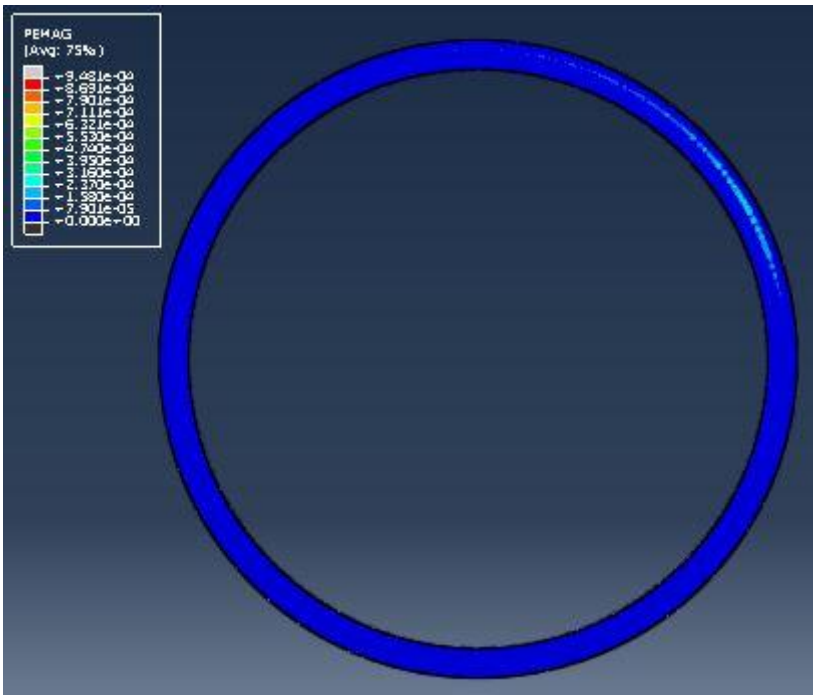

Appendix IX, 2

0.175 °/s

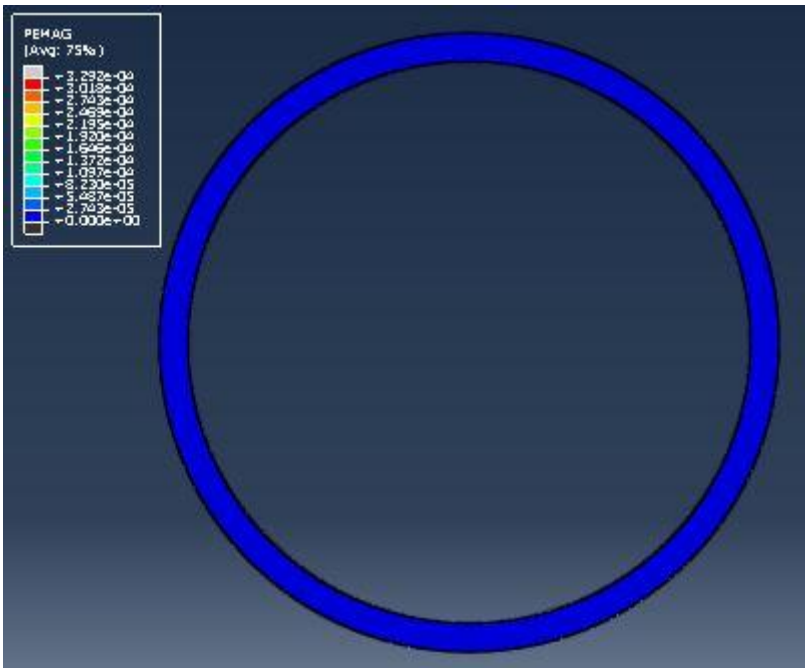

Appendix X, 1

Distribution of residual stresses for speeds 0.125, 0.15 and 0.175 °/s.

0.125 °/s

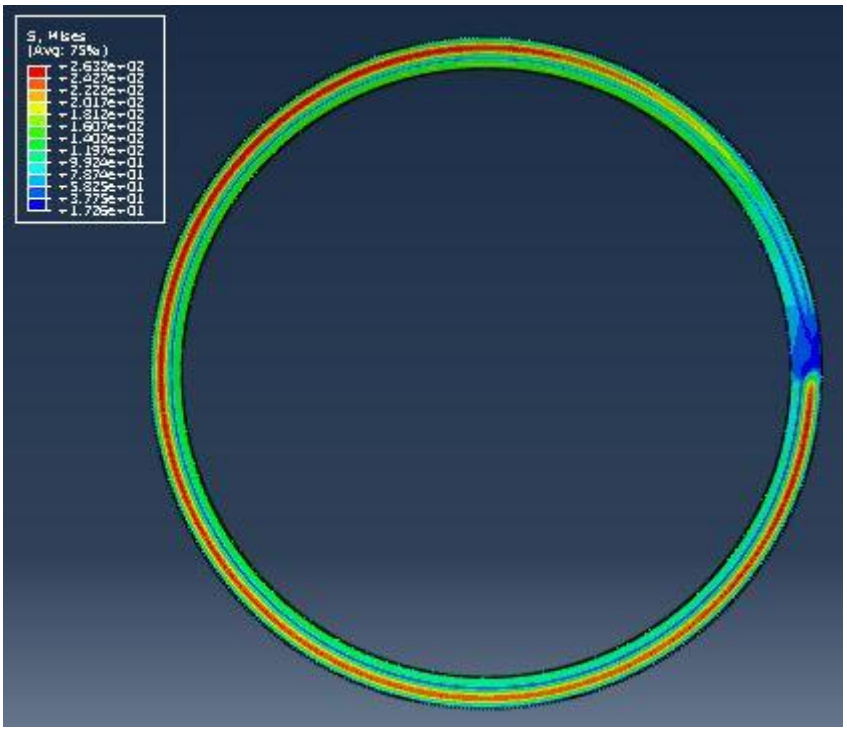

0.15 °/s

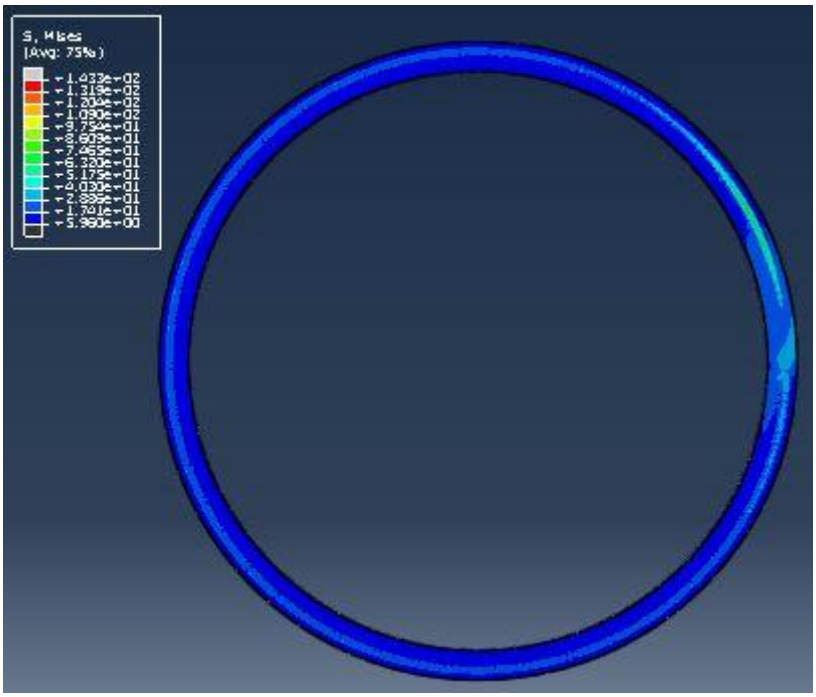

Appendix X, 2

0.175 °/s

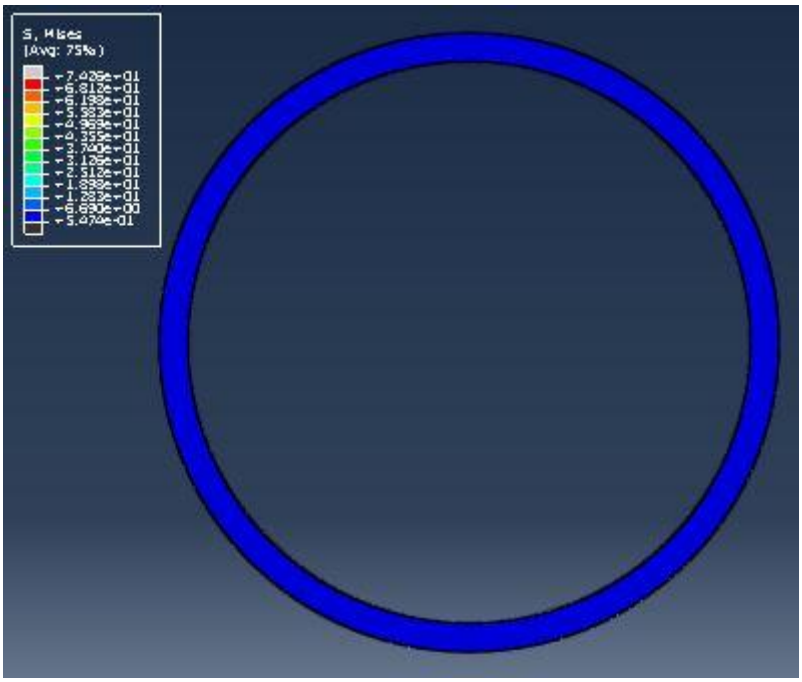

Appendix XI

Distribution of temperatures during heating for the different ring heights 25, 30 and 35 mm.

25 mm

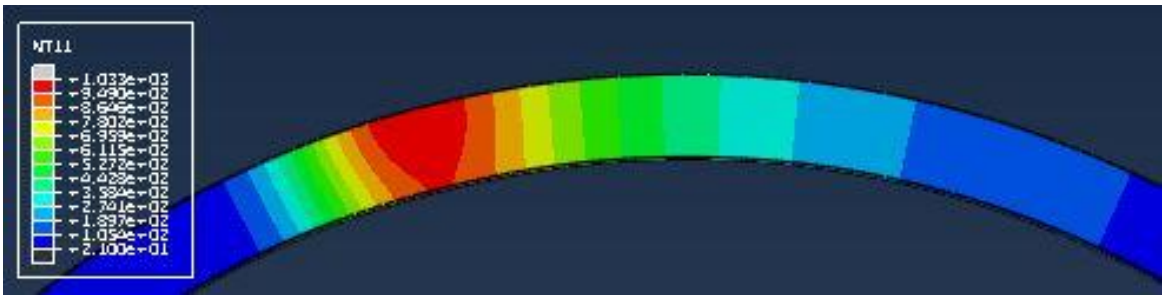

30 mm

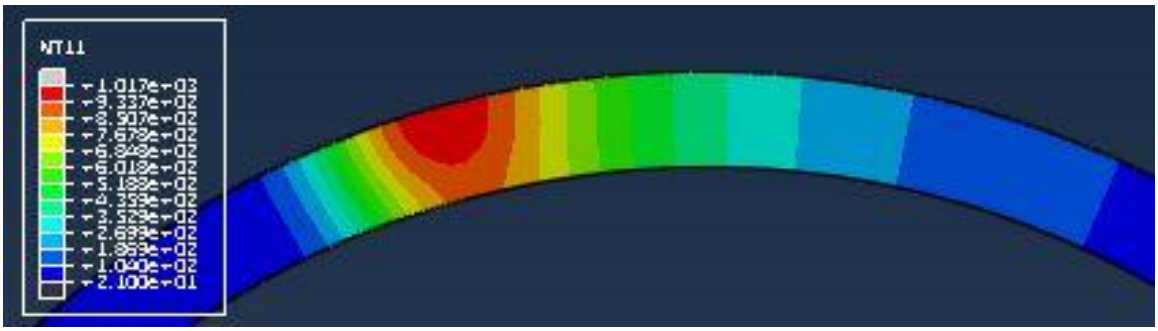

35 mm

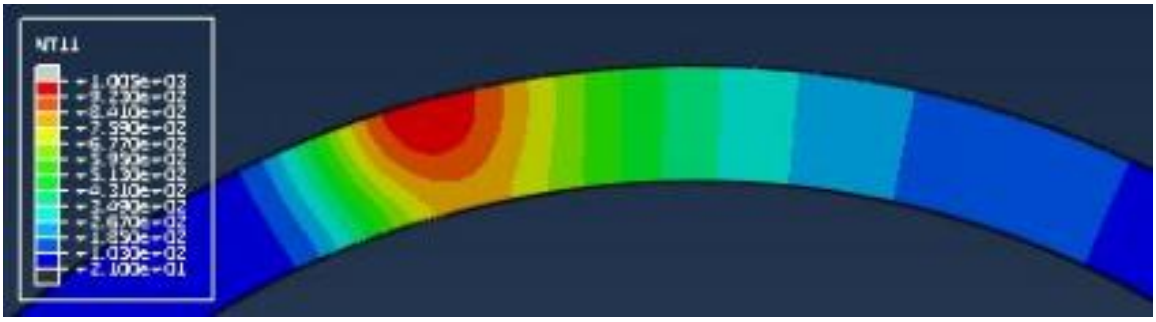

Appendix XII

Distributions of temperatures on the top and bottom surfaces for different ring thicknesses 4, 6, 8 and 10 mm.

4 mm, top surface (right) and bottom surface (left)

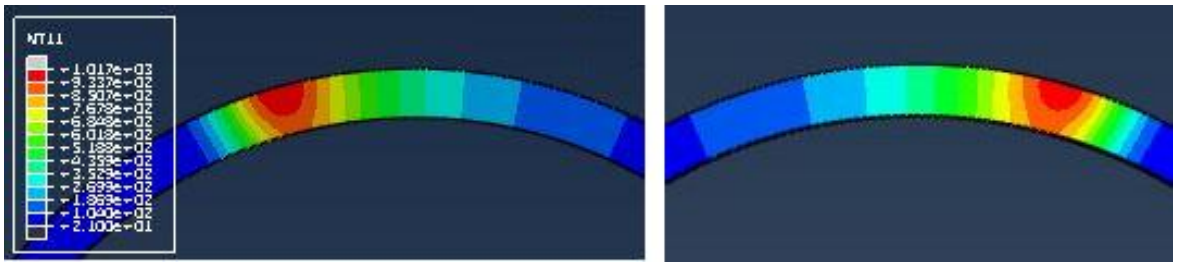

6 mm, top surface (right) and bottom surface (left)

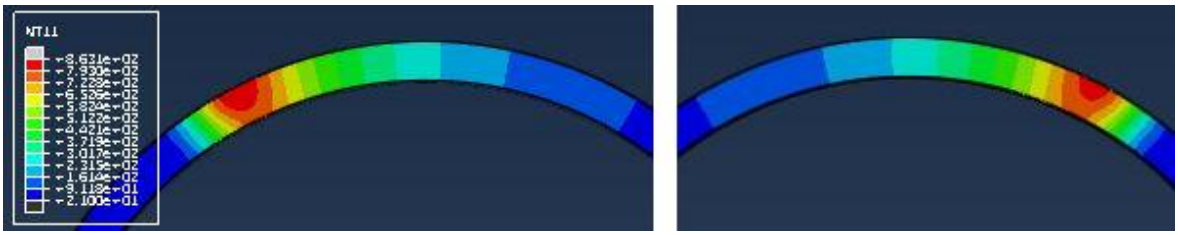

8 mm, top surface (right) and bottom surface (left)

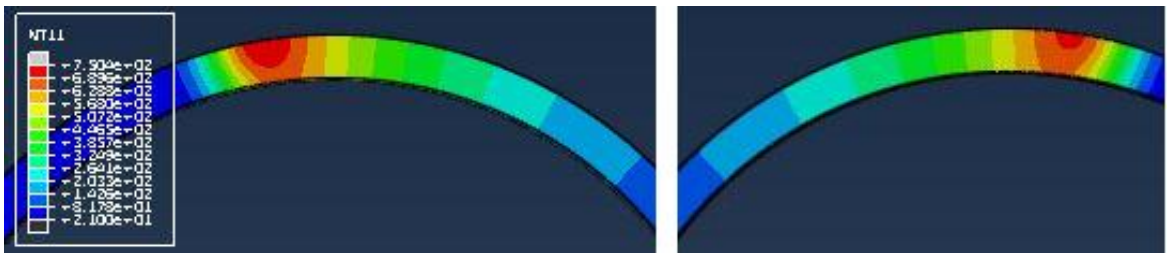

10 mm, top surface (right) and bottom surface (left)

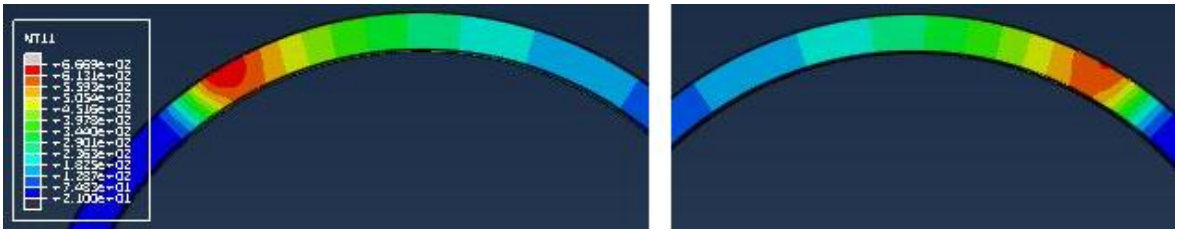

Appendix XIII, 1

Overall distribution of displacements on the top surface for 500, 550 and 575 wires.

500 wires

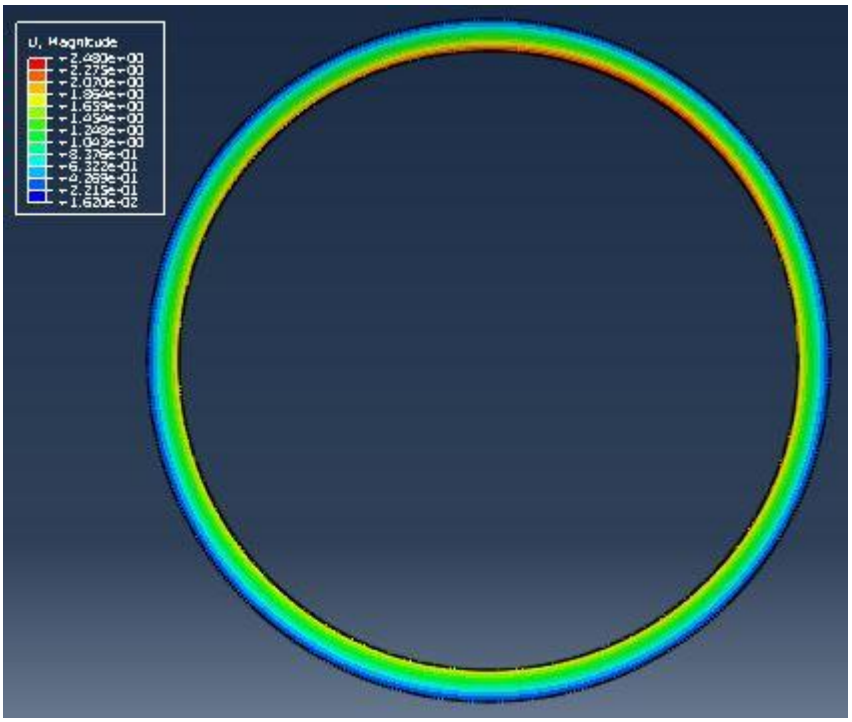

550 wires

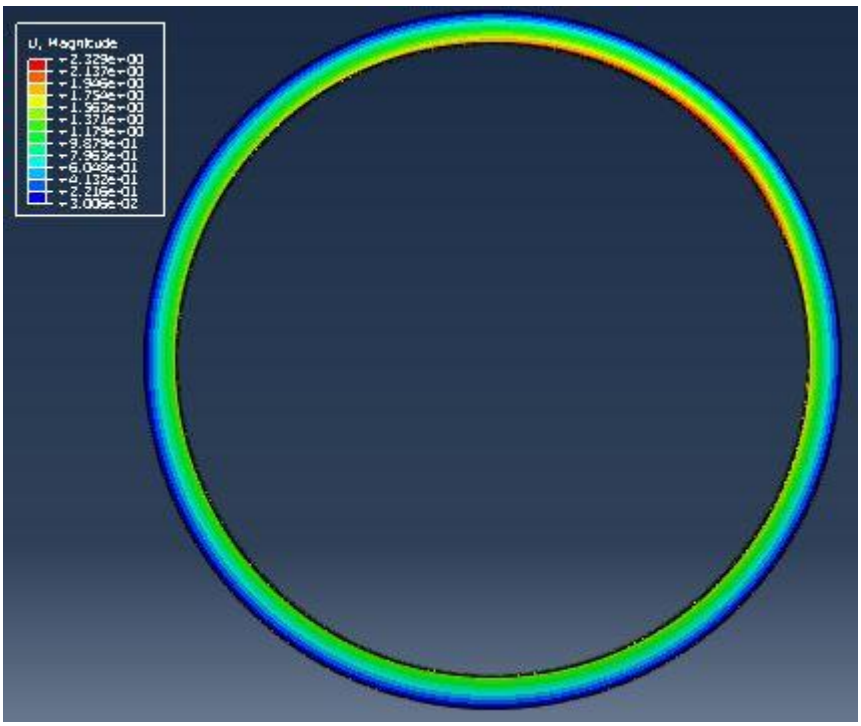

Appendix XIII, 2

575 wires

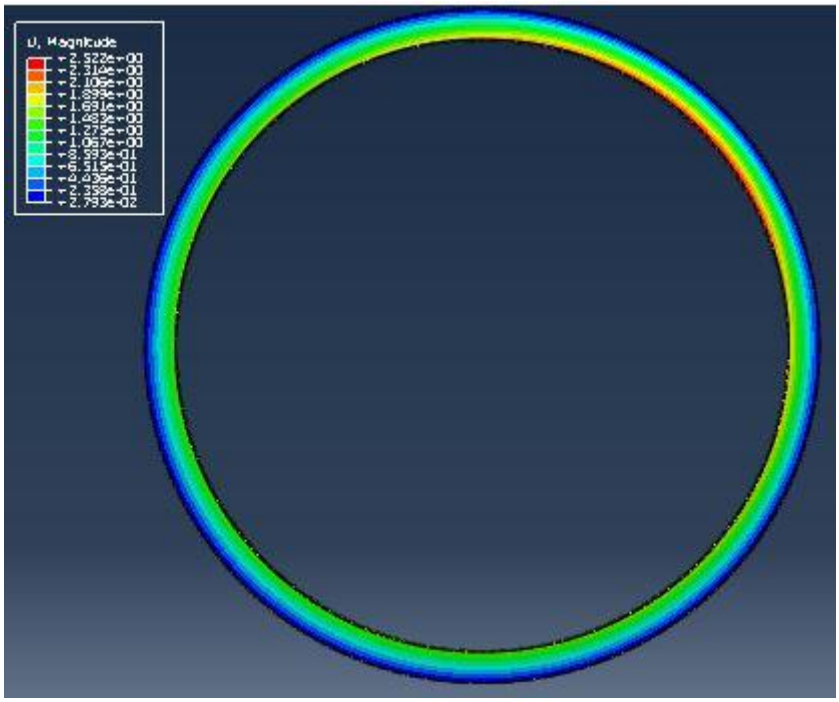

Appendix XIV, 1

Distributions of plastic strains on the top surface for 475, 500, 550 and 575 wires.

475 wires

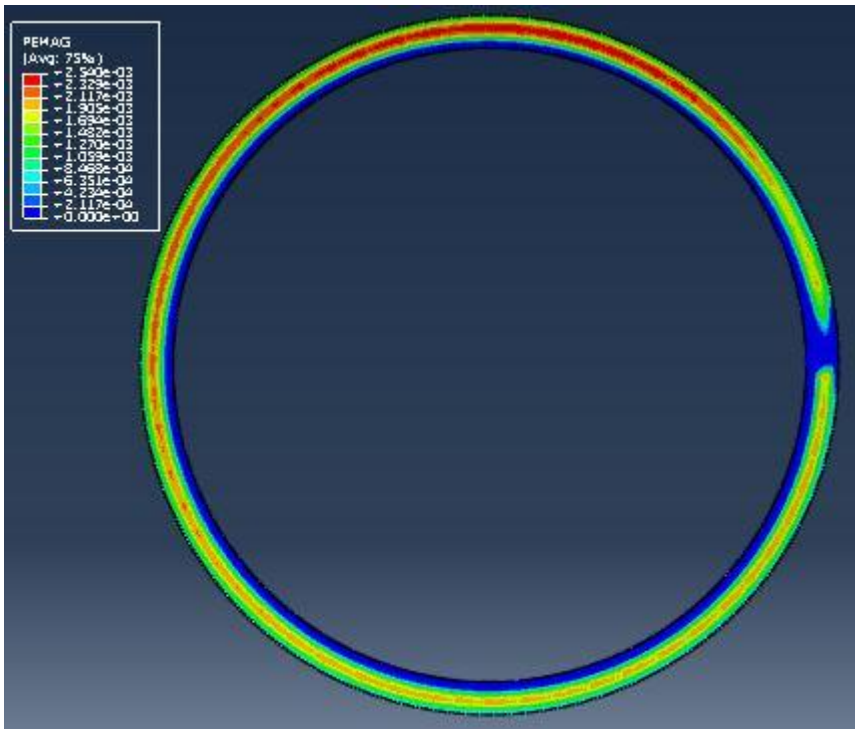

500 wires

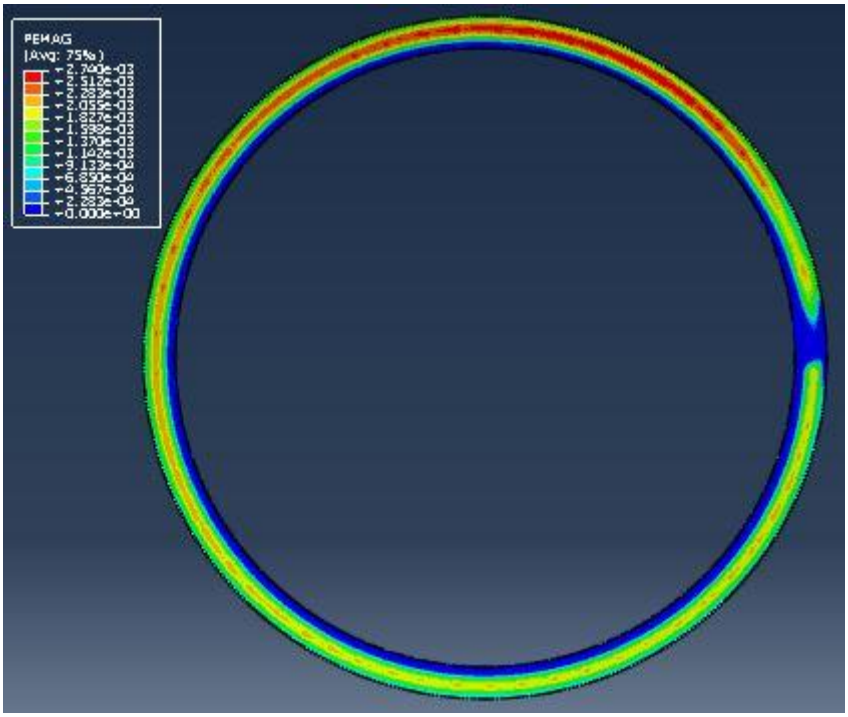

Appendix XIV, 2

550 wires

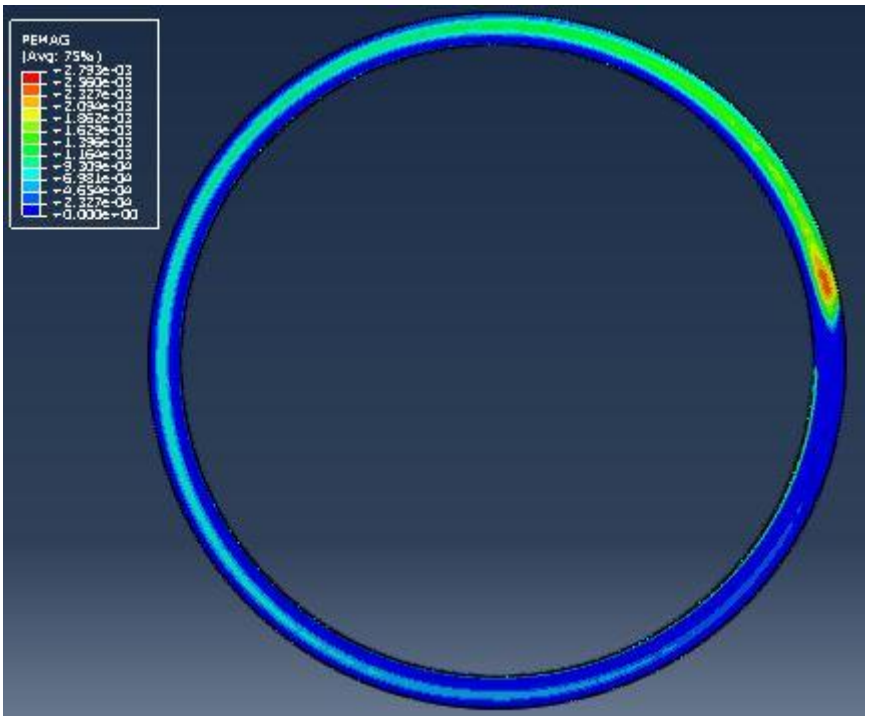

575 wires

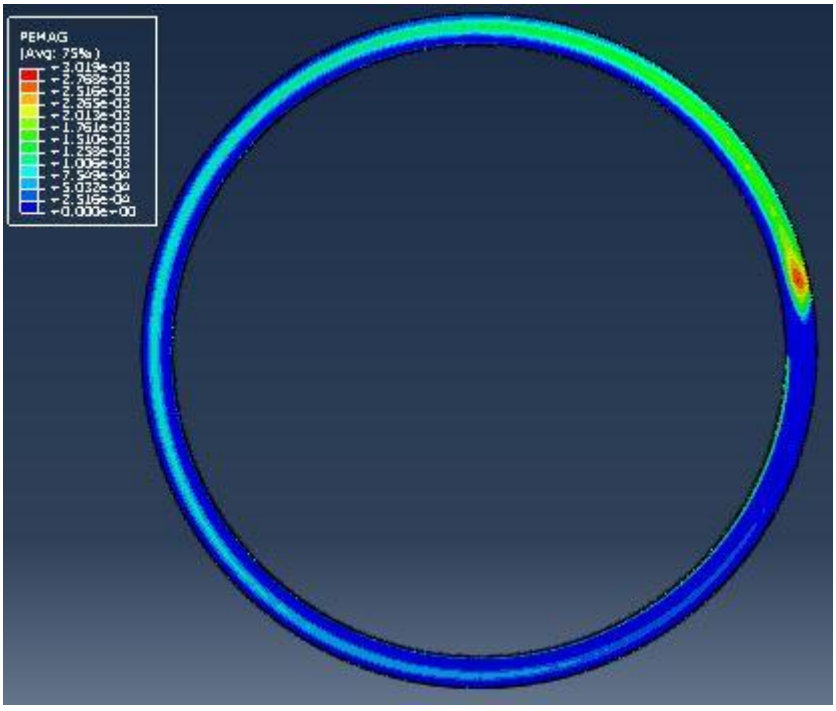

Appendix XV, 1

Distributions of residual stresses on the top surface for 475, 500, 550 and 575 wires.

475 wires

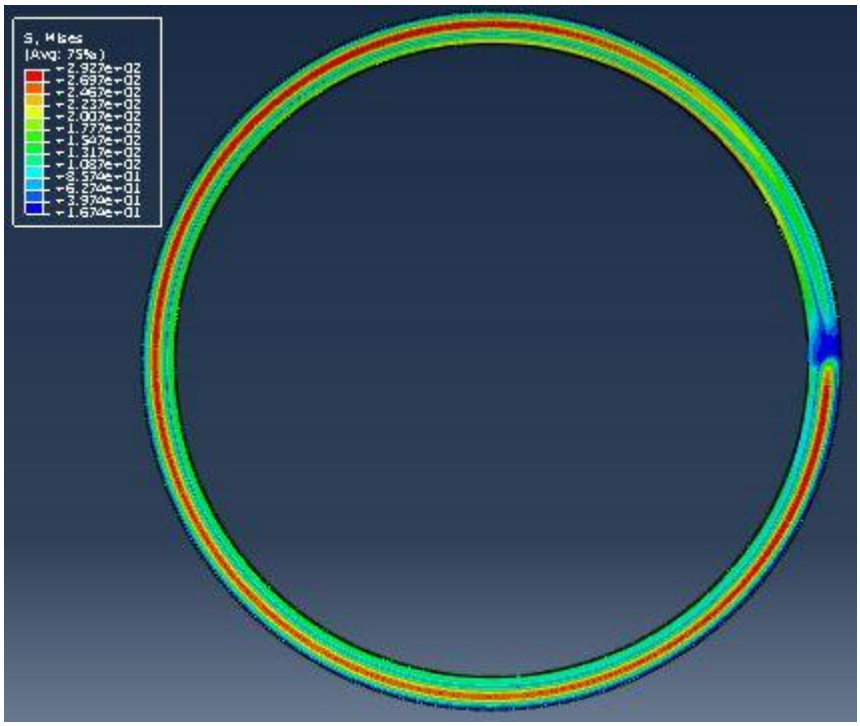

500 wires

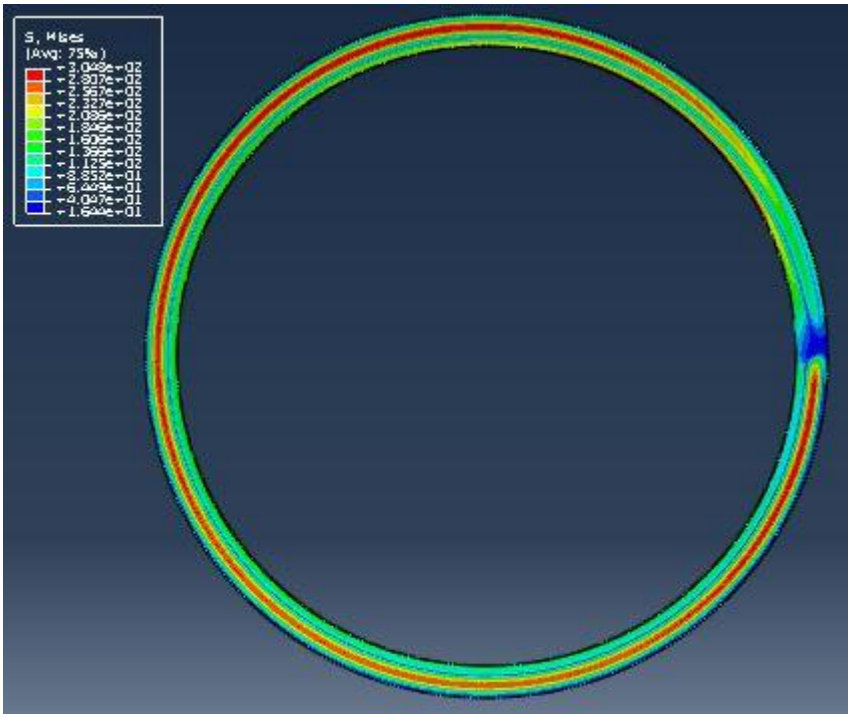

Appendix XV, 2

550 wires

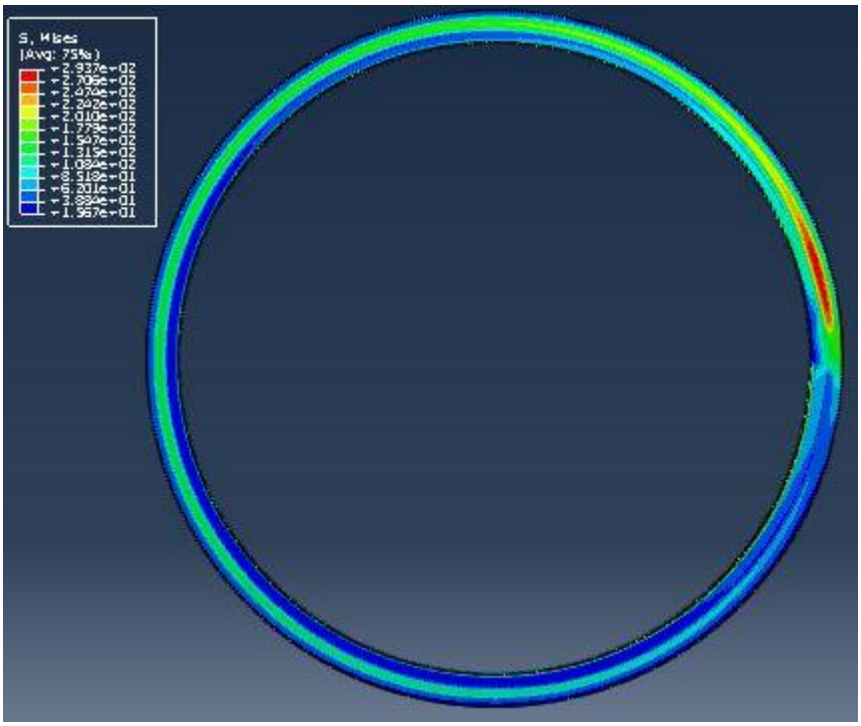

575 wires